UNIVERSITY OF CAPE TOWN

FACULTY OF ENGINEERING

DEPARTMENT OF MECHANICAL ENGINEERING

CREEP PREDICTIONS FOR TURBOMACHINERY COMPONENTS

a dissertation submitted towards the degree of
Master of Science in Engineering

H. O. SIEBURG
B. Sc. Eng. (Mech.) (Witwatersrand)

April 1989

ABSTRACT

Several theories of creep and creep rupture are reviewed. Specific attention is devoted to the brittle damage theory proposed by Kachanov. Creep, damage and life predictions for rectangular or circular cross section beams under bending and tensile loads are presented. Comparison with data for a Ni Superalloy showed life predictions could be 30% in excess of experimental values. This beam model also revealed that it is imperative that no bending moments be inadvertently applied during tensile creep testing. The creep-damage material model is extended to multidimensional situations. A refinement, whereby no damage accumulates in compression, is incorporated. A User-Material subroutine for this constitutive model has been formulated, and incorporated into the ABAQUS FEM package. Several verification examples are presented; one example is the creep-damage behaviour of a notched bar in tension. The value of reference stress techniques is discussed. Reference stress estimates for a centrifugally loaded bar, as well as for a cantilever under distributed loads, are presented. These could be useful in turbine blade design.

CONTENTS

1.0 Introduction

At high temperatures, typically above 3/10 of the melting point, materials behave differently to the familiar elastic-plastic responses at room temperature: There is a continual, although slight, increase in deformation under load. Then after several hundred (or thousand) hours of apparently safe operation, the component fails catastrophically and without much prior warning. This creep phenomenon is not yet fully understood.

In many applications such as steam generators, furnaces, steam or gas turbines, creep has been observed to occur. The designers of such apparatus cannot predict with acceptable confidence what the time to failure under operating conditions is likely to be. Yet the prevention of a catastrophic failure is imperative.

Researchers and Engineers are continuously striving towards a better understanding of this creep phenomenon, so as to develop better analysis and design tools.

This work has been conducted in order to become familiar with contemporary thinking on this subject, and to become familiar with some of the creep analysis tools.

1.1 Scope of proposed work

Firstly the theories of creep deformation and damage were reviewed in order to assess those characteristics needed for the design of structures operating in the creep range. The finite lifetimes of creeping structures were of particular interest.

Reference stress techniques were studied. The technique is an approximate, but useful aid for component design in the creep range.

As an introduction to the topic, creep-damage in beams of various cross-sections, under bending and/or axial loads, were investigated.

To perform advanced calculations, non-linear finite element methods were used. The ABAQUS finite element package was used, as it provided the possibility for a user to define his own material constitutive relations. A subroutine UMAT, capable of portraying creep and damage behaviour, was developed and verified.

It was proposed that ultimately these relevant theories and finite element subroutines should be used in design calculations of creep damage of structures at high temperatures such as turbine blades and thin walled structures.

Non-isothermal and thermal transient conditions, although very pertinent to the creep problem, were not considered here.

2.0 Literature survey

2.1 Creep deformation under constant stress

When a specimen, maintained at a suitably high temperature, is subjected to constant uniaxial tension, a time dependent deformation over and above an elastic deformation is observed. Early investigators have tended to identify 4 distinct phases of the deformation response:

1) Immediate elastic deformation.

2) Primary creep, characterised by a decreasing strain rate.

3) Secondary creep, during which the strain rate is constant.

4) Tertiary creep, where the strain rate increases and finally the specimen parts, i.e. rupture.

illustrated in fig. (2.1) from [1]:

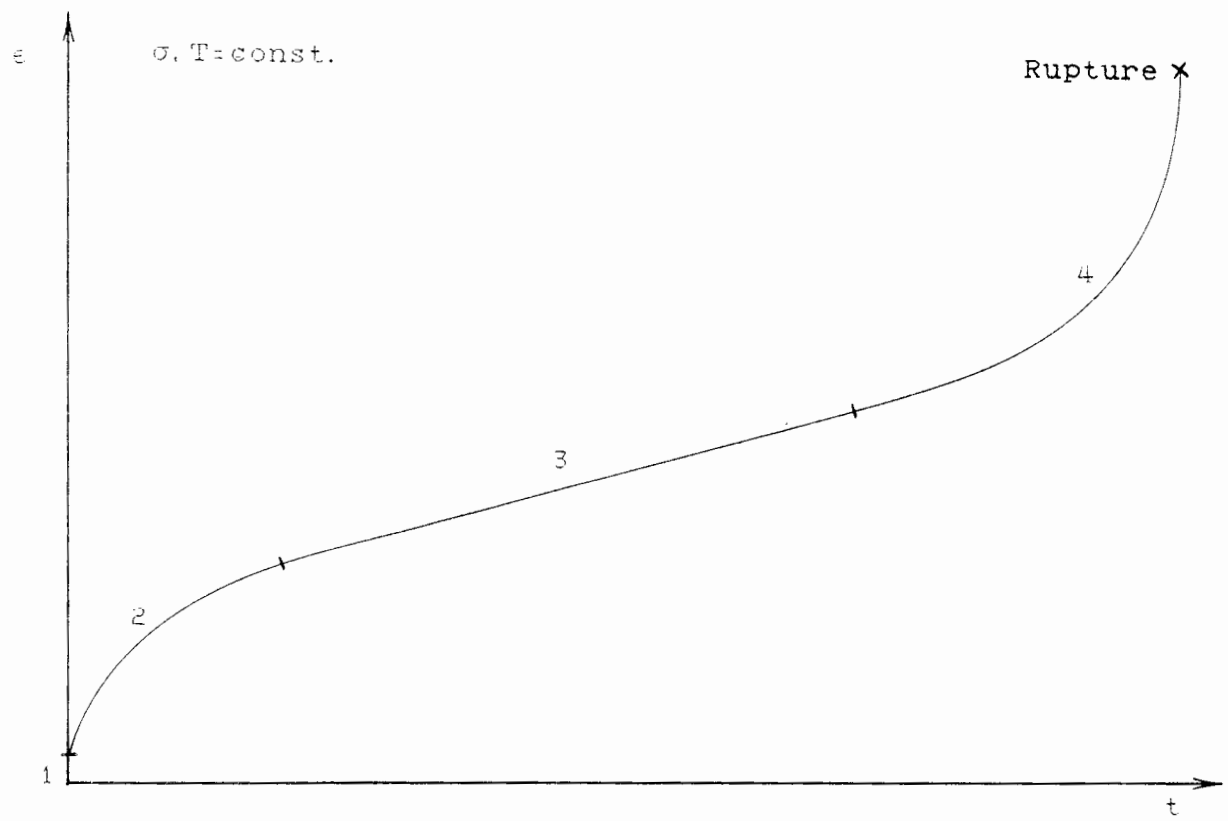

fig. (2.1) Creep response to a uniaxial load

It is claimed that different deformation mechanisims dominate during primary, secondary and tertiary creep phases.
Besides geometry and material properties, the deformation was found to be dependent on three major parameters: stress (σ), time (t) and temperature (T) [1], i.e.

$$\epsilon_{cr} = f(\sigma, t, T)$$

The proposal that the variables can be separated is mathematically convenient and widely accepted, but is however not conclusively proven. So:

$$\epsilon_{cr} = f_1(\sigma)\ f_2(t)\ f_3(T)$$

Early investigators proposed many function types for f_1, f_2 and f_3 based on empirical considerations on rate processes. By curve-fitting procedures they described the creep phenomenon with some success. However a unifying empirical rationale remains elusive.

Norton (from [1]) proposed a power relationship for f_1 which yields good results for lower stresses:

$$f_1(\sigma) = A\ \sigma^m \qquad \ldots \quad (2.1)$$

Dorn [2] proposed an exponential relationship for f_1 which gives better results at higher stresses:

$$f_1(\sigma) = C\ \exp(\sigma/\sigma_o)$$

And Mc. Vetti [3] attempted to unify the above approaches by stating:

$$f_1(\sigma) = \sinh^m(\sigma/\sigma_o)$$

noting that a sinh function approaches a power function for lower stress values, and an exponential function at high stress values.

The Norton relationship is however most widely used.

Functions f_2 for the time dependence are variations of a power relation, for example:

$$f_2(t) = \alpha\ t^n \qquad 1/3 < n < 1/2 \qquad \ldots \quad (2.2)$$

attributed to Bailey [1]. Graham and Walles proposed:

$$f_2(t) = \sum_i \alpha_i t^{n_i}$$

and the specific form:

$$f_2(t) = \alpha t^{0.33} + \beta t + \gamma t^3$$

is frequently used [4] as it gives good results for many materials.

Temperature affects creep response in several ways. Firstly, the material properties are functions of temperature. So for f_1 and f_2 above:

$$A = A(T)\ ,\quad m = m(T)\ ,\quad \alpha = \alpha(T)\ ,\quad n = n(T) \qquad \text{etc.}$$

Secondly, different deformation and damage mechanisims dominate the creep response at increasing operating temperature. At lower temperatures dislocation mobility and consequent slip

within crystals predominate. At higher temperatures increased dislocation mobility and diffusion cause intercrystalline slip and void formation to dominate.

The general consensus appears to be that the effect of temperature should be described by the form:

$$f_3(T) = f_3\left[\exp\left[\frac{-Q}{RT}\right]\right]$$

where Q = activation energy and R = Bolzmann constant. Power functions for f_3 are generally used. There is significant evidence, however, to suggest that functions for the time and temperature variables must not be separated, but should be treated as some time-temperature parameter. Dorn proposed a power function [2]:

$$f_{2,3} = \alpha\left[t\,\exp\left[\frac{-Q}{RT}\right]\right]^n$$

Time-temperature relationships have been used successfully to extrapolate rupture data using the Larson-Miller or Manson-Halferd parameters for instance [5]. The relative success in using such parameters is evidence that time and temperature must be seen in conjunction.
A more complete list of possible functions can be found in [6].

2.2 Creep under variable stresses

A multitude of theories have been proposed, many of which are significant and useful, however no one single theory is acceptable for all conditions. As before only the more widely used theories will be described [1].

2.2.1 Time hardening

is based on the assumption that the major factor affecting the creep rate is the length of exposure to a temperature and stress level, irrespective of the strain history [5]. It asserts therefore that only material changes are significant. If f_1 and f_2 are chosen as eq. (2.1) and (2.2) respectively, and for constant temperature:

$$\dot{\epsilon}_{cr} = nA\,\sigma^m\,t^{n-1} \qquad \ldots \quad (2.3)$$

A graphic procedure is summarised in fig. (2.2) from [5].

2.2.2 Strain hardening

is based on the assumption the the major factor affecting the creep rate is the state of strain, irrespective of its exposure time [5]. So it is claimed that an equation of state governs the creep response. If eq. (2.1) and (2.2) are chosen as before, and given constant temperature:

$$\dot{\epsilon}_{cr} = \frac{nA^{1/n}\,\sigma^{m/n}}{\epsilon_{cr}^{(1-n)/n}} \qquad \ldots \quad (2.4)$$

Strain hardening is illustrated graphically in fig. (2.3) from [5].

2.2.3 Life fraction rule (Robinson)

This refinement attempts to compromise between time hardening and strain hardening. Instead of moving vertically (fig. 2.2) or horisontally (fig. 2.3) to determine the starting point on the new curve, an intermediate starting point is chosen so that the ratios of exposure time to rupture-life on the curve and a subsequent curve are equal, i.e.:

$$\frac{t_i}{t_{Ri}} = \frac{t_f}{t_{Rf}} \qquad t_f = \frac{t_{Ri}}{t_{Rf}}\,t_i$$

t_f thus determines the starting point on a curve for the following stress level. The procedure is illustrated in fig. (2.4) from [5].

A close relationship can be shown to exist [1] between Kachanov damage accumulation and Robinsons Life Fraction rule.

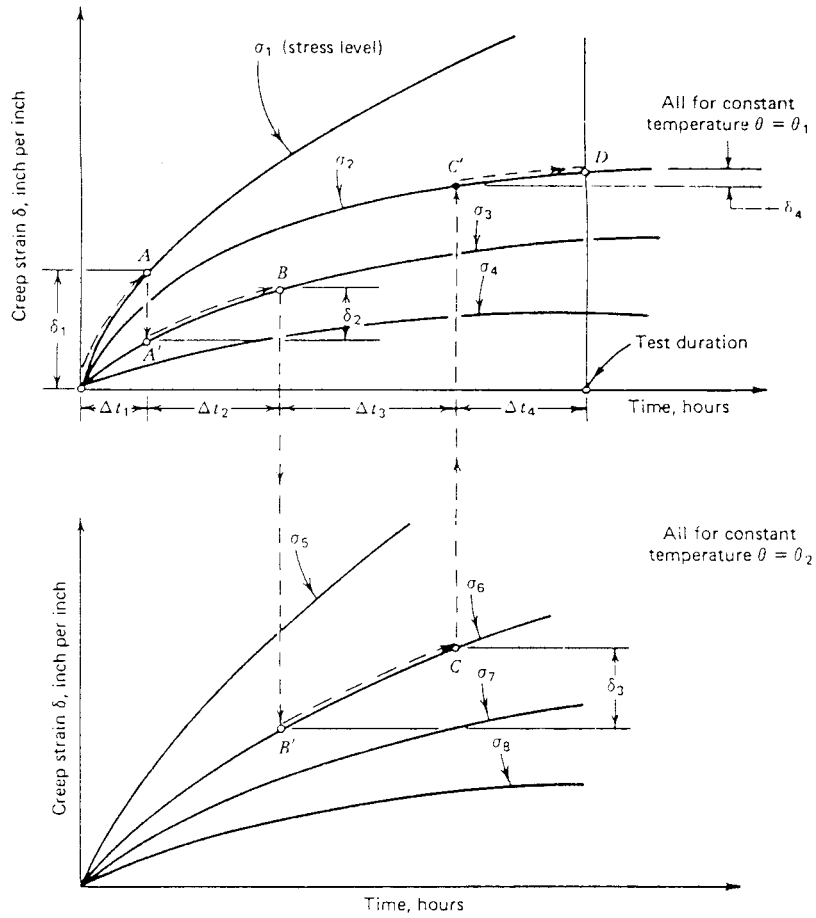

fig. (2.2) Creep strain accumulation under time-hardening assumptions

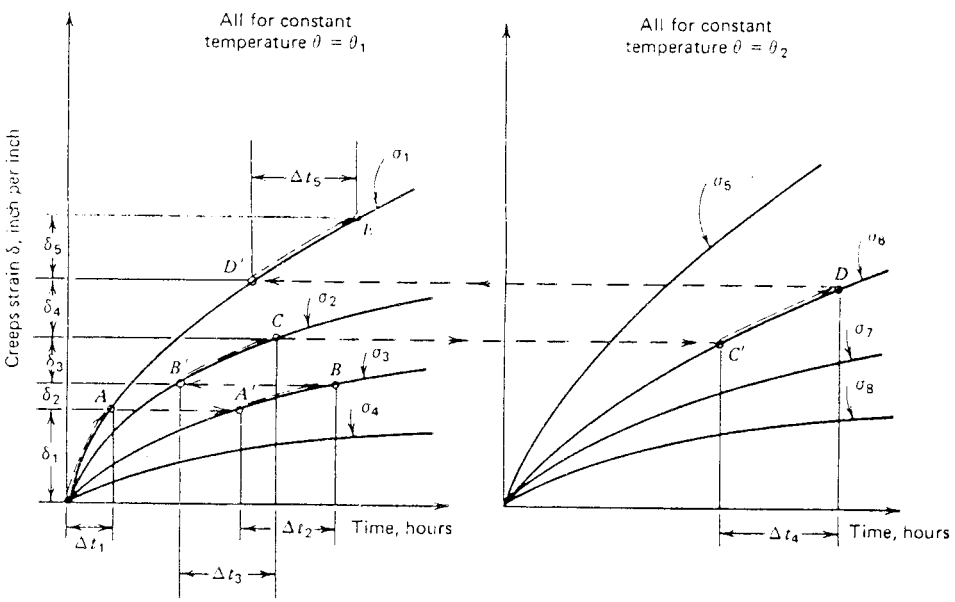

fig. (2.3) Creep strain accumulation under strain-hardening assumptions

2.2.4 Total strain theory

proposes that a one to one relationship between strain and time exists, even for variable stress. There is an immediate and complete response to stress changes. The theory is included, despite its inaccuracy, for its simple application and demonstrated in fig. (2.5) from [1].

The above theories can be compared by examining how each predicts primary creep response to a step load, as shown in fig(2.6):

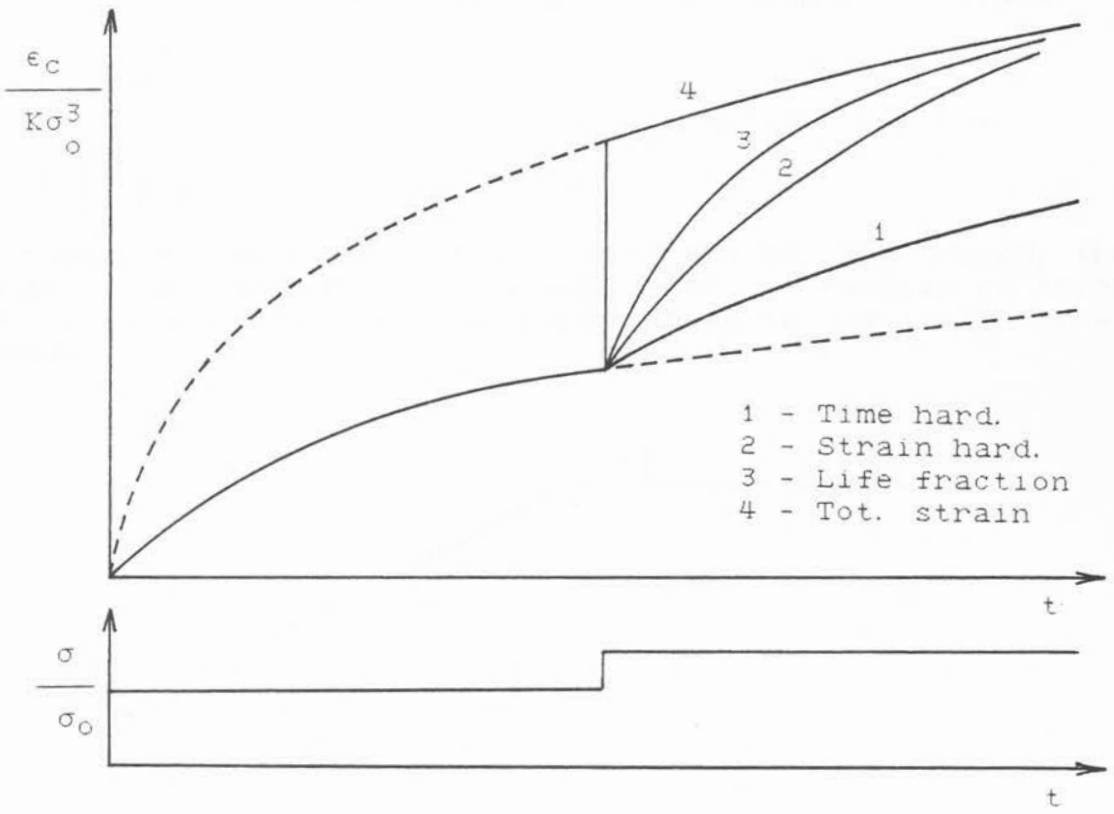

fig. (2.6) Response to a step load change

The predictions vary widely. With the exeption of the time hardening theory, all theories approach the total strain solution with time. The strain hardening theory correlates best with experimental data, and so would be the best theory to use. Time hardening and total strain theories, despite their inaccuracies, could serve to set upper and lower limits to creep curves. The real behaviour would lie between the time hardening and total strain extremes, and strain hardening would give a fair indication of the response.

2.2.5 Viscoelastic models

Attempts have been made to describe creep in terms of linear or nonlinear visco-elasticity, i.e. as an analogy to the behaviour of linear elasticity and viscosity of Newtonian fluids [7]. The approach is particularly useful when analysing variable loads [8].

Maxwell's model considers equilibrium of a spring and dashpot in series:

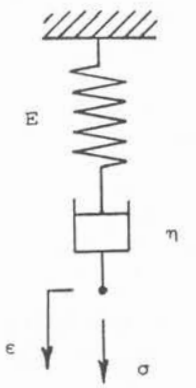

$$\sigma = E\epsilon + \eta\dot{\epsilon} \quad \text{ie.} \quad \sigma + p_1\dot{\sigma} = q_1\dot{\epsilon} \qquad p_1 = \eta/E\ ,\ q_1 = \eta$$

and using Laplace transforms the response to any loading function can be obtained:

$$\epsilon(t) = \int_0^t \sigma(\tau)\left[1/\eta + 1/E\ \dot{\delta}(t-\tau)\right]\partial\tau$$

Although primary and tertiary creep are not reproduced, the model does qualitatively reproduce the interaction of secondary creep with elastic deformation as shown in fig. (2.7) for a step load.

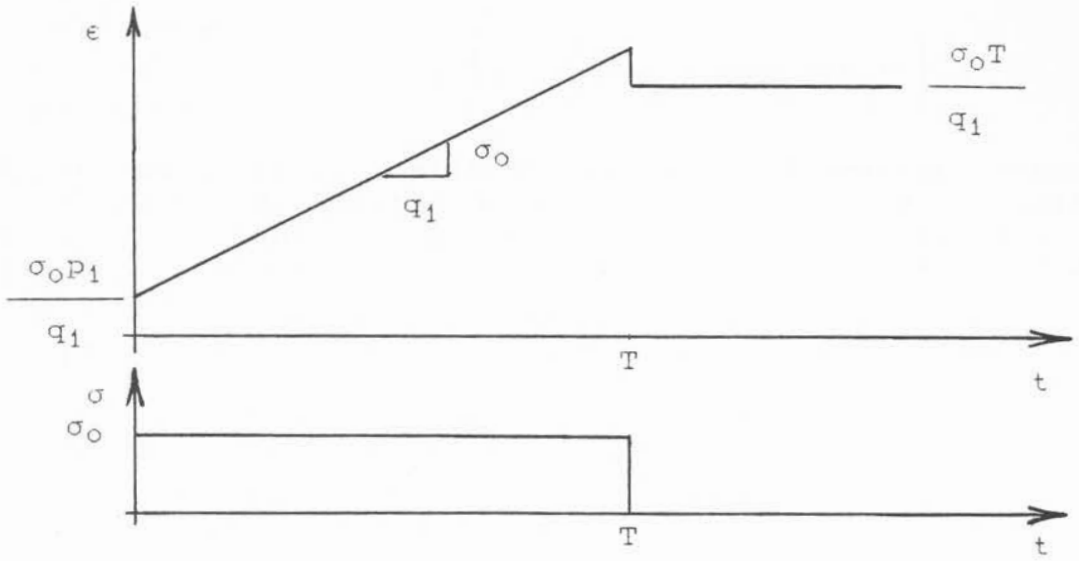

fig. (2.7) Response to step load changes

A Kelvin solid considers a spring and dashpot in parallel, and by a similar analysis obtains the response to any loading function to be:

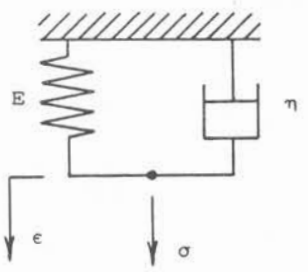

$$\epsilon(t) = 1/\eta\int_0^t \sigma(\tau)\ \exp\left[E/\eta(\tau-t)\right]\ \partial\tau$$

Only primary creep and recovery is reproduced as illustrated in fig. (2.8) for a step load:

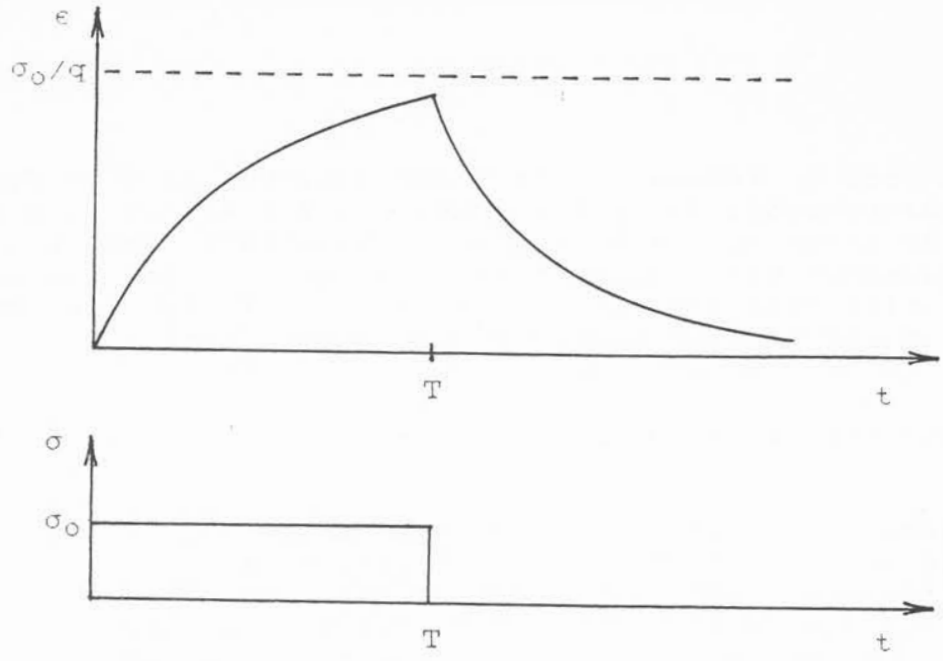

fig. (2.8) Response to step load changes

A Standard viscous solid is modelled by superimposing a Maxwell fluid and a Kelvin solid, and the response to any load function is:

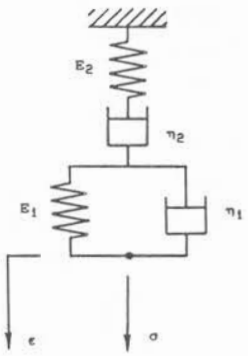

$$\epsilon(t) = 1/\eta_1 \int_0^t \sigma(\tau)\ \exp\left[(\tau-t)/m\right]\ \partial\tau + \int_0^t \sigma(\tau)\left[1/\eta_2 + 1/E_2\,\delta(t-\tau)\right]\ \partial\tau$$

With the exeption of tertiary creep all deformation phenomena can be described. Elastic deformation for loading and unloading are correctly modelled, and primary creep (modelled as a transient) asymptotically approaches secondary creep. This is illustrated in fig. (2.9):

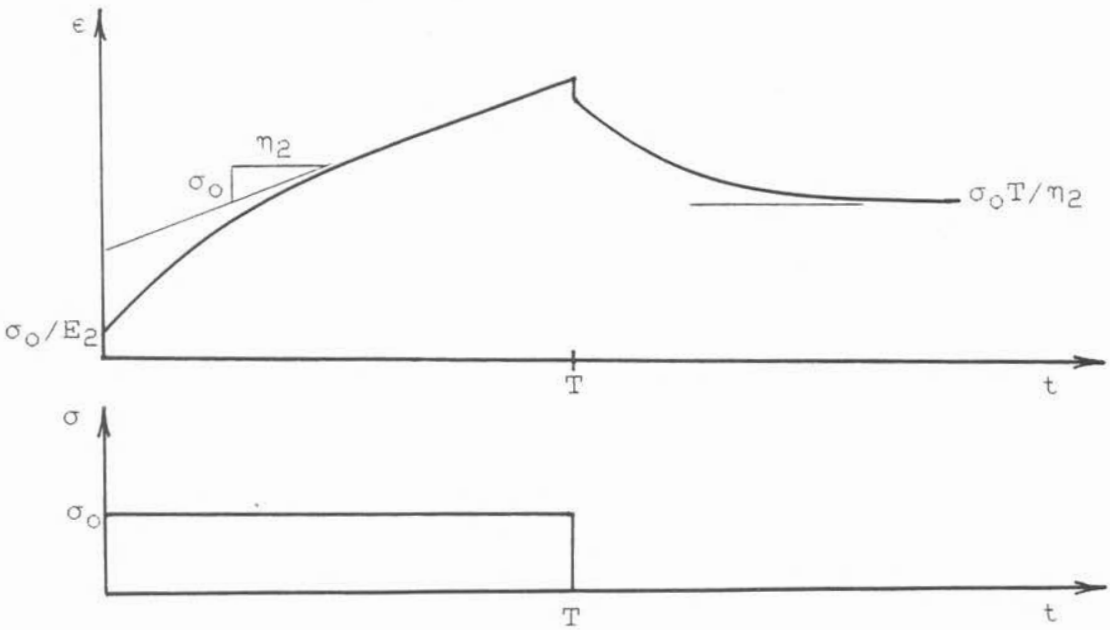

fig. (2.9) Response to step load changes

Although such an approach has been successful in describing the response of non-metals, it was found to be inappropriate when analysing creep behaviour of metals. Metallic creep is not only a viscous process, but rather diffusion and void formation are the dominant phenomena. However, purely qualitatively, primary and secondary creep are described using this approach.

Extensions to the above visco-elastic theories have been attempted:

1) By including more spring and dashpot elements in various arrangements, higher derivatives of stress and strain are introduced to the differential equation of equilibrium and solved. So for example, Besseling used several Maxwell-elements in parallel with some success.

2) By introducing non-linearities, i.e. terms p_i and q_i as variables of stress and temperature, very good theories were developed by Graham and Walles as well as Rabotnov (reviewed in [1]). These yield better correlation with experiment.

3) Gittus [9] has attempted to relate viscous terms in the differential equation of equilibrium to crystal dislocation processes and void formation.

2.3 Multiaxial creep

The largest proportion of creep tests are uniaxial tension tests. However realistic service applications involve multiaxial stresses. The uniaxial constitutive equations can readily be extended into the multiaxial domain.

Investigators have seen remarkable similarities between the creep process and plasticity. Both could be described as path dependent viscous flow. The similarity in stress distributions, once a steady-state is attained, supports the connection. The resulting model should comply with several requirements [1, 25]:

1) The multiaxial flow rule should reduce to the familiar uniaxial formulations when applied to a uniaxial tension test.

2) The model should reflect the observations that the material volume is (nearly) constant, and that the hydrostatic stress does not materially influence the creep process.

3) For isotropic materials, the principal stress and strain rate directions should coincide.

From 2), the creep strain rate is proportional to the stress deviator s_{ij}:

$$\frac{\partial \epsilon_{crij}}{\partial t} = \lambda \, s_{ij} \qquad \ldots \quad (2.5)$$

λ being a proportionality constant. This flow rule is an extension of the incremental Prandtl-Reuss plasticity flow rule to the creep regime.

Let the effective (v. Mises) stress and effective creep strain rate be:

$$\sigma_e = \frac{1}{\sqrt{2}}\left[(\sigma_{11}-\sigma_{22})^2+(\sigma_{22}-\sigma_{33})^2+(\sigma_{33}-\sigma_{11})^2+6\sigma_{12}^2+6\sigma_{23}^2+6\sigma_{31}^2\right]^{1/2} \qquad \ldots \quad (2.6a)$$

$$\frac{\partial \epsilon_{cre}}{\partial t} = \frac{\sqrt{2}}{3}\left[\left[\frac{\partial \epsilon_{11}}{\partial t}-\frac{\partial \epsilon_{22}}{\partial t}\right]^2+\left[\frac{\partial \epsilon_{22}}{\partial t}-\frac{\partial \epsilon_{33}}{\partial t}\right]^2+\left[\frac{\partial \epsilon_{33}}{\partial t}-\frac{\partial \epsilon_{11}}{\partial t}\right]^2+ 6\left[\frac{\partial \epsilon_{12}}{\partial t}\right]^2+6\left[\frac{\partial \epsilon_{23}}{\partial t}\right]^2+6\left[\frac{\partial \epsilon_{31}}{\partial t}\right]^2\right]_{cr}^{1/2} \qquad \ldots \quad (2.6b)$$

then:

$$\frac{\partial \epsilon_{crij}}{\partial t} = \frac{3}{2}\,\frac{\partial \epsilon_{cre}}{\partial t}\,\frac{s_{ij}}{\sigma_e} \qquad \ldots \quad (2.7)$$

The proportionality constant λ can be experimentally obtained from a uniaxial tension test, where the effective stress and strain reduce to the axial stress and strain respectively. Alternatively, a constitutive model and hardening hypothesis from chapter 2.2 can be used. So in general:

$$\epsilon_{cre} = f_1(\sigma_e)\ f_2(t)\ f_3(T)$$

Using the Norton and Bailey relationships under isothermal conditions (ie f_3=const.):

$$\epsilon_{cre} = a\sigma_e^{m}\ t^{n}$$

yields [25]:

$$\frac{\partial \epsilon_{crij}}{\partial t} = \frac{3}{2}\, an\sigma_e^{m-1}\, s_{ij}\, t^{n-1} \qquad \ldots \quad (2.8a)$$

for time-hardening, and

$$\frac{\partial ecrij}{\partial t} = \frac{3}{2}\, na^{1/n}\, \sigma_e^{(m/n-1)} s_{ij}\, \epsilon_{cre}^{(1-1/n)} \qquad \ldots \quad (2.8b)$$

for strain-hardening assumptions. The effect of damage can be incorporated by noting that:

$$\sigma_e = \frac{\sigma_{eN}}{1-\omega} \qquad \text{and} \qquad s_{ij} = \frac{s_{ijN}}{1-\omega}$$

The subscript N refers to stresses in the undamaged state.

In order to cast the time-hardening constitutive equations into a more useful (integrable) form, Penny [1] utilised the time transformation:

$$\tau = \int_0^t aE\, \sigma_o^{m-1}\, f_2(t)\, dt \quad = at^n$$

together with the normalisation of stress and strain quantities with respect to their corresponding reference stress and strain. If the non-dimensional quantities:

$$\Sigma_{ij}=\frac{\sigma_{ij}}{\sigma_o} \quad \Sigma_{ijN}=\frac{\sigma_{ijN}}{\sigma_o} \quad \Sigma_e=\frac{\sigma_e}{\sigma_o} \quad \Sigma_{eN}=\frac{\sigma_{eN}}{\sigma_o} \quad D_{ij}=\frac{s_{ij}}{\sigma_o} \quad D_{ijN}=\frac{s_{ijN}}{\sigma_o}$$

$$\lambda_{ij}=\frac{\epsilon_{ij}}{\epsilon_o} \quad \lambda_e=\frac{\epsilon_e}{\epsilon_o} \quad \lambda_{crij}=\frac{\epsilon_{crij}}{\epsilon_o}$$

are used, then the time transformation yields:

$$\dot{\lambda}_{crij} = \frac{3}{2}\, \frac{\dot{\lambda}_{cre}}{\Sigma_e}\, D_{ij} \qquad \text{with} \quad \dot{(\ )} = \frac{\partial (\ )}{\partial \tau}$$

and:

$$\dot{\lambda}_{cre} = \Sigma_e^m$$

Incorporating damage effects, the final creep constitutive equation is:

$$\dot{\lambda}_{crij} = \frac{3}{2} \frac{\Sigma_{eN}^{m-1} D_{ijN}}{(1-\omega)^m} \quad \ldots (2.9)$$

If the refined damage model is used, whereby damage and damage accumulation is supressed in compression, equation (2.9) becomes:

$$\dot{\lambda}_{crij} = 3/2 \; \Sigma_{Ne}^{m-1} \; S_{Nij} \qquad \Sigma_1 < 0 \quad \ldots (2.9a)$$

whenever the maximum principal stress is compressive.

2.4 Damage and creep rupture

Creep rupture is the culmination of the tertiary stage of creep, where the creep rate increases from a constant value (at the onset of tertiary creep) to infinity at rupture. Depending on stress and temperature, different microstructural processes dominate deformation behaviour, resulting in either a ductile or brittle fracture [1].

For temperatures above 0.4-0.6 of the melting temperature, failure is predominantly brittle. At such high temperatures diffusion becomes significant. Diffusion, coupled with increased dislocation mobility, results in the grain-boundaries becoming weaker than the grains themselves. Thus deformation occurs by slip along grain-boundaries. Also, prior to tertiary creep, there is little deformation. To maintain material continuity, the grains will deform. However, given suitable grain geometries and grain boundary slippage [1], the weaker grain boundaries separate, creating voids.

Metallographic investigations reveal that as tertiary creep begins, internal micro-voids do occur at grain boundaries. The voids are distributed throughout the material, but especially in high stress regions. It was shown that voids preferentially grow on a plane normal to the direction of maximum principal stress. Voids grow and coalesce to eventually form a macroscopic crack which at rupture has grown to a critical size [13].

For lower temperatures and higher stresses, different mechanisims predominate, causing ductile behaviour [14]. Due to lower temperatures, diffusion is markedly reduced. Slip occurs largely within the grains due to dislocation movement, but is restricted by the stable grain boundaries. Slip occurs preferentially along planes parallel to the maximum shear stress, so large strains and necking are observed. Excessive slip along a slip plane will cause cracks to be initiated at the surface [1]. Unlike brittle behaviour, cracks are not evenly distributed. There are only a few, ultimately only one dominant crack which grows along a slip plane.

The majority of creep tests are conducted under isothermal conditions to establish a relationship between rupture time and a constant uniaxial stress, shown in fig. (2.10).

The high stress, short time portion of the curve can be correlated to predominantly ductile behaviour. The low stress, long time part of the curve describes predominantly brittle behaviour. Both ductile and brittle rupture can be approximated by straight lines. A significant transition region shows that brittle and ductile mechanisims interact. So only when low stresses prevail, resulting in very long lifetimes, can ductile behaviour be safely neglected, and only when the stresses are very high can brittle void formation be safely ignored. As finite life at zero load is unreasonable, one would expect the rupture curve to asymptotically approach $t=\infty$ for extremely low stresses.

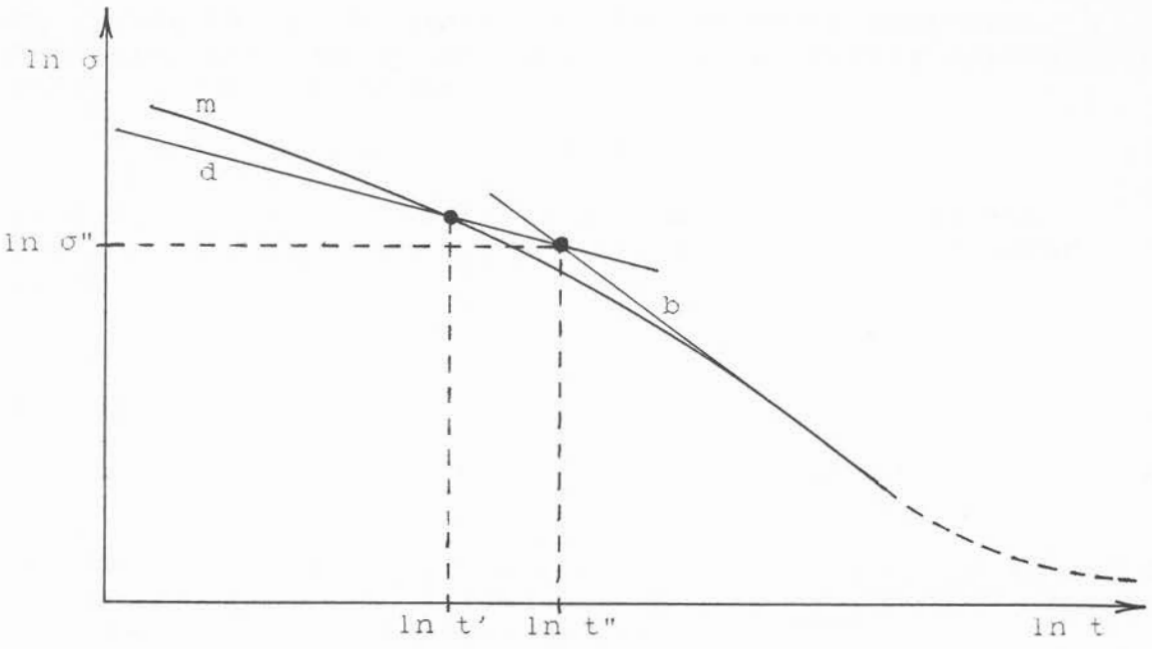

fig. (2.10) Time to rupture in uniaxial tension

The above description is a gross simplification of real behaviour, as oxidation, corrosion effects, phase transformations of crystal structure and recrystallisation contribute, and under certain circumstances even dominate, final response.

Until the complex creep process is more fully understood and described, a designer can only resort to phenomenological theories. One such theory, which appears especially promising, was proposed by Kachanov.

2.4.1 Kachanov brittle damage theory

Kachanov [14, 15] proposed that the observed growth and coalescence of microcracks can be described in terms of damage accumulation, irrespective of the mechanisim whereby they grow. So damage is defined as the progressive reduction of the cross section area of the material that bears load [25]. If $A(0)=A_N$ is the area of the undamaged component, then:

$$A(t) = A(0)\left[1-\omega(t)\right] \quad \text{i.e.} \quad A = A_N(1-\omega) \qquad 0 \leq \omega \leq 1$$

$\omega=0$ corresponds to virgin material containing no microcracks, and $\omega=1$ indicates complete seperation, i.e. rupture. Specifically, $\omega=1$ indicates the presence of a macroscopic crack of critical dimensions, whereupon rupture follows immediately. The requirement $\omega=1$ is thus the Kachanov criterion for rupture. Under constant loads, the stress will increase due to a reduction in area, so:

$$\sigma = \frac{\sigma_N}{(1-\omega)}$$

$\sigma_N = F/A_N$ being the stress in the undamaged component. Realising that damage accumulation is primarily dependent on stress, time, and temperature,

$$\omega = F_1(\sigma)\ f_2(t)\ F_3(T)$$

Kachanov proposed a power relationship for the stress dependence, similar to Norton's law for creep. So under isothermal conditions (F_3=const.):

$$\omega = b\ \sigma^k\ t^n$$

so that

$$\frac{\partial \omega}{\partial t} = b\ \sigma^k\ n t^{n-1} \approx b\left[\frac{\sigma_N}{1-\omega}\right]^k \quad . \ . \ . \quad (2.10)$$

The exponent n does in practice not differ greatly from 1.0, so the explicit time dependence is often neglected. Rabotnov [14] generalised the above to obtain:

$$\frac{\partial \omega}{\partial t} = b\ \frac{\sigma_N{}^k}{(1-\omega)^r} \quad \text{and} \quad \frac{\partial \epsilon_{cr}}{\partial t} = a\ \frac{\sigma_N{}^m}{(1-\omega)^q}$$

However, the simplifying assumptions whereby m=q and k=r are acceptable considering scatter in experimental data. It was also found that for a wide range of materials, $k \approx 0.75\ m$ [15].

If we consider the stresses to have attained a steady-state, (σ=const.) the Kachanov and Norton equations above can in turn be integrated w.r.t. time:

$$\int_0^1 (1-\omega)^k\ d\omega = b\sigma_N{}^k n \int_0^{t_R} t^{n-1}\ dt$$

if ω=1 the time to brittle rupture is:

$$t_R{}^n = \frac{1}{b(k+1)\sigma_N{}^k} \quad . \ . \ . \quad (2.11)$$

so

$$(1-\omega)^{k+1} = 1 - \frac{t}{t_R}$$

These results correlate well with experiment. Eq. (2.11) is plotted in fig. (2.10) as line b, and ductile fracture shown as line d. Substituting back into the Norton equation for creep strain and integrating we get:

$$\epsilon_{cr} = a\sigma_N{}^m t_R{}^L \left[1-\left[1 - \frac{t}{t_R}\right]^{1/L}\right] \quad \text{with} \quad L=\frac{k+1}{k+1-m} \quad . \ . \ . \quad (2.12)$$

Upon rupture, when $t=t_R$ and $\epsilon_{cr}=\epsilon_R$:

$$\epsilon_{crR} = a\sigma_N{}^m t_R{}^L = L/(k+1)\ a/b\ \sigma_N{}^{m-k}$$

The new material property L is the creep ductility. It measures the ability of the material to accommodate damage by redistributing stresses more evenly throughout the component [28].

The constants a and m can be obtained from short time creep tests. For many materials m=3 yields good results. If k≈3/4 m, the constants b and k can be obtained from rupture data and eq. (2.11) [15]. However eq. (2.11) is very sensitive to error, and rupture data is known to scatter considerably. So subsequent creep predictions will vary greatly for even small differences in b. Having obtained values for the constants from the limited data that is usually availible, creep curves can be constructed. Rupture times so predicted could, due to the extreme sensitivity mentioned, be 20-50 % in error.

A strain criterion for rupture ("e" criterion [1]) involves the Monkman-Grant constant ϵ_*. The criterion states simply that the minimum creep rate multiplied by the rupture time is a constant, a material property [19]. Noting that $a\sigma_N^m$ is the minimum creep rate, i.e. the steady-state creep rate which neglects damage-accumulation,

$$\epsilon_* = a\sigma_N^m \, t_R$$

This criterion can also be applied to obtain a further estimate for a.

As mentioned, the above analysis presumes constant stress; that the stress redistribution is complete. However, damage also accumulates during primary creep, where stresses redistribute. Also, the damage accumulation itself causes stresses to redistribute to maintain overall component equilibrium. It is thus questionable if a steady-state as such exists, although there are phases during the creep process where stresses vary only slightly with time (=secondary creep). In section 2.5, the numerical integration of the constitutive equations subject to varying stresses will be presented.

Multiaxial damage evolution involves the observation that for some materials the rupture life (and thus the damage accumulation) is governed by the maximum principal stress σ_1, whereas for other materials the effective (v.Mises) stress σ_e is more appropriate. Hayhurst [29] suggested that the shape of the isochronous rupture surface is:

$$\alpha \frac{\sigma_1}{\sigma_o} + (1-\alpha)\frac{\sigma_e}{\sigma_o} = 1.0$$

where the rupture time t_o is the life of a uniaxial tension test at the reference stress σ_o. The parameter α is a material constant. Kachanov's power relationship can now be extended to the multiaxial case:

$$\omega = b\left[\alpha\sigma_1 + (1-\alpha)\sigma_e\right]^k t^n$$

Utilising the same t-τ time transformation and non-dimensional quantities as in section 2.3, the multiaxial damage evolution equation is:

$$\dot{\omega} = \frac{b\sigma_o^{k+1-m}}{aE} \frac{\left[\alpha\Sigma_{1N} + (1-\alpha)\Sigma_{eN}\right]^k}{(1-\omega)^p} \qquad \ldots (2.13)$$

A further refinement in the damage evolution equation can be incorporated [18], to model void closure. It is argued that whenever the maximum principal stress is compressive, voids close. So in compression the entire (undamaged) cross-section area A_N becomes available to transmit loads. Thus

$$\omega=0 \ , \ \dot{\omega}=0 \text{ and } \sigma_{ij}=\sigma_{Nij} \qquad \text{if } \sigma_{N1}<0$$

The observation [18] that for comparable load magnitudes, the creep rupture times in compression are orders of magnitude higher than in tension, substantiates the model refinement.

2.4.2 Viscous failure (Hoff)

Given high loads and moderate temperatures, ductile materials will behave in a viscous manner [16]. Microvoids are less prevalant. The stress is increased by the Poisson effect reducing the cross sectional area. At a point of weakness, localised necking will occur, resulting in rupture. As the total strains are high, elastic strains may be neglected, but true stress and strain expressions must be used [14]. Here, only the uniaxial case will be discussed.

Differentiating the true stress-strain relationship, and substituting:

$$\dot{\epsilon}_{cr} = a\sigma^m \qquad \text{yields:} \qquad a\sigma^{m+1} = \dot{\sigma}$$

which can be integrated to obtain an estimate of the time to rupture:

$$t_R = \frac{1}{am\sigma_o^m}\left[1 - \left[\frac{\sigma_o}{\sigma_R}\right]^m\right] \qquad \ldots (2.14)$$

where σ_R is the stress when a localised neck occurs, and subsequent deformation is unstable to fracture. Rosenblyum [14] considered an elastic - perfectly plastic response by setting $\sigma_R=\sigma_y$, the yield stress at that operating temperature. For very very ductile materials, (especially pure materials) necking is extenive, and σ_R=infinity. Then the Hoff rupture life is:

$$t_R = \frac{1}{am\sigma_o^m} \qquad \ldots (2.15)$$

These times to ductile rupture are plotted in fig. (2.10) as line d. Brittle fracture is also shown as line b in fig. (2.10), so delineating the regions for brittle and ductile failure.

The intersection of the two curves b and d is at:

$$t'' = \frac{1}{am}\left[\frac{am}{b(k+1)}\right]^{-m/(m-k)} \qquad \text{and} \qquad \sigma'' = \left[\frac{b(k+1)}{am}\right]^{1/(m-k)}$$

This gives a rough indication that if $t>t''$ or $\sigma<\sigma''$ brittle fracture is likely, and if $t<t''$ or $\sigma>\sigma''$ ductile fracture is indicated.

Under variable loads, the Hoff ductile rupture equations also reduce to the familiar Robinsons Life Fraction rule.

For a work-hardening material with α the strain hardening exponent the Life Fraction rule in continuous form is:

$$\int_0^{\infty}\left[\frac{\epsilon_{cr}}{\epsilon_o}\right]^{\alpha}\exp(-m\epsilon_{cr})\,d\epsilon_{cr} = \int_0^{t} a\sigma_o^{m}\,dt = 1/m'$$

then:

$$t_R = \frac{1}{am'\sigma_o^{m}}$$

Besides integrating, m' is best obtained by experiment. It was found, however, that m' is not significantly different from m. Robinsons Life Fraction rule also applies to a work hardening material.

2.4.3 Kachanov mixed failure

Kachanov's brittle failure theory can be extended [14] by using true stress and strain when deformations are large. It is an attempt to extend the damage concept ω to the region of viscous failure. This can be done by noting that ω is defined as the reduction of cross-section area, by whatever mechanisim (ductile or brittle) it occurs. Kachanov proposed damage accumulation and creep progress independently, as they describe entirely different processes:

$$\dot{\epsilon}_{cr} = a\sigma_o^{m}\exp m\epsilon_{cr} \qquad \sigma = \left[\frac{\sigma_o}{1-\omega}\right]\exp(\epsilon_{cr})$$

and integrating:

$$\exp(\epsilon_{cr}) = \left[1 - am\sigma_o^{m}t\right]^{-1/m}$$

Kachanov proposed that damage accumulates according to:

$$\frac{\partial\omega}{\partial t} = b\sigma^{k} = b\left[\frac{\sigma_o}{1-\omega}\right]^{k}\exp(k\epsilon_{cr})$$

substituting for strain:

$$\frac{\partial\omega}{\partial t} = b\left[\frac{\sigma_o}{1-\omega}\right]^{k}(1-am\sigma_o^{m}t)^{-k/m}$$

Integrating over the lifetime, the rupture life predicted by the mixed Kachanov hypothesis is:

$$t_R = \frac{1}{am\sigma_o^m}\left[1-\left[1-\sigma_o^{m-k}\frac{a(m-k)}{b(k+1)}\right]^{m/(m-k)}\right] \quad \ldots \quad (2.16)$$

which is shown by line m in fig. (2.10). The time t':

$$t' = \frac{1}{am}\left[\frac{b(k+1)}{a(m-k)}\right]^{-m/(m-k)}$$

in fig. (2.10) indicates whether mixed Kachanov or ductile theories apply.

2.4.4 Robinsons life fraction rule

A different view of damage was proposed by Robinson. The component deteriorates in proportion to the ratio of time spent at a particular load and temperature to the rupture time at that load and temperature [1], i.e. the deterioration accumulated during t_i at s_i and T_i, is:

$$d_i = t_i/t_{Ri}$$

The damage from each load case i is independent of any previous loading, but accumulates with damage from previous loads. For step loading, rupture is taken to occur when [5]:

$$d_f = \sum_i t_i/t_{Ri} = 1.0$$

Or for continuously varying loads, rupture occurs when:

$$\int \frac{dt}{t_R} = 1.0$$

In practice, rupture was found to occur at cumulative damage values significantly different from 1.0, ranging between 0.4 and 2.0 depending on the load sequence. It was shown [17] that the cumulative life fraction at failure is less than 1.0 when stresses increase with time, and greater than 1.0 for stresses decreasing with time.

Also the life fraction rule makes no distinction between damage accrued under stress and temperature. Creep-damage behaviour under changing stresses is, however, fundamentally different from creep damage behaviour under changing temperature.

Despite these misgivings, the life-fraction rule yields acceptable results, considering scatter in rupture data. It is simple to apply using readily availible data. In [17] lines of constant damage were correlated with the Larson-Miller parameter, indicating that the life fraction rule is also

consistent for temperature changes. Although it is inaccurate for load changes, it could still be applied successfully if tests could indicate what cumulative damage fraction other than 1.0 applies to the load sequence in question.

Although Kachanov defines damage differently, it can be shown [1] that the Kachanov approach under variable loads reduces to the life fraction rule, indicating that the theories are consistent with one another.

2.5 Integration of the constitutive model

Of the various creep and damage evolution theories discussed in sections 2.3 and 2.4, the creep equation (2.9) and damage equation (2.13) will be chosen for further development. The complete material constitutive model thus is:

$$\dot{\lambda}_{crij} = \frac{3}{2} \frac{\Sigma_{eN}^{m-1} D_{ijN}}{(1-\omega)^m} \qquad \ldots (2.9)$$

and

$$\dot{\omega} = \frac{b\sigma_o^{k+1-m}}{aE} \frac{\left[\alpha\Sigma_{1N} + (1-\alpha)\Sigma_{eN}\right]^k}{(1-\omega)^p} \qquad \ldots (2.13)$$

Because the stresses continually vary in time, the constitutive equations must be integrated numerically. The time increment $\Delta\tau$ is chosen sufficiently small so that constant stresses can be assumed during that time step. The damage evolution equation can be integrated analytically within the time step ${}_n\tau < \tau < {}_{n+1}\tau$ to obtain the damage at the end of the step n:

$${}_{n+1}\omega = 1 - \left[(1-{}_n\omega)^{p+1} - \Delta\tau/\tau_R\right]^{1/(p+1)} \qquad \ldots (2.17)$$

with:

$$\tau_R = \frac{1}{C(p+1)\left[\alpha\Sigma_{1N} + (1-\alpha)\Sigma_{eN}\right]^k} \qquad \ldots (2.18)$$

This τ_R does not provide an indication of the time to failure of the component, as the stresses are not constant. If the nominal stresses were to remain constant, as in the uniaxial case, then τ_R would indicate the component lifetime. Noting that:

$$[1-\omega(t)]^m = [(1-{}_n\omega)^{p+1} - (\tau-{}_n\tau)/\tau_R]^{m/(p+1)} \qquad {}_n\tau<\tau<{}_{n+1}\tau$$

the creep evolution equation can be analytically integrated over the time step, so that the creep strain increment during the timestep n is:

$$\Delta\lambda_{crij} = \frac{3\Sigma_{Ne}^{m-1} D_{Nij}}{2C(p+1-m)\left[\alpha\Sigma_{N1}+(1-\alpha)\Sigma_{Ne}\right]^k}\left[(1-{}_n\omega)^{p+1-m} - (1-{}_{n+1}\omega)^{p+1-m}\right]$$

The creep strain at the end of the time step is:

$${}_{n+1}\lambda_{crij} = {}_n\lambda_{crij} + \Delta\lambda_{crij} \qquad \ldots (2.19)$$

This forward-difference algorithim can now be used by noting that at $\tau=0$, $\omega=0$ $\lambda_{cr}=0$ and the stresses are obtained from the elastic solution. At each subsequent time step $n=1,2 \ldots n_R$, τ_R and thus ${}_{n+1}\omega$ and ${}_{n+1}\lambda_{cr}$ can be found. The equilibrium and continuity equations applied at the end of every time increment will yield the changes in the stress pattern. Whenever $\omega \approx 1$, rupture has occurred, and the damage and creep accumulation must cease.

If the refined damage model is used, damage is suppressed in compression. Then equations (2.17) and (2.18) are modified, whenever the maximum principal stress is compressive, to:

$$\omega = 0 \qquad \Sigma_1 < 0 \qquad \ldots \quad (2.17a)$$

$$\tau_R = \infty \qquad \Sigma_1 < 0 \qquad \ldots \quad (2.18a)$$

The integration of equation (2.9a) yields in compression:

$$^{n+1}\lambda_{crij} = {}^{n}\lambda_{crij} + 3/2\Sigma_{Ne}^{m-1}S_{Nij}\,\Delta\tau \qquad \Sigma_1 < 0 \quad \ldots \quad (2.19a)$$

A simple forward-difference algorithim is acceptable as the time step is chosen such that the stress can be considered constant over the interval. Also, equation (2.19) was derived using a forward-difference algorithim of comparable accuracy.

3.0 Creep predictions for bending beams

3.1 Primary creep and stress redistribution in a beam subject to bending and axial loads

Upon loading virgin material, an initially very high strain rate is observed, which progressively decreases to a constant creep strain rate referred to as the steady state. Secondary creep is then seen as a continuation of this steady state [1].
The primary creep phenomenon can be explained to be a result of an interaction between creep and elastic strains caused by a redistribution of stress.

When a component is loaded, the stress distribution is initially elastic. However, since the creep strain rate is a nonlinear function of stress, the stresses must redistribute so as to maintain equilibrium and continuity at all times. At the steady state the redistribution is complete (to a sufficiently high degree) and the stresses remain constant thereafter.
The analysis for a beam in bending and axial load follows to illustrate the method used to predict primary creep. In principle the same method is used to predict primary creep in any geometry.

For every case the analysis method comprises the following procedure [1]:

1) Solve the elastic problem subject to its boundary conditions for stresses and strains, i.e. solve the relevant governing differential equations at t=0.

2) Choose a constitutive relationship to describe creep behaviour. Usually a power function of stress is sufficient.

3) Noting that subsequent (t>0) strain comprises the sum of elastic and creep strains, obtain the rate form of the governing differential equations. This will include additional terms incorporating creep strain.

4) Solve the rate equations subject to the boundary conditions, bearing in mind that the complete solution at each time step comprises a particular integral (obtained in 1 above) and a complementary function. Expressions for strain rate, stress rate and creep rate (as appropriate) are obtained. These are integrated numerically (forward difference is amenable and sufficient) to obtain all quantities at the following time step. Equilibrium must be enforced to obtain the complete solution at that time step.

5) Step 4) is repeated from time step to time step using the most current infomation until a steady-state is reached. Criteria for the attainment of the steady-state would be either a sufficiently constant strain rate or a sufficiently small stress rate.

In practice this method becomes very complicated for more realistic geometries, and a finite element method would be more appropriate. However in principle the method is still applicable [1].

The analysis neglects strains other than elastic and creep strains, as well as damage accumulation, but does include the possibility of step loads.

3.1.1 Time hardening

Consider a beam-element in tension and bending [11]:

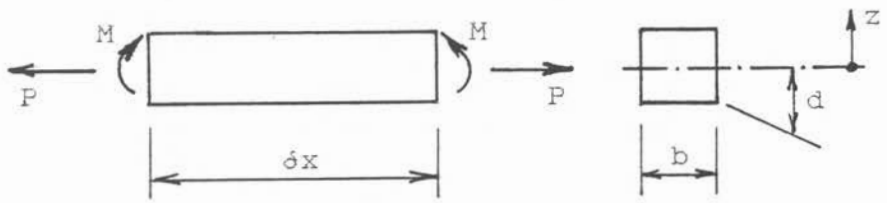

The strain comprises the sum of the elastic and creep strains, or alternatively, the sum of the strains due to bending and tension. Continuity requires [1]:

$$\epsilon_x = \frac{\sigma_x}{E} + \epsilon_{cr} = \kappa z + \epsilon_x(0) \qquad \ldots \quad (3.1)$$

Solving for stress:

$$\sigma_x = E\left[\epsilon_x(0) + \kappa z - \epsilon_{cr}\right] \qquad \ldots \quad (3.2)$$

Force and moment equilibrium require:

$$P = \int_A \sigma_x \, dA \qquad \text{and} \qquad M = \int_A \sigma_x \, z \, dA$$

which after partial integration yield:

$$P = EA\epsilon_x(0) - E\int_A \epsilon_{cr} \, dA$$

$$M = EI\kappa - E\int_A \epsilon_{cr} \, z \, dA \qquad \ldots \quad (3.3)$$

If creep strain is zero, the above reduces to the familiar elastic case.

Non-dimensionalising, using:

$$\Sigma = \sigma/\sigma_o \qquad \lambda = \epsilon/\epsilon_o \qquad \xi = z/d$$

$$\alpha = d^2/A \qquad \beta = d^4/I$$

where σ_o is the reference stress, equations (3.1), (3.2) and (3.3) become:

$$\lambda_x = \Sigma_x + \lambda_{cr} = \lambda_o + \frac{\kappa d}{\epsilon_o}\xi \qquad \ldots \quad (3.1a)$$

$$\Sigma_x = \lambda_{xo} + \frac{\kappa d}{\epsilon_o}\xi - \lambda_{cr} \qquad \ldots \quad (3.2a)$$

$$\frac{P}{\sigma_o} = \frac{d^2\,\lambda_{xo}}{\alpha} - \int_{-1}^{+1} \lambda_{cr}\, d^2\eta\, d\xi$$

$$\frac{M}{\sigma_o} = \frac{d^4\,\kappa}{\beta\,\epsilon_o} - \int_{-1}^{+1} \lambda_{cr}\, d^3\eta\xi\, d\xi \qquad \ldots \quad (3.3a)$$

A non-dimensional time-parameter is used, and is defined as:

$$\tau = \int E\sigma_o^{m-1}\, f_2(t)\, dt$$

and all the following time derivatives ($\dot{}$) are with respect to this τ. This is convenient as the analysis is now independent of f_2, and f_2 only affects the transformation from the τ domain to real time.

Using f_1 from section 2.1 the time hardening creep law is:

$$\dot{\lambda}_{cr} = \Sigma_x^m \qquad \ldots \quad (3.4)$$

At τ=0: the elastic solution is found by noting that τ=0.

$$\lambda_x = \Sigma_x \qquad \ldots \quad (3.1b)$$

$$S_x = \frac{P}{A\sigma_o} + \frac{Md}{I\sigma_o}\xi \qquad \ldots \quad (3.2b)$$

$$\lambda_{xo} = \frac{P}{A\sigma_o}$$

$$\frac{\kappa}{\epsilon_o} = \frac{M}{I\sigma_o} \qquad \ldots \quad (3.3b)$$

At τ>0: the rate equations are obtained by differentiating equations (3.1a), (3.2a) and (3.3a) with respect to τ, and substituting from (3.4):

$$\dot{\lambda}_x = \dot{\Sigma}_x + \dot{\Sigma}_x^m \qquad \ldots \quad (3.1c)$$

$$\dot{\Sigma}_x = \frac{\dot{P}}{A\sigma_o} + \frac{\dot{M}d}{I\sigma_o}\xi + \alpha\int_{-1}^{+1}\Sigma_x^{m_\eta}\,\partial\xi + \beta\xi\int_{-1}^{+1}\Sigma_x^{m_{\eta\xi}}\,\partial\xi - \Sigma_x^m \qquad \ldots \quad (3.2c)$$

taking $\dot{P}$ and $\dot{M}$ =0:

$$\dot{\lambda}_{xo} = \alpha\int_{-1}^{+1}\Sigma_x^{m_\eta}\,d\xi \qquad \ldots \quad (3.3c)$$

$$\frac{\dot{\kappa}}{\epsilon_o} = \frac{\beta}{d}\int_{-1}^{+1}\Sigma_x^{m_{\eta\xi}}\,d\xi$$

Two approaches can be used in the algorithim:

First Approach:
Numerically integrate [1] $\dot{\Sigma}_x$, $\dot{\lambda}_{xo}$, $(\dot{\kappa}/\epsilon_o)$ thus:

$$\Sigma_x^{j+1} = \Sigma_x^j + \dot{\Sigma}_x^j\,\Delta t \qquad \text{and} \qquad \lambda_{xo}^{j+1} = \lambda_{xo}^j + \dot{\lambda}_{xo}^j\,\Delta t$$

$$\text{and} \qquad (\kappa/\epsilon_o)^{j+1} = (\kappa/\epsilon_o)_j + (\dot{\kappa}/\epsilon_o)^j\,\Delta\tau$$

$$\text{so:} \qquad \lambda_{cr}^{j+1} = \Sigma_x^{j+1} - \lambda_{xo}^{j+1} - (\kappa/\epsilon_o)^{j+1}d\xi$$

$$\text{and:} \qquad \lambda_x^{j+1} = \lambda_{xo}^{j+1} + (\kappa/\epsilon_o)^{j+1}d\xi$$

and check errors made by using equation (3.3a) at regular intervals.

Second Approach:
Numerically integrate [12] $\dot{\lambda}_{cr}$ only.

$$\lambda_{cr}^{j+1} = \lambda_{cr}^j + \dot{\lambda}_{cr}^j\Delta\tau$$

and obtain λ_{xo} and (κ/ϵ_o) from eq. (3.3a), λ_x from eq. (3.1a), and Σ_x from (3.2a). A refinement is possible when instead of using Σ_x at the beginning of the interval, the average Σ on that interval is chosen:

$$\lambda_{cr}^{j+1} = \lambda_{cr}^j + \left[\Sigma_x^j + 1/2\dot{\Sigma}_x^j\Delta\tau\right]^m\Delta\tau$$

Check errors by comparing results from equation (3.2a) with:

$$\Sigma_x^{j+1} = \Sigma_x^j + \dot{\Sigma}_x^j\Delta t$$

3.1.2 Strain hardening

The analysis is exactly the same as for time hardening [12] up to the point where a creep law is used in equation (3.4). From there:

Using f_1 from section 2.1 the strain hardening law is:

$$\dot{\lambda}_{cr} = \frac{nA^{1/n}\sigma_o^{(m-1)/n}\Sigma_x^{m/n}}{\lambda_{cr}^{(1-n)/n}} \qquad \ldots \quad (3.5)$$

For $\tau=0$: the elastic solution is as before.

For $\tau>0$: the rate equations are:

$$\dot{\lambda}_x = \dot{\Sigma}_x + \dot{\lambda}_{cr} \qquad \ldots \quad (3.1d)$$

$$\dot{\Sigma}_x = \dot{\lambda}_{xo} + (\dot{\kappa}/\epsilon_o)d\xi - \dot{\lambda}_{cr} \qquad \ldots \quad (3.2d)$$

for $\dot{P}$ and $\dot{M} = 0$:

$$\dot{\lambda}_{xo} = \alpha\eta\int_{-1}^{+1}\dot{\lambda}_{cr}\,d\xi \quad , \quad (\dot{\kappa}/\epsilon_o) = \beta\eta/d\int_{-1}^{+1}\dot{\lambda}_{cr}\,\xi\,d\xi \qquad \ldots \quad (3.3d)$$

The two approaches that can now be followed are the same as for the time hardening case exept that now the equation set (*.*d) must be used.

A subsequent step change in load can be dealt with in exactly the same way as a constant load applied to virgin material, exept that now the material has initial stresses, strains and deflections.

The results of time hardening and strain hardening primary creep, and the stress redistribution are illustrated in fig. (3.1):

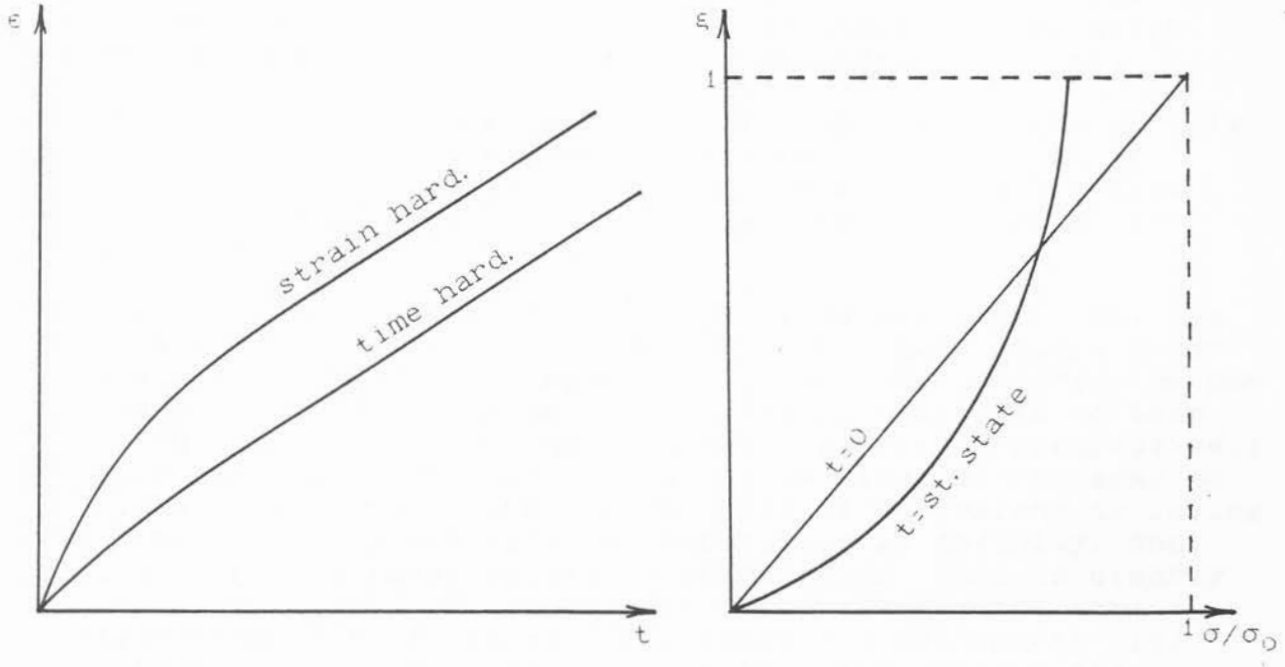

fig. (3.1) Primary creep - time and strain hardening

For the special case of a beam subject to an axial load only, no stress redistribution takes place. For loads other than step loads, equations (3.3c) or (3.3d) will have to be re-evaluated to incorporate additional load rate terms.

3.2 Creep predictions for a beam subject to damage

In order to predict the complete creep response of a beam to steady axial and bending loads, a constitutive relationship must be found that models the tertiary phase of creep. Kachanov's notion of damage [4], defined as a progressive reduction of the load-bearing area, appears to reproduce the trends observed during tertiary creep rather well. This damage equation must be combined with the algorithims describing stress redistribution (section 3.1), as damage accumulation rates have been shown to be strongly dependent on stress.

The Kachanov brittle damage theory will be used, although this theory is limited to the lower stress region, as shown in section 2.4.1. This is not considered to be too restrictive, as in most design situations only the long life, low stress regions are of interest.

Further, the refinement of the Kachanov damage theory will be used, whereby an attempt is made to model crack closure under compression. It has been argued [18] that under compression any cracks close, and so the undamaged area is available to bear load, whereas in tension the load bearing area is progressively reduced by damage. Further, it is claimed that microcracks do not grow under compressive stress. This is equivalent to saying that the creep rupture life in compression is infinity, and that no tertiary phase exists in compression. This is clearly not true, as graphs of compressive creep display the same tertiary characteristics as their tensile counterparts [19]. The graphs in [19] seem to indicate that the rupture life in compression is about an order of magnitude higher than the rupture life in tension for the similar loads. So damage rates are significantly lower in compression than in tension, and a component will have ruptured in a region of tensile stress long before any appreciable damage could accumulate in the regions of compressive stress. On the other hand, for other materials, noticeably copper, no differences between tensile and compressive damage rates were observed [22]. So to disallow damage in compression is valid for specific materials only. To set damage in compression equal to zero appears to be acceptable whenever there are tensile loads that dominate damage accumulation and rupture. Should the entire component be under compressive loads however, it would be invalid to assume no damage accumulation in compression. The damage accumulation rate in compression would be significantly lower than the rate in tension.

It has repeatedly been observed that microcracks in tension preferentially grow on planes perpendicular to the maximum principal stress (i.e. an opening mode I crack). It has been shown [22] that under compression damage accumulates on a different plane, namely the plane of maximum principal shear stress (i.e. a sliding mode II or tearing mode III type crack).

Questions now arise in how to calculate the accumulation of damage that is generated on different planes. Tests conducted on tubes in tension and reverse torsion indicate that damage accumulated on different planes do not interact. Tensorial representations of damage [30] have been formulated in order to

capture not only the amount, but also the orientation of damage. Hayhurst [20] used principal damage rates in three principal stress directions with some success.

The damage equations that will be used here are:

$$\frac{\partial \omega}{\partial t} = b\sigma^{k} \qquad \sigma > 0$$

$$\omega \,, \quad \frac{\partial \omega}{\partial t} = 0 \qquad \sigma \leq 0$$

Concerning this non-linear Kachanov constitutive relationship, a further point can been raised [18]. Should loads change between tension and compression, damage will be a discontinuous function: Damage is accumulated under tension, and as the loads become compressive damage "jumps" to zero. Clearly, finite damage exists, although during compressive loads damage is not incorporated into the equations, thus simulating crack closure. During the compressive phase, the material "remembers" the damage accumulated in tension. Upon resumption of the tensile load, damage "jumps" back to its original value and continues to accumulate.

A further complication arises out of the non-linear damage equation, in that equilibrium can only be maintained if the stresses redistribute during damage accumulation. So stresses change not only during primary creep, but during tertiary creep also, and the notion of a steady-state stress distribution no longer exists.

It has been shown [21] that in bending the neutral axis shifts away from the region of high damage. Stresses redistribute in such a way so as to relieve highly damaged areas from bearing load, but at the expense of higher stresses in lesser damaged areas.

The analysis that follows is an enlargement on the theory presented in section 3.1.1. and incorporates non-linear damage accumulation. The time-hardening assumption has been retained although it is conceded that the response to varying loads will be poorly modelled. In principle any beam cross section can be considered, however only rectangular and circular cross sections will be elaborated on in the appendix A.

Consider a beam under tension and/or bending:

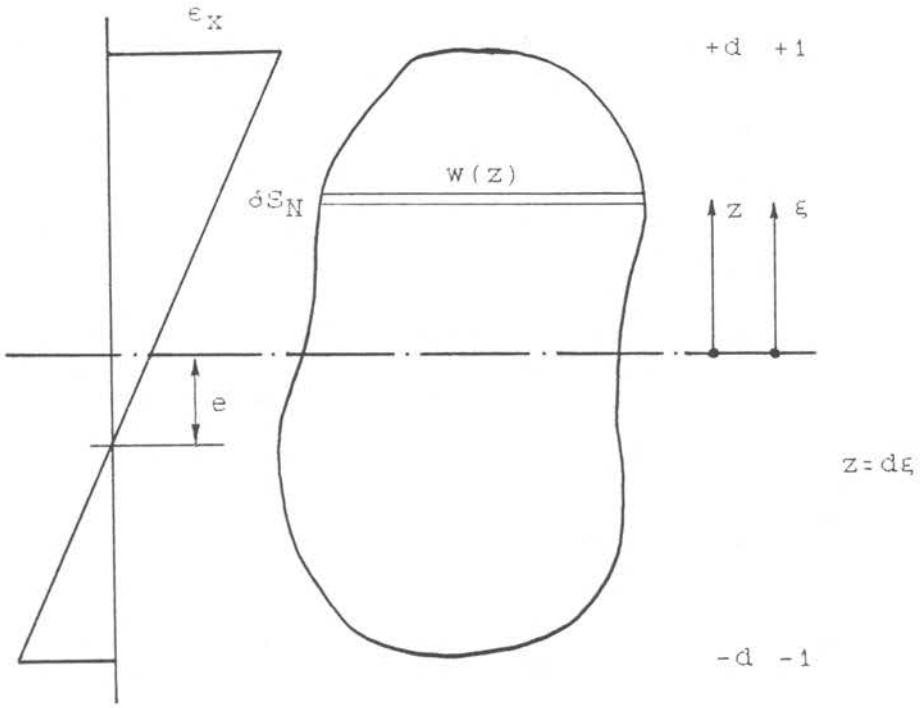

fig. (3.2) Beam section

As plane sections remain plane,

$$\epsilon_x = \epsilon_x(z=0) + \kappa z = E^{-1}\sigma_x + \epsilon_{cr} \qquad \ldots \quad (3.1)$$

$$\sigma_x = E[\epsilon(0) + \kappa z - \epsilon_{cr}] \qquad \ldots \quad (3.2)$$

Non dimensionalising:

$$\lambda_x = \lambda_{x0} + (\kappa/\epsilon_0)*d\xi = \Sigma_x + \lambda_{cr} \qquad \ldots \quad (3.1e)$$

$$\Sigma_x = \lambda_{x0} + (\kappa/\epsilon_0)*d\xi - \lambda_{cr} \qquad \ldots \quad (3.2e)$$

At the neutral axis $\epsilon(e)=0$, so:

$$e = -\epsilon(0)/\kappa$$

Equilibrium must consider the actual stress σ_x acting on the load bearing area (dS), which is reduced by damage:

$$P = \int_S \sigma_x \, dS \qquad\qquad M = \int_S \sigma_x z \, dS$$

As the limits of integration vary with damage, the current load bearing area dS is related to the original, undamaged area dS_N by:

$$dS = (1-\omega)\, dS_N$$

so that:

$$P=\int_{S_N} \sigma_x (1-\omega)\ dS_N \qquad M=\int_{S_N} \sigma_x (1-\omega) z\ dS_N \qquad \ldots \quad (3.3)$$

Or in non-dimensional form:

$$\frac{P}{\sigma_0}=\int_{S_N} \Sigma_x (1-\omega)\ dS_N \qquad \frac{M}{\sigma_0}=\int_{S_N} \Sigma_x (1-\omega) z\ dS_N \qquad \ldots \quad (3.3e)$$

Substituting from equation (3.2e):

$$\begin{bmatrix} I_1 & I_2 \\ I_2 & I_3 \end{bmatrix} \begin{bmatrix} \lambda_{x0} \\ \dfrac{\kappa}{\epsilon_0} \end{bmatrix} = \begin{bmatrix} \dfrac{P}{\sigma_0} + I_4 \\ \dfrac{M}{\sigma_0} + I_5 \end{bmatrix}$$

where:

$$I_1=\int_{S_N} (1-\omega)\ dS_N \qquad I_2=\int_{S_N} (1-\omega) d\xi\ dS_N \qquad I_3=\int_{S_N} (1-\omega) d^2\xi^2\ dS_N$$

$$I_4=\int_{S_N} \lambda_{cr} (1-\omega)\ dS_N \qquad I_5=\int_{S_N} \lambda_{cr} (1-\omega) d\xi\ dS_N$$

In appendix A the integrals are given for both rectangular and circular beam cross sections. So:

$$\begin{bmatrix} \lambda_{x0} \\ \dfrac{\kappa}{\epsilon_0} \end{bmatrix} = \frac{1}{I_1 I_3 - I_2^2} \begin{bmatrix} I_3 & -I_2 \\ -I_2 & I_1 \end{bmatrix} \begin{bmatrix} \dfrac{P}{\sigma_0} + I_4 \\ \dfrac{M}{\sigma_0} + I_5 \end{bmatrix} \qquad \ldots \quad (3.6)$$

Given loads and creep strains at any time, the equilibrium stress distribution can be obtained from equations (3.6) and (3.2e) after evaluating the integrals I_1 to I_5.

The equilibrium-rate equations are from equation (3.3e):

$$\frac{\dot{P}}{\sigma_0} = \int_{S_N} \dot{\Sigma}_x (1-\omega)\, dS_N - \int_{S_N} \Sigma_x \dot{\omega}\, dS_N$$

$$\frac{\dot{M}}{\sigma_0} = \int_{S_N} \dot{\Sigma}_x (1-\omega)\, d\xi\, dS_N - \int_{S_N} \Sigma_x \dot{\omega} d\xi\, dS_N$$

where the first and second terms in either equation describe stress redistribution during primary and tertiary creep respectively.

From equation (3.2e):

$$\dot{\Sigma}_x = \dot{\lambda}_{x0} + (\kappa/\epsilon_0)\dot{d\xi} - \dot{\lambda}_{cr} \qquad \ldots \quad (3.7)$$

and proceding similarly as before:

$$\begin{bmatrix} \dot{\lambda}_{x0} \\ \dot{\kappa}/\epsilon_0 \end{bmatrix} = \frac{1}{I_1 I_3 - I_2^2} \begin{bmatrix} I_3 & -I_2 \\ -I_2 & I_1 \end{bmatrix} \begin{bmatrix} \dot{P}/\sigma_0 + I_6 + I_8 \\ \dot{M}/\sigma_0 + I_7 + I_9 \end{bmatrix} \qquad \ldots \quad (3.8)$$

with:

$$I_6 = \int_{S_N} \dot{\lambda}_{cr} (1-\omega)\, dS_N \qquad I_7 = \int_{S_N} \dot{\lambda}_{cr} (1-\omega)\, d\xi\, dS_N$$

$$I_8 = \int_{S_N} \Sigma_x \dot{\omega}\, dS_N \qquad I_9 = \int_{S_N} \Sigma_x \dot{\omega} d\xi\, dS_N$$

Also see appendix A.

By substituting equation (3.8) back into equation (3.7), the stress rate at any time is known. This enables a time step to be chosen: Integrating the constitutive equations presupposes a constant - or rather an acceptably constant - stress during a time step $\Delta\tau$. If a 1% variation in stress is considered acceptable,

$$\Sigma_{x\,j} + \dot{\Sigma}_{x\,j}\Delta\tau = \Sigma_{x\,j+1} = 1.01\Sigma_{x\,j}$$

As Σ_x and $\dot{\Sigma}_x$ vary throughout the cross section, the smallest quotient is selected:

$$\Delta\tau = 0.01 \left| \frac{\Sigma_x}{\dot{\Sigma}_x} \right| \text{ smallest} \qquad \ldots (3.9)$$

as proposed in [1].

So far the analysis has been general, and at this point the non linear Kachanov constitutive equation can be introduced.

Creep	Damage	
$\epsilon_{cr} = f_1(\sigma)\ f_2(t)\ f_3(T)$	$\omega = F_1(\sigma)\ f_2(t)\ f_3(T)$	$\sigma_N > 0$
	$= 0$	$\sigma_N \leq 0$

For constant temperature, using the Norton and Bailey relationships:

$\epsilon_{cr} = a\sigma^m\ t^n$	$\omega = b\sigma^k\ t^n$	$\sigma_N > 0$
	$= 0$	$\sigma N \leq 0$

with

$$\sigma_x = \frac{\sigma_{xN}}{(1-\omega)} \qquad \sigma_N > 0$$

$$= \sigma_{xN} \qquad \sigma_N \leq 0$$

Non-dimensionalising the above using the non dimensional time parameter τ:

$$\tau = At^n \quad \text{with} \quad A = aE\sigma_0^{m-1} \quad \text{and} \quad B = \frac{b\sigma_0^{k+1-m}}{aE}$$

yields:

$$\dot{\lambda}_{cr} = \left[\frac{\Sigma_{xN}}{1-\omega} \right]^m \qquad \Sigma_{xN} > 0$$

$$= \Sigma_{xN}^m \qquad \Sigma_{xN} \leq 0 \qquad \ldots (3.10)$$

and

$$\dot{\omega} = B \left[\frac{\Sigma_{xN}}{1-\omega} \right]^k \qquad \Sigma_{xN} > 0$$

$$\omega\ ,\ \dot{\omega} = 0 \qquad \Sigma_{xN} \leq 0 \qquad \ldots (3.11)$$

The analysis that follows is taken from [15] and has been reproduced in section 2.4.1 for the case of steady state creep. Here, stress redistribution due to damage is included.

Integrating equation (3.11) yields:

$$\tau_R = \frac{1}{B(k+1)\Sigma_{xN}^{k}} \qquad \Sigma_{xN}>0$$

$$= \infty \qquad \Sigma_{xN}\leq 0 \qquad \ldots (3.12)$$

and transforming back to the real time domain:

$$t_R^{n} = \frac{1}{b(k+1)\sigma_{xN}^{k}} \qquad \sigma_{xN}>0$$

$$= \infty \qquad \sigma_{xN}\leq 0 \qquad \ldots (3.12a)$$

Given sufficiently constant stresses over the time interval $\Delta\tau$ (a 1% variation is considered acceptable), the damage increment between τ_i and $\tau_i+\Delta\tau_i$ is:

$$\omega_{i+1} = 1-\left[(1-\omega_i)^{k+1} - \frac{\Delta\tau}{\tau_R}\right]^{(1/(k+1))} \qquad \Sigma_{xN}>0$$

$$= \omega_i \qquad \Sigma_{xN}\leq 0 \qquad \ldots (3.13)$$

Integrating equation (3.10) over $\Delta\tau$ yields the creep strain increment :

$$\Delta\lambda_{cri} = \frac{\Sigma_{xN}^{m-k}}{B(k+1-m)}\left[(1-\omega_i)^{k+1-m} - (1-\omega_{i+1})^{k+1-m}\right] \qquad \Sigma_{xN}>0$$

$$= \Sigma_{xN}^{m}\,\Delta\tau \qquad \Sigma_{xN}\leq 0 \qquad \ldots (3.14)$$

so:

$$\lambda_{cr\ i+1} = \lambda_{cr\ i} + \Delta\lambda_{cri}$$

Transforming back to the real time domain:

$$\epsilon_{crR} = \frac{a\sigma^{m-k}}{b(k+1-m)} \qquad \sigma_{xN}>0$$

$$= \infty \qquad \sigma_{xN}\leq 0 \qquad \ldots (3.14a)$$

Also:

$$\lambda_{crR} = \dot{\lambda}_{cr\ min}\, L\, \tau_R \quad \text{where} \quad L = \frac{k+1}{k+1-m} \text{ the creep ductility.}$$

Now the constants a and b and the exponents m, n, K must be found. This ammounts to curvefitting selected equations against experimental data. For this purpose data from [19] for the alloy Mar-M 246 at 900 C has been chosen. It must be noted from the outset that finding equation constants that yield acceptable results is no easy matter, in view of the extreme sensitivity of the predicted creep response to even the slightest variations in an equation constant.

As there is no closed form solution to the curve fitting process, trial and error methods prevail.

From equation (3.12a), a linear relationship for log t_R vs. log σ is predicted.

$$\log \sigma_N = \frac{1}{k} \log \left[\frac{1}{b(k+1)} \right] - \frac{n}{k} \log t_R \qquad \ldots \quad (3.12b)$$

Further information is obtained by relating the minimum creep strain rate to the applied stress and to the time to rupture. In both cases log-linear relationships are predicted by theory, and over limited stress ranges log-linear relationships are also suggested by data [19], barring scatter.

$$\log \sigma_N = \frac{-1}{m} \log \left[a n t_{ss}^{n-1} \right] + \frac{1}{m} \log \left(\frac{\partial \epsilon_{cr}}{\partial t} \right)_{min.} \qquad \ldots \quad (3.10a)$$

$$\log t_R = \frac{k}{mn} \log \left[\frac{a n t_{ss}^{n-1}}{b^{m/k} (k+1)^{m/k}} \right] - \frac{k}{mn} \log \left(\frac{\partial \epsilon_{cr}}{\partial t} \right)_{min.} \qquad \ldots \quad (3.10b)$$

Data provided by [19] can be fitted to equations (3.12b), (3.10a) and (3.10b). Extending the piecewise linearisation over a fairly wide range of stress, namely 290 MPa - 450 MPa, the equation constants in table 3.1 were found to give the best results.

Table 3.1: Mar-M 246 at 900 C (290 - 450 MPa)		
k=7.9	m=8.4	n=1.0
a=1.9 10E-76	b=3.5 10E-71	

Computer predictions using the above differed from data by as much as 25% , although on a log-log scale the predictions fell within the scatter band for data plotted against equation (3.10a).

Scatter in data fitted to equation (3.10a) especially, can cause large changes in the resulting equation constants. So, for instance by selecting data that pertains to a fairly narrow range of stress (from 290 MPa to 340 MPa) the straight line equation (3.10a) fitted the data with greatly reduced scatter. Using the selected data, the trial and error curvefitting yielded the equation constants in table 3.2.

Table 3.2: Mar-M 246 at 900 C (290 - 340 MPa)		
k=8.5	m=8.4	n=1.076
a=1.67 10E-77	b=5.58 10E-76	

The computer predictions with equation constants from table 3.2 correlated very well with data from [19], however only over the narrow stress range. Using these equation constants to predict the response to stresses outside the range 290-340 MPa, yielded worse results than if the constants from table 3.1 were used.

A computer program was developed on the basis of the damage model outlined above. A program listing is provided in appendix B . In view of the fact that the stresses continually redistribute, the time increments will remain small throughout the component lifetime. Thus the computing time can be long.

3.2.1 Uniaxial tension

In fig. (3.3) computer predictions using the constants from table 3.2, a circular beam cross section of 20 [mm] diameter, and constant uniaxial stresses of 290 [MPa] and 340 [MPa], are compared with data from [19]. The very good correlation attained indicates that the curve fitting procedure to obtain the equation constants was successful. However, it must be restated that a very selective curve fitting procedure was used, and large discrepancies between prediction and experiment were found for stresses outside this narrow range.

If the constants from table 3.1 were used, errors of about 20% were noted. However the error was found to be consistent over a wider range of stresses.

Also included in fig. (3.3) is a predicted response to a step change in load after 200 [h] from 290 [MPa] to 340 [MPa]. As the assumption of time-hardening was made, one would expect that this prediction would not be very accurate. If nothing else, it serves to illustrate the program's ability to deal with step load changes, given that damage has accumulated under previous loads. In effect the prediction is arrived at by "transferring" from one creep curve to the next along lines of constant damage, as illustrated in fig. (2.4). The program thus utilises a life fraction rule in predicting the response to step load changes. As the life fraction rule has received the favourable comment [5] of being better than the time or strain hardening rules, the prediction in fig. (3.3) might not be so bad after all.

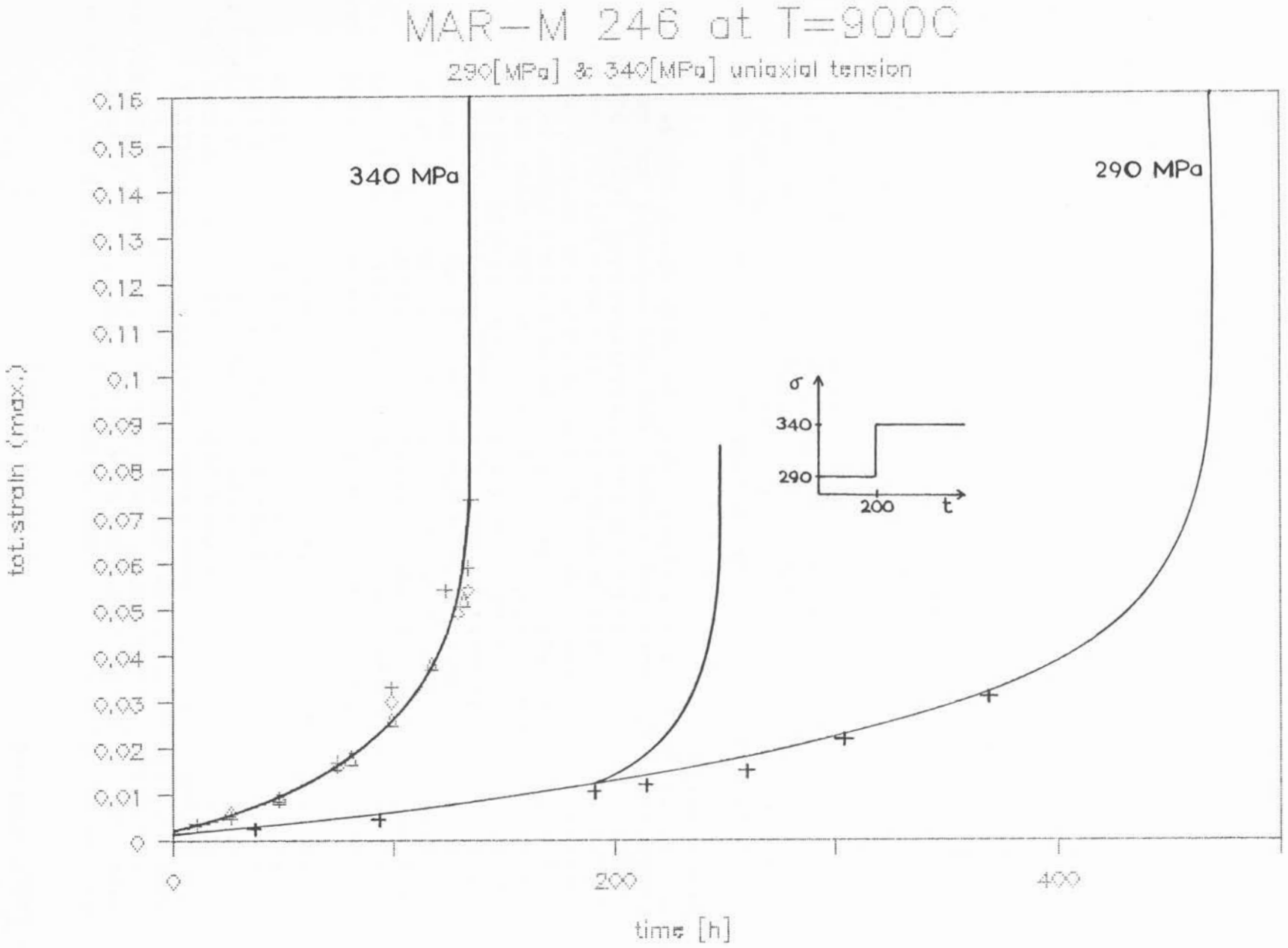

fig. (3.3) Uniaxial tension under 290 and 340 MPa

3.2.2 Bending

Having established the computer methods credibility in uniaxial tension, the creep response to a bending moment is attempted. Only a moment M=380 [Nm] is applied to a circular cross section beam 20 [mm] in diameter so that the reference stress is 290 [MPa]. As the stresses exceed 340 [MPa], the equation constants from table 3.1 were used. The predicted rupture time in fig. (3.4) of t_R=560 [h] compares favourably with the rupture time predicted by the reference stress in equation (3.12b) of t_R=517 [h] - a difference of 8%. The approximate reference stress techniques in section 4.1 give similar results.

In fig. (3.5), the stress distribution is shown at selected time intervals, and the continual stress redistribution becomes apparent. Also it can be observed that tertiary stress redistribution due to damage occurs by a progressive shifting of the neutral axis, also shown in [21]. A change in shape of the stress distribution takes place only during primary creep. In tension (z positive) the stresses rise between times C to F due to damage accumulation in tension. Yet they rise less than they would have, had there been no stress redistribution. In compression however, stresses rise because the neutral axis shifts so as to leave progressively less material to bear compressive loads. Had no stress redistribution taken place, compressive stresses would have remained constant during secondary and tertiary creep, and the beam would not be in equilibrium.

A further observation that can be made is that there appears to be a skeletal point [11] at z=-0.002[m] and σ=-300[MPa]. A skeletal point is a point within the continuum where the stress is invariant with time. The stress at this skeletal point appears to concur in magnitude with the reference stress σ_o=290 [MPa]. However it is felt that this skeletal point is of little significance as a reference stress, as it will be seen from fig. (3.8) that the skeletal point and reference stress do not coincide.

In fig. (3.6) the distribution of damage throughout the beam is shown for the same selected time intervals. The assumption was made that plane sections remain plane, i.e. a linear strain distribution. From equations (3.10) and (3.11) it is clear that damage is proportional to creep strain, and so proportional to total strain. The damage should, as shown in fig. (3.6), be linearly distributed. As damage is zero at the neutral axis, the curves' intercept with the z-axis show the movement of the neutral axis as damage accumulates.

Micrographic studies [22] of rectangular cross section beams show that grain boundary fissures and cracks grow most rapidly near the tensile surface of the beam, and there is very little evidence of damage close to the center of the beam cross section. Micrographs of beams in reverse loading showed deterioration only in regions that had experienced tension immediately prior to examination. An explanation could be that cracks close under compression, rendering them unobservable under a microscope.

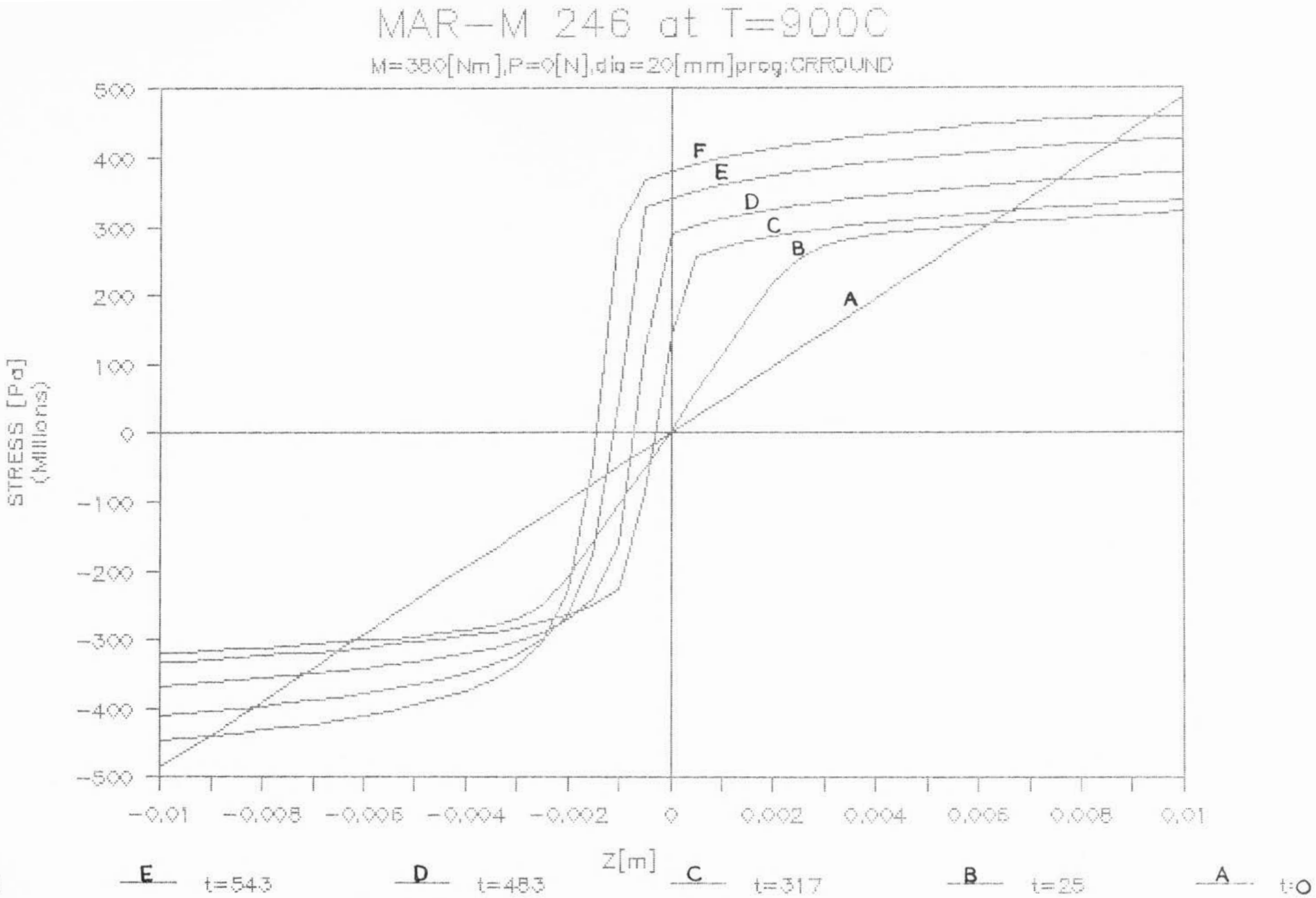

fig. (3.5) Stress distributions across the beam section

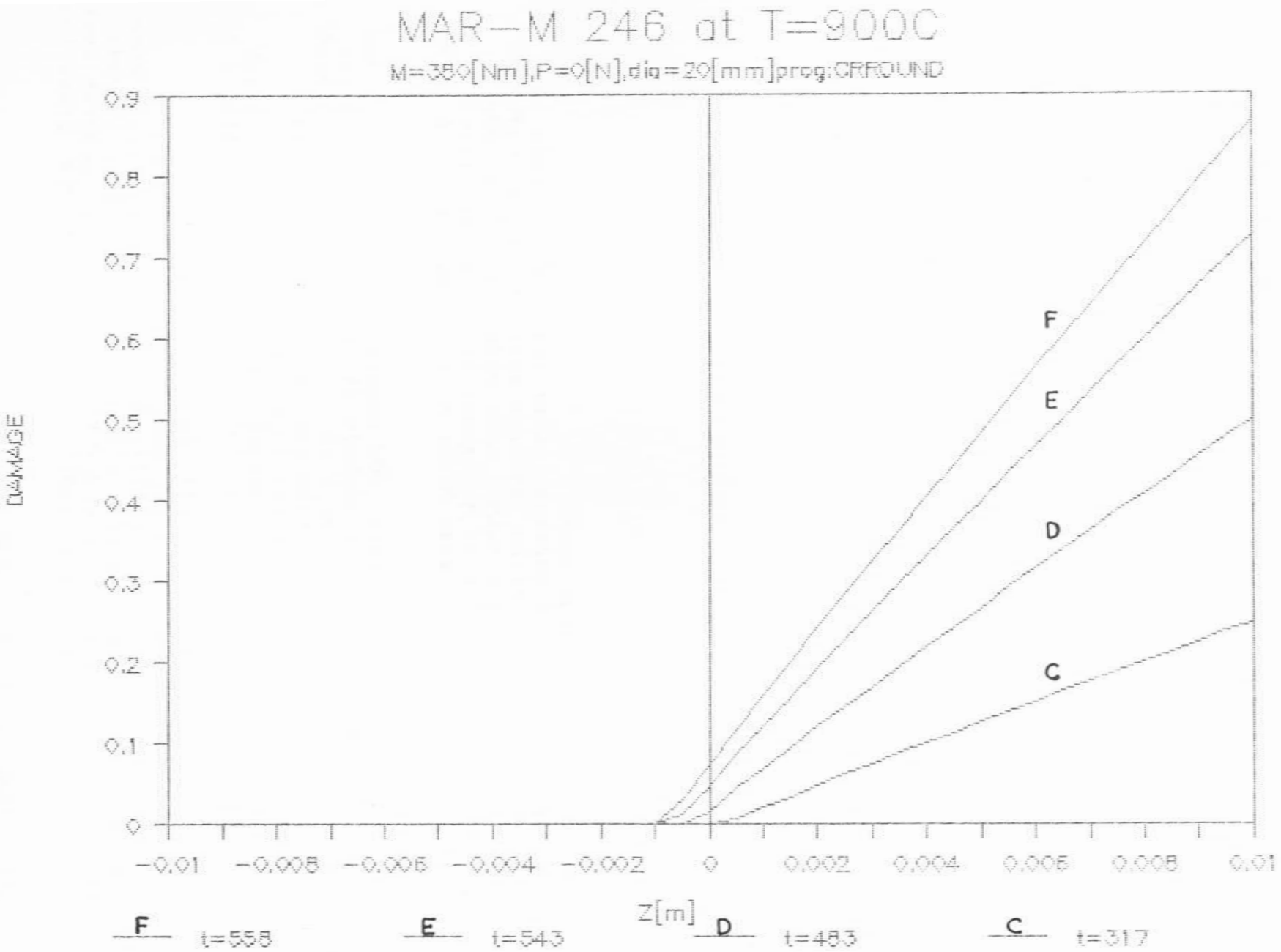

fig. (3.6) Damage distributions across the beam section

3.2.3 Combined bending and tension

In fig. (3.7,) tensile and bending loads are combined. Dimensions and equation constants are unchanged from the pure bending case. The reference stress for this case can be found to be 290+34= 324 [MPa]. The life of a uniaxial specimen at that stress from eq. (3.12b) is t_R=189 [h]. The computed prediction of t_R=210 [h] compares favourably, being 11% in excess.

The stress distribution at various times is shown in fig. (3.8). The stresses rise fairly uniformly over the greatest portion of the beam, similar to stress increases during uniaxial tension. As damage in the beam reaches an advanced stage however, the outer fibres at z=-0.01 are predicted to be under high compressive stress, a surprising result considering the relative magnitudes of axial and bending loads (M=45 [Nm] and P=91106 [N]).

A very distinctive skeletal point at z=-0.008 and σ=220 [MPa] is observed. However it is different from the calculated reference stress of 324 [MPa]. What might be significant however is the observation that the skeletal point occurs at the same place in the material where the damage curves in fig. (3.9) tend towards zero.

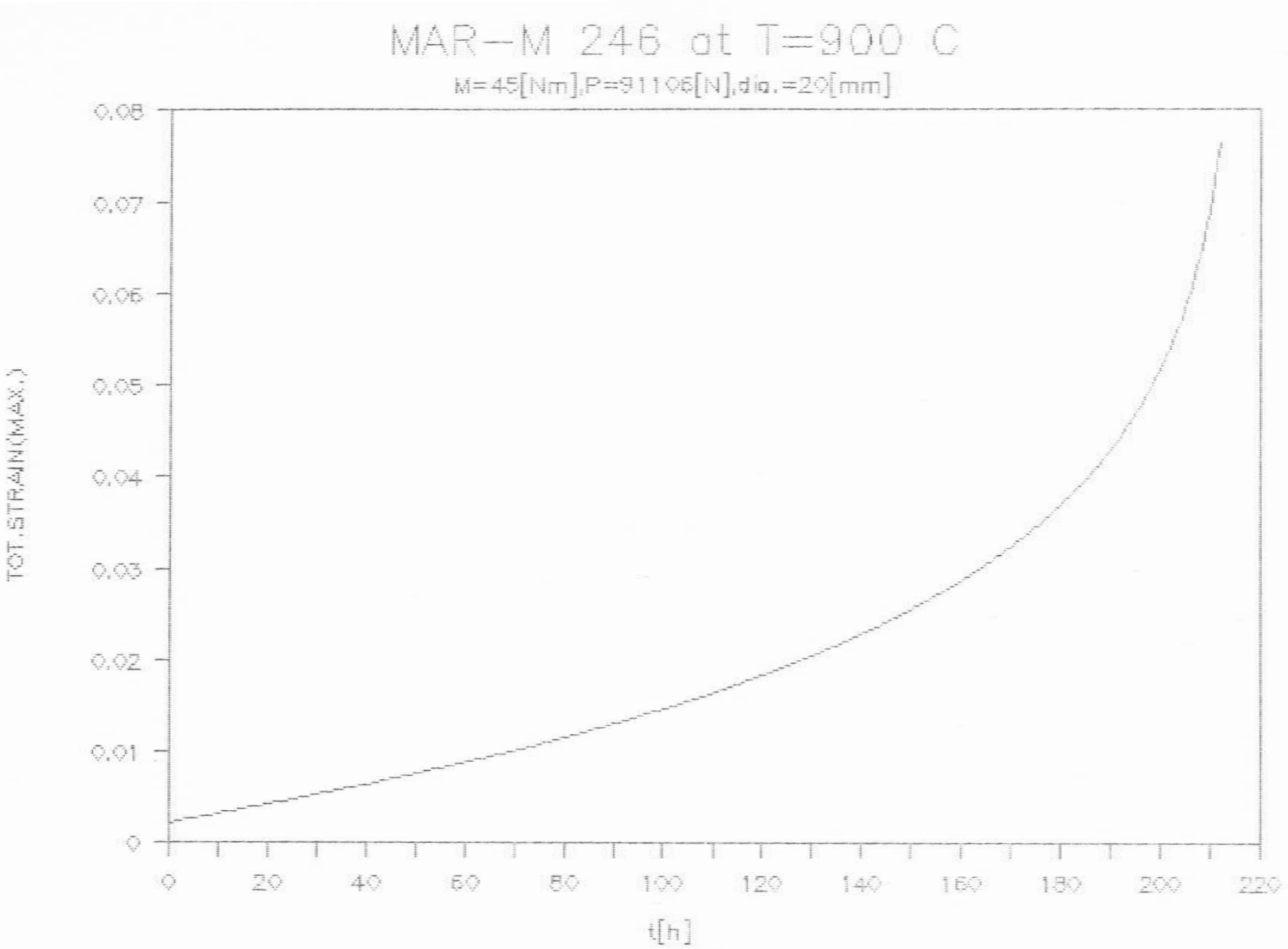

fig. (3.7) Strain history of the extreme tension fibre

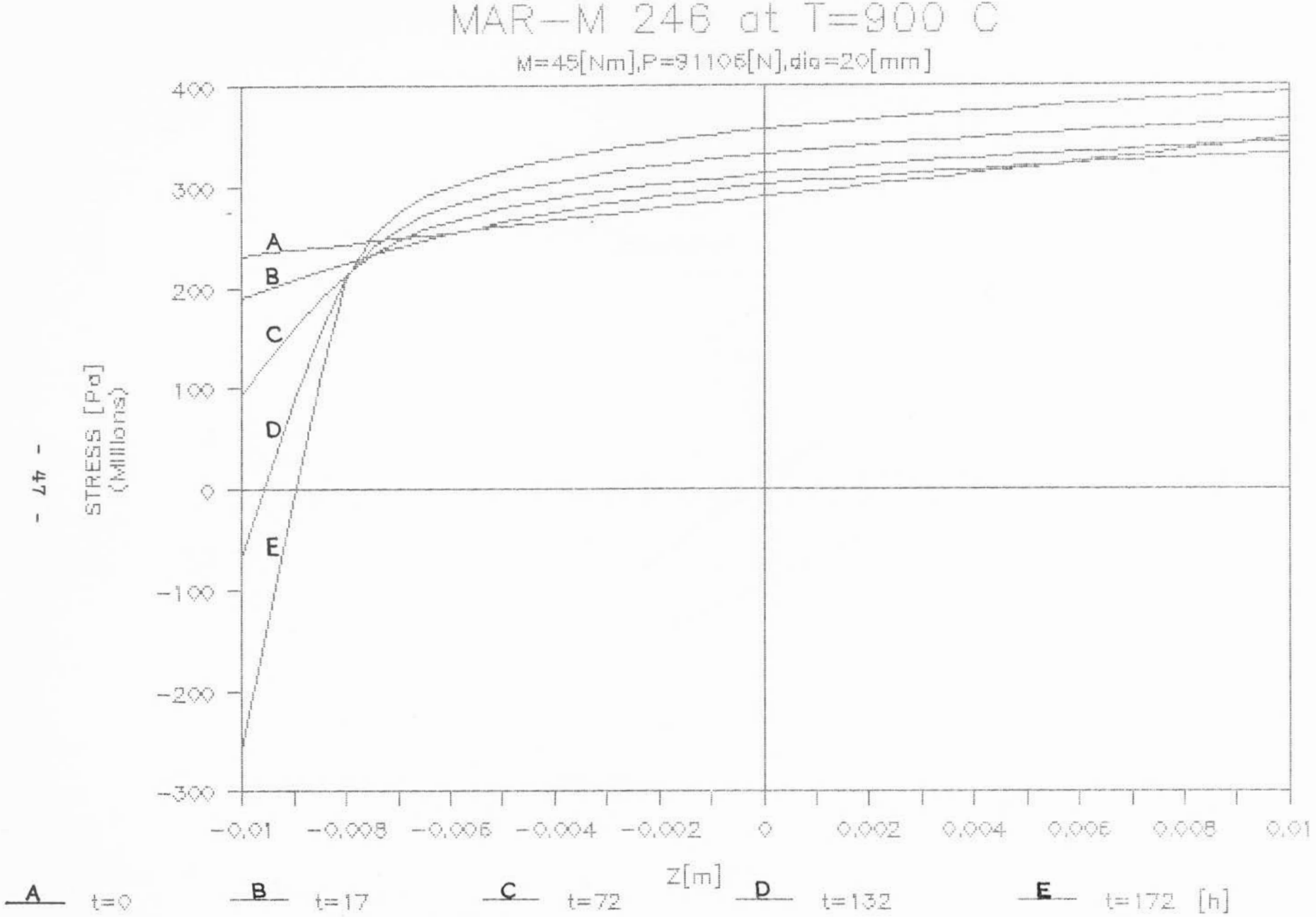

fig. (3.8) Stress distributions across the beam section

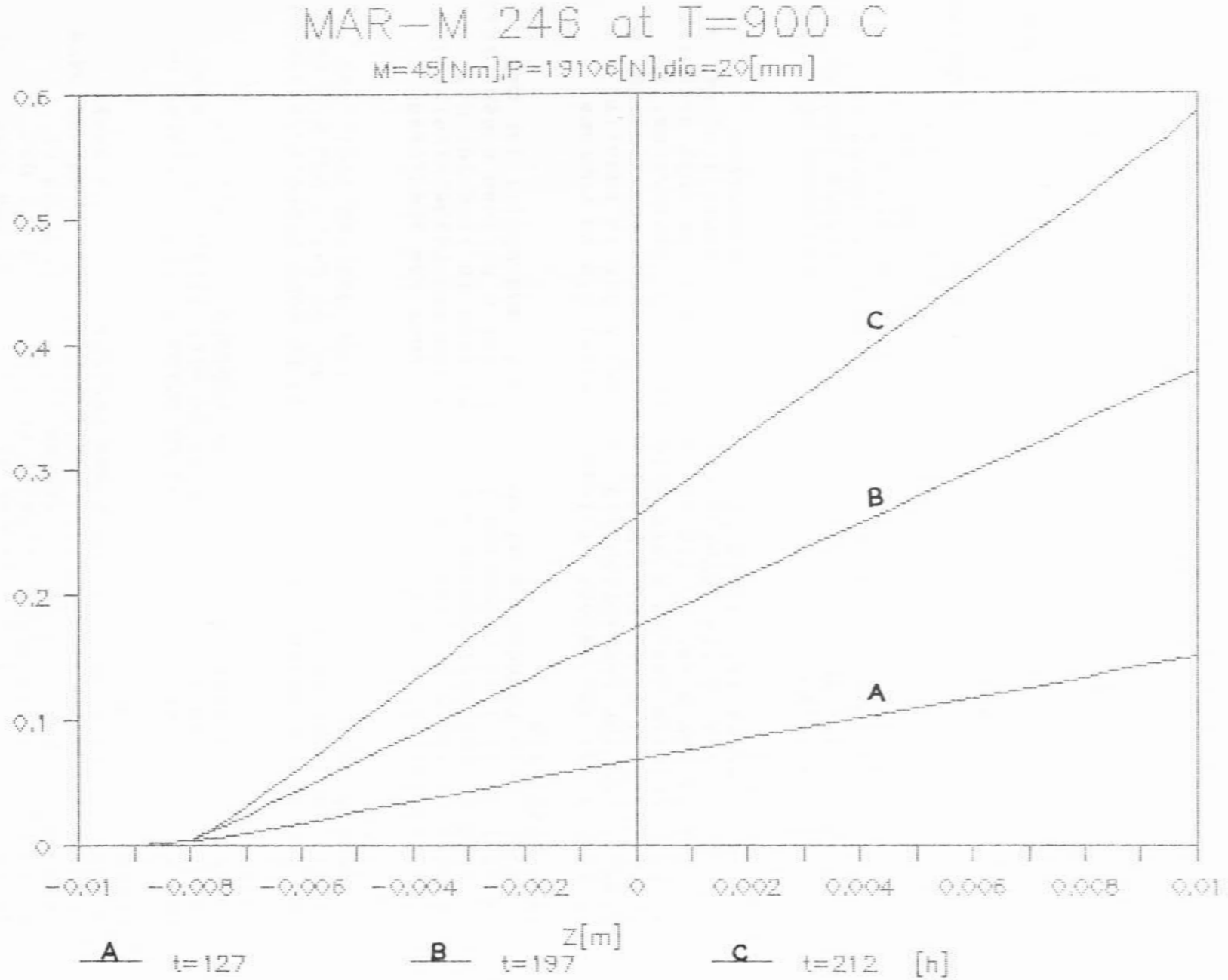

fig. (3.9) Damage distributions across the beam section

3.2.4 The effects of bending during tensile testing

In this section, an assessment will be made of the effects of eccentric loading during tensile creep testing. It has been shown that even small bending loads introduced by inappropriate arrangements to apply the tensile load can have a deleterious effect on the creep response [1], and cause premature failure.

The effect of eccentric loading on primary creep response has been documented [1], and shown to be significant. Now, also the effect of eccentric loading on rupture life will be assessed.

The equation constants were chosen to be more representative of steels. No specific material is implied, so n=1/3 and k=m was chosen. A beam of circular cross section, dia.=20 [mm], was modelled.

Figs. (3.10), (3.12) and (3.11), (3.13) show the predicted effects of eccentric loading for m=3 and m=5 respectively. A 1% load eccenticity causes a 15% reduction in life for m=3, as against a 27% life reduction for m=5. For a 5% load eccentricity, however, life reductions of 60% for m=3, and 90%(!) for m=5 were predicted.

In fig. (3.14) the effect of load eccentricity on rupture predictions for conventionally cast MAR-M 246 is equally dramatic. A 4% eccentricity caused a 58% reduction in life, a 8% eccentricity caused a 81% life reduction. Directionally solidified MAR-M 246 in fig. (3.15) appears to be only slightly less sensitive to the adverse effects of eccentric loading: 4% and 8% eccentricity caused 52% and 74% life reductions respectively.

It has been shown that conventional testing equipment applies eccentric loads well in excess of 1%. Inappropriate loading arrangements have been singled out as the major source of scatter that have plagued creep reseachers to date [23]. Such extreme sensitivity of the creep response to load illustrates that the correct testing technique is imperative to eliminate the possibility of applying bending moments during tensile testing.

Possibly, when comprehensive, more reliable creep data becomes more freely available, can creep predictions be made with more confidence.

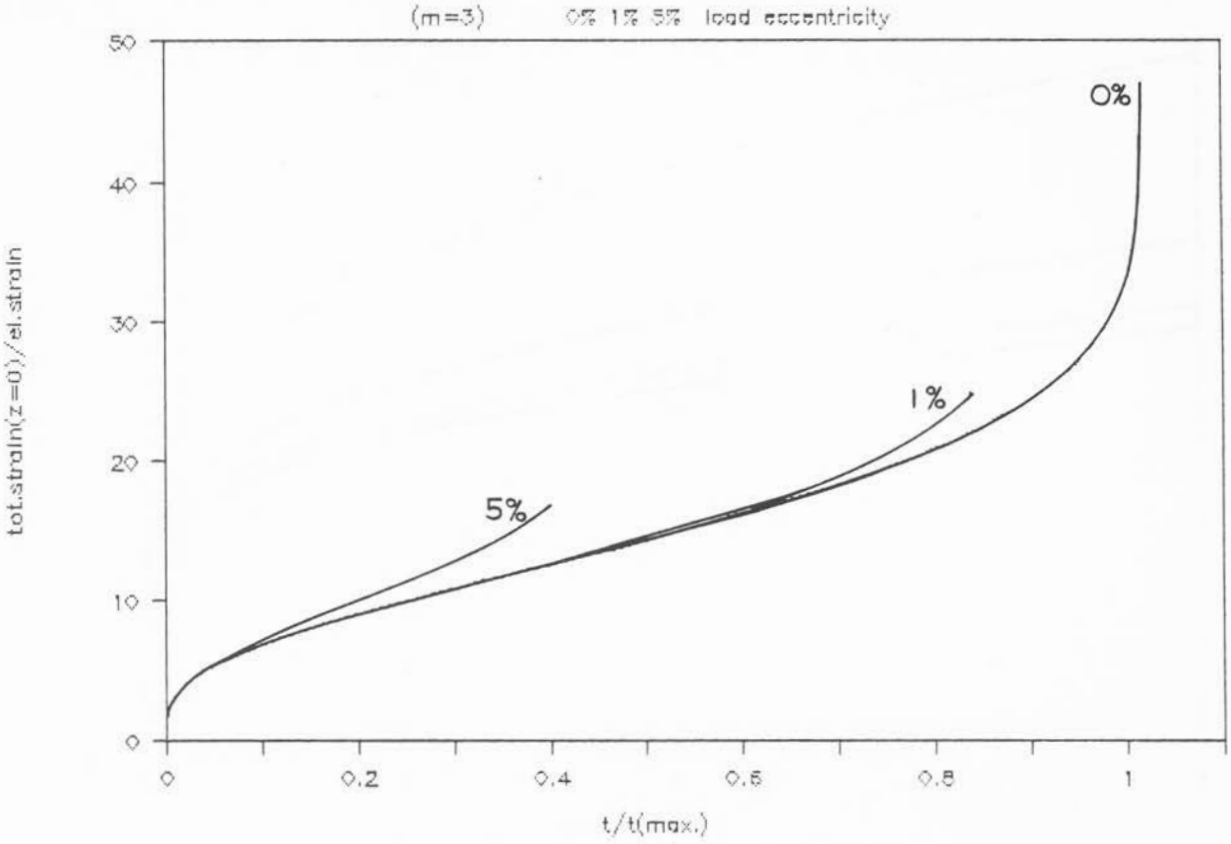

fig. (3.10) Life predictions under eccentric loading (m=3)

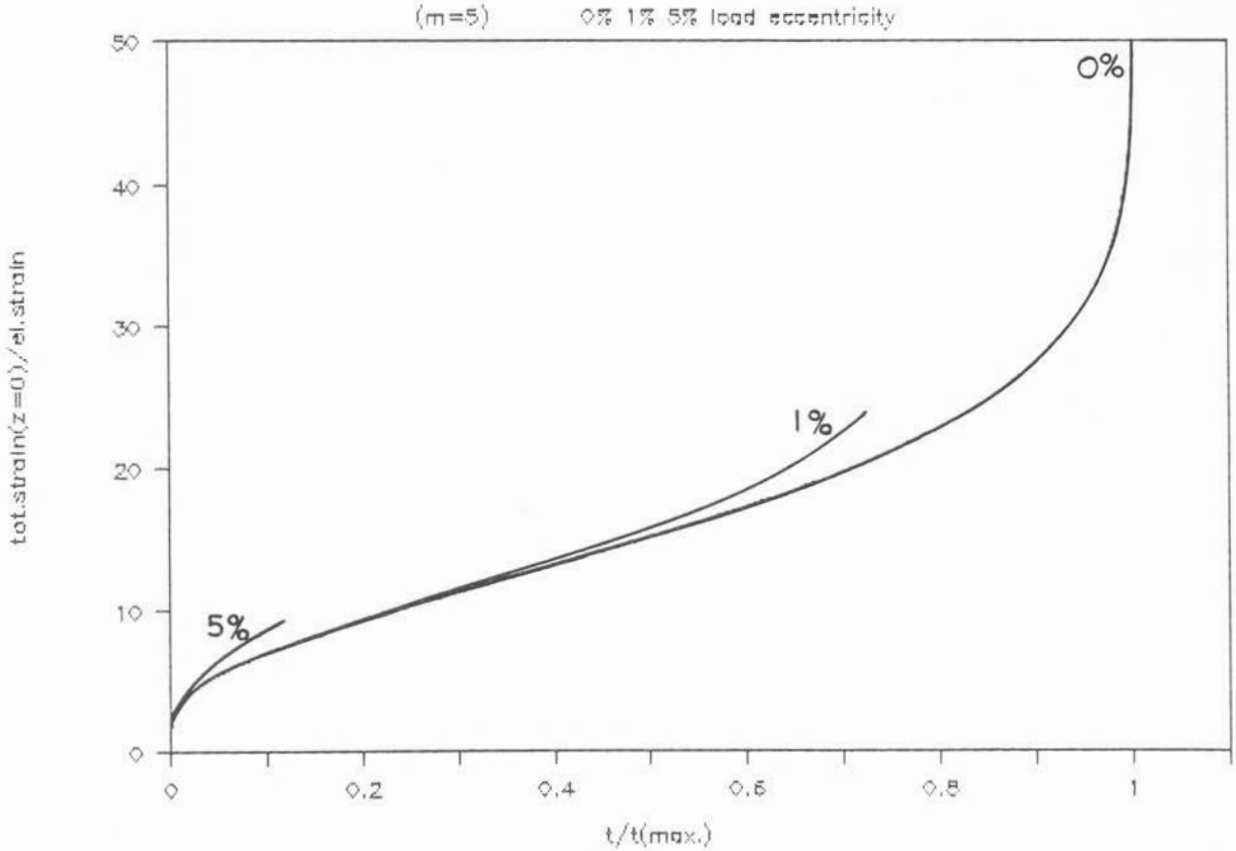

fig. (3.11) Life predictions under eccentric loading (m=5)

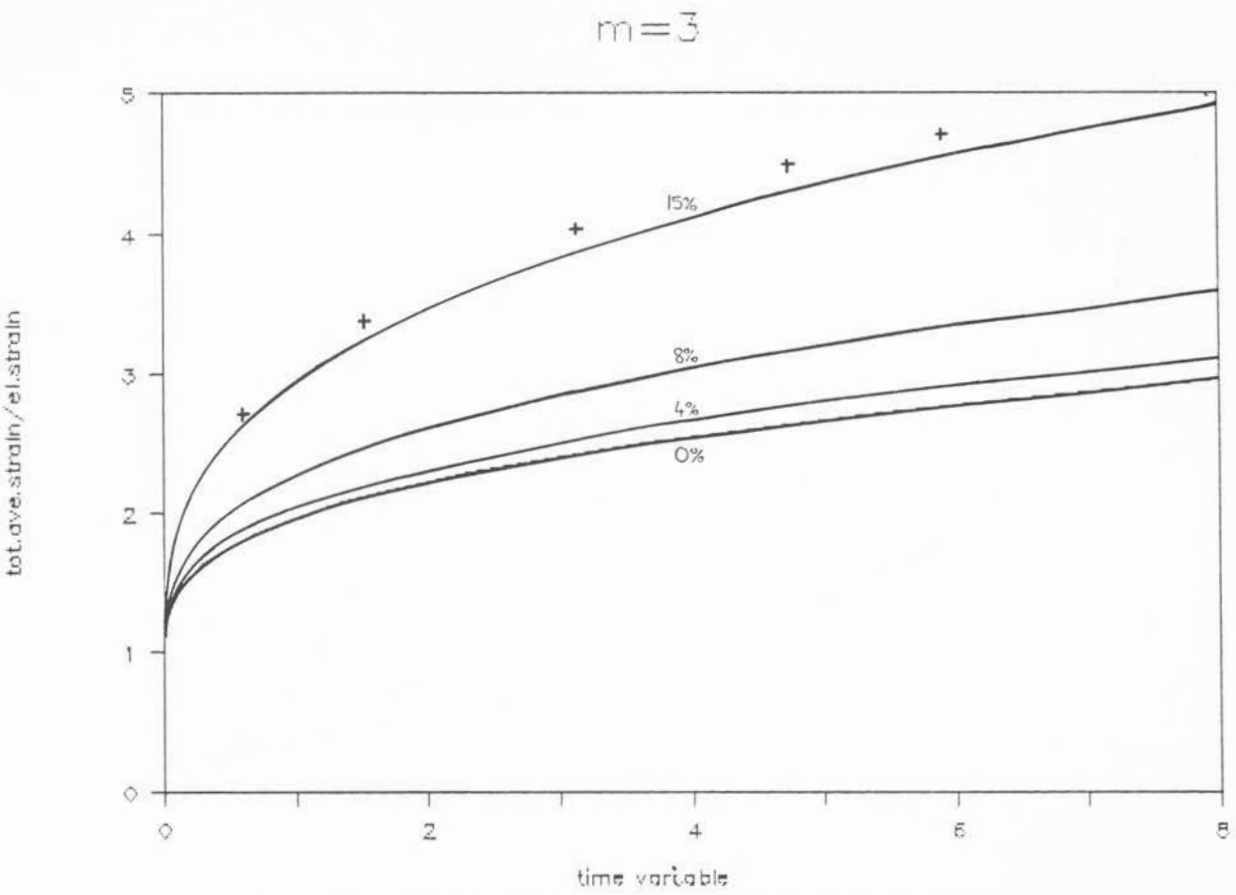

fig. (3.12) Primary creep under eccentric loading (m=3)

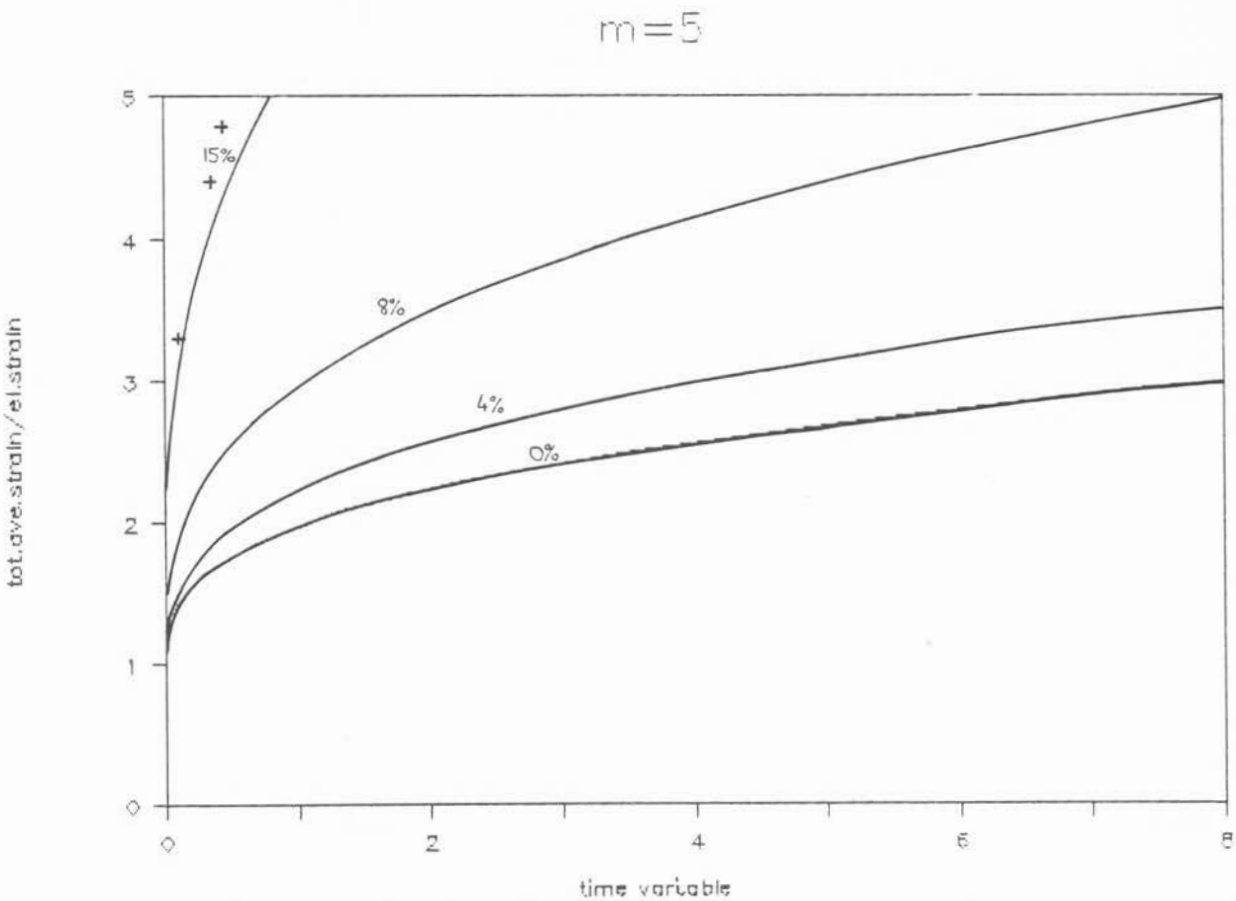

fig. (3.13) Primary creep under eccentric loading (m=5)

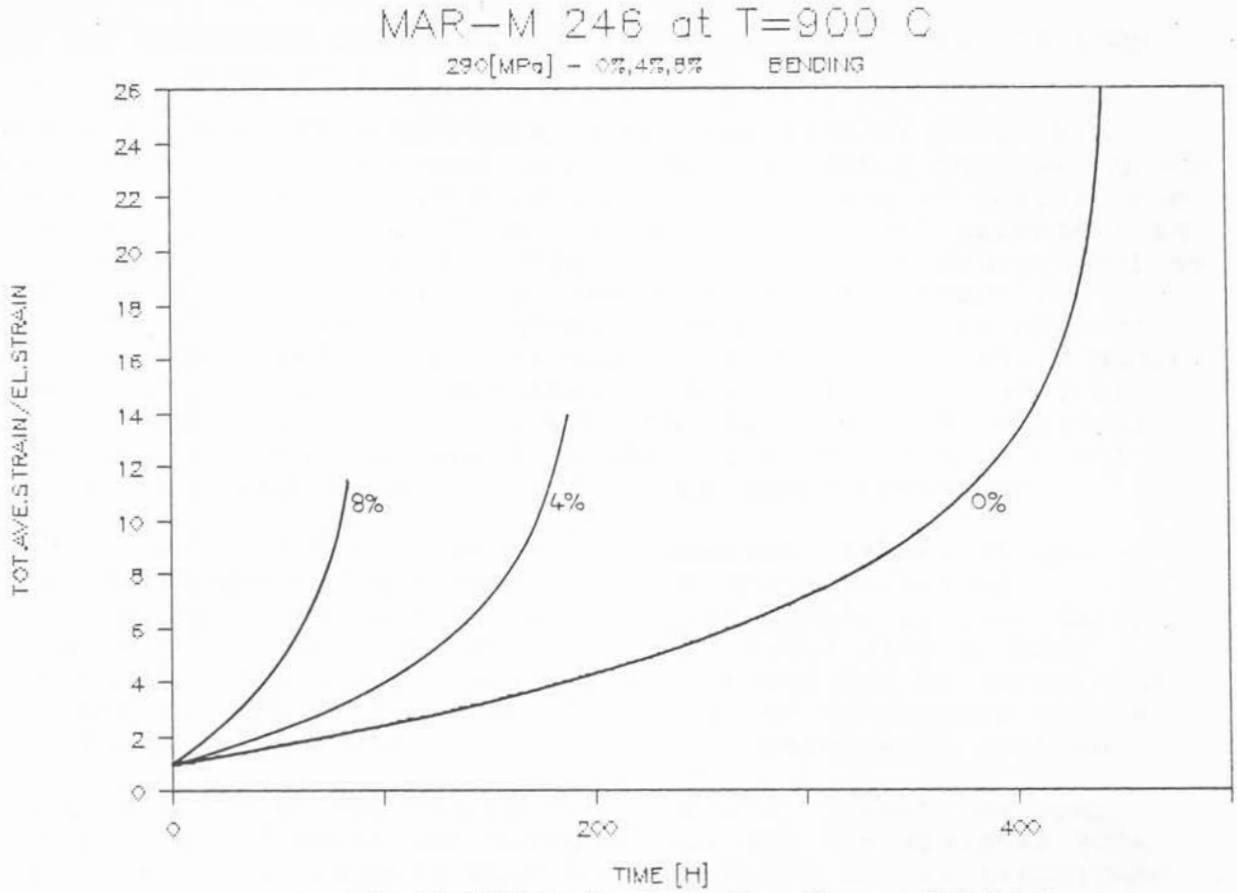

fig. (3.14) Life predictions for conventionally cast MAR-M 246 under eccentric loading

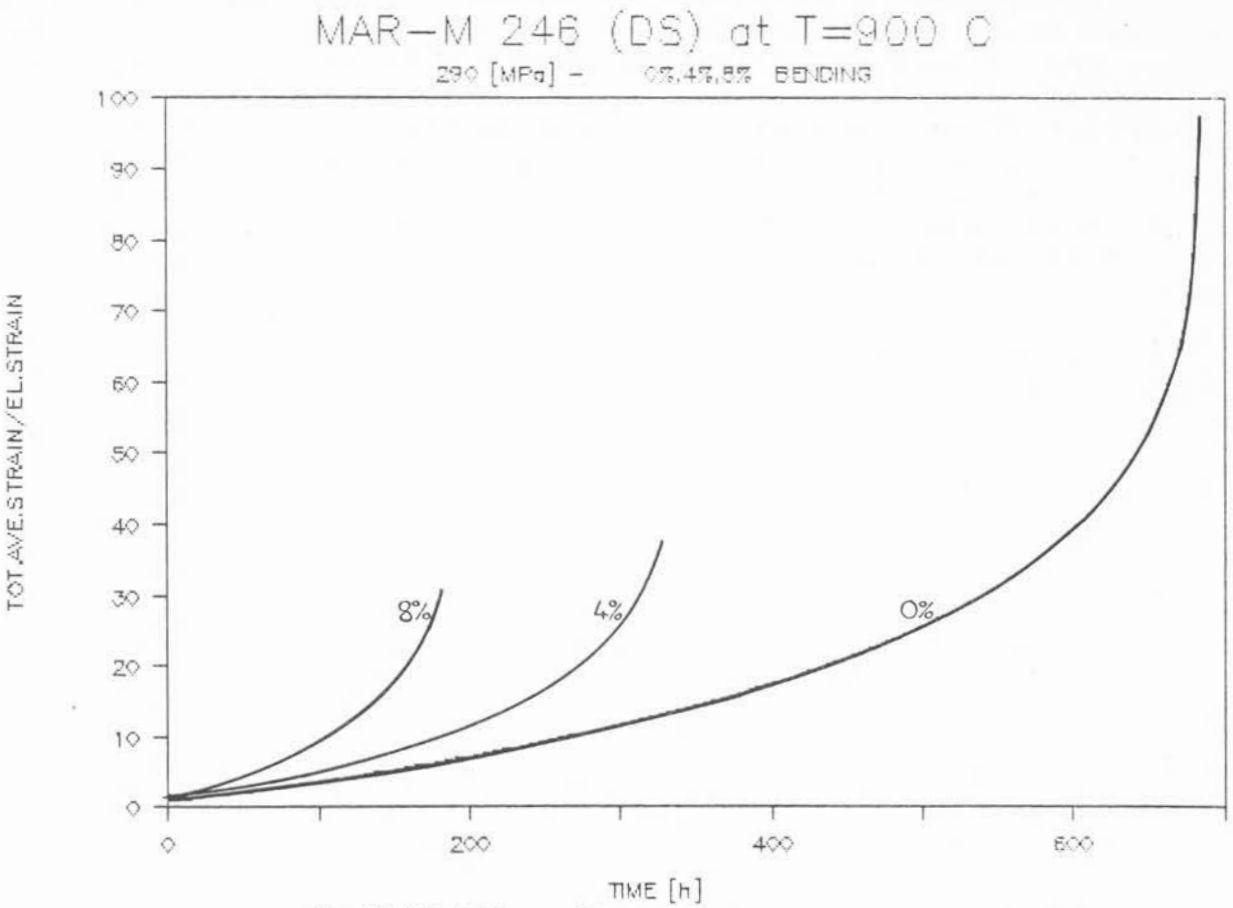

fig. (3.15) Life predictions for directionally solidified MAR-M 246 under eccentric loading

4.0 The reference stress method and some design applications

To the designer of components, creep analysis is beset with difficulties [22]. Firstly, a mathematical model must be chosen. There is usually a variety of idealistic models to choose from, (outlined briefly in section 2.1) with only scant agreement as to which model is most suitable for a particular design purpose. Some approximations, such as constancy of temperature for example, are neccessary to develop formulations that are not unwieldy. Such approximations might however not be valid under operational conditions, and thus be a significant source of error. Also, the initial state of the material, the residual stress imposed during manufacturing, is more often than not unknown, yet significantly impact upon creep behaviour.

Having however chosen some model, numerical values of the equation parameters are needed. These are obtained by "best estimate" curve-fitting the creep models to test data, which is notoriously prone to scatter. Faced with so many sources of error and variability, it should not be surprising that predictions of the creep behaviour of components can be significantly in error, and should be treated with caution.

Concurrently with the search for complete, "exact" methods, simple order-of-magntiude methods that aid the designer were sought after. It is here that the reference stress techniques become prominent.

Reference stress techniques are useful in several ways [24]: Firstly, at an initial design stage the extent and importance of the creep behaviour can be assessed vis-a-vis other failure modes, such as fatigue. Secondly, reference stress methods augment, and often replace, exact analyses where design data is inadequate or unreliable, or when "exact" analyses become prohibitively expensive. Thirdly, reference stress techniques aid in effectively planning the expensive and time consuming creep tests, by recommending at what stress levels and temperatures tests should be conducted, so that optimal design use can be made of a minimum number of tests. Finally, this approach is invaluable when components under variable loads are considered [1].

The aim of reference stress methods is to improve the accuracy of a creep prediction by reducing the exposure to uncertainties arising out of [22]:

1) the mathematical model used

2) the sensitivity of the equation constants to data scatter

3) greatly varying equation constants obtained from different curve fitting procedures

Attempts are made to correlate the creep deformation in a structure *directly* to the creep behaviour of a uniaxial tension test specimen. This is only possible as a remarkable similarity exists between the geometric shape of the creep curves of a

component and a uniaxial test specimen [1]. So a material independent scaling factor is sought that relates component and specimen creep curves.

In a reference stress analysis, the expression for the total creep response can be separated into terms that are only material-dependent, and others that depend only on the component geometry and loading [24]. By a suitable choice of reference stress, the effect of the material-dependent terms can be reduced to be almost constant, so minimising their effect on the total creep response. In this way a significant source of error in using possibly inappropriate material models or equation constants is largely removed. However, it should be noted that strictly speaking reference stress methods apply only to secondary creep, i.e. when the stress distribution remains constant in time, and stresses vary only in proportion to the applied load [1].

Using a Norton relationship with a reference stress σ_o to describe a uniaxial tension test:

$$\frac{\dot{\epsilon}}{\dot{\epsilon}_o} = \left[\frac{\sigma}{\sigma_o}\right]^m \qquad \ldots \quad (4.1)$$

we attempt to relate a characteristic deformation U of the structure directly to the uniaxial data (obtained at the reference stress σ_o) through a geometric scaling factor β, so that [25]:

$$\dot{U}(t) = \beta(\text{geometry, loads, boundary cond., } m, \sigma_o) \cdot \dot{\epsilon}_o(t, \sigma_o)$$

The reference stress is chosen as some multiple α of a stress that is dependent on load and geometry only:

$$\sigma_o = \alpha \cdot \sigma \text{ (loads, geometry)}$$

in such a way that material dependence, geometry and load dependence occur in separate terms:

$$\dot{U}(t) = \beta(m, \alpha) \cdot f(\text{geometry}) \cdot \dot{\epsilon}_o(t, \sigma_o)$$

The reference stress, i.e. α, is then chosen in such a way that the scaling factor β varies as little as possible with variations in the material parameter m. So the correct choice of α results in a β that is effectively constant.

The above approach, refined by MacKenzie [26], is illustrated briefly by considering the curvature-rate of a rectangular cross-section beam (width b, height 2d) in pure bending:

$$\dot{\kappa} = \left[\frac{(2m+1)}{2m} \quad \frac{M}{bd^2\sigma_o}\right]^m \frac{\dot{\epsilon}_o}{d}$$

If the reference stress were chosen as

$$\sigma_o = 1.004 \frac{M}{bd^2} \quad \text{i.e.} \quad \alpha = 1.004$$

the term in square brackets will be seen to be practically constant for a wide range of m:

$$\left[\frac{(2m+1)}{2m\,\alpha}\right]^m \approx 1.572 \qquad 3 < m < 11$$

So for a rectangular beam in bending:

$$\text{if } \sigma_o = 1.004\frac{M}{bd^2} \quad \text{then } \kappa = 1.572\frac{\epsilon_o}{d}$$

where ϵ_o is the strain response obtained by subjecting a similar material to a uniaxial tension test at a load of σ_o and at the same temperature as the beam.

The MacKenzie method however has the disadvantage that it depends on analytical, closed-form solutions [25], which, except for some simple cases, are not available. In general, numerical solutions are obtained by computer, and so Sim [27] developed a numerical technique whereby it is proposed that the reference stress should be chosen so as to obtain equal deflections of a component for any two arbitrary values of the material exponent m [25]. So if U_1 and U_2 are the component deflections obtained numerically using exponent m_1 and m_2 respectively, a very good approximation to the reference stress is given by:

$$\alpha = \left[\frac{U_1}{U_2}\right]^{1/(m_1 - m_2)} \qquad \ldots \quad (4.2)$$

With this method however, a complete numerical creep analysis for the component would have to be carried out for at least two values of m. In view of the fact that for most cases the information at hand is only approximate, costly analyses become difficult to justify, especially if a further and fairly good order-of-magnitude method exists to estimate the reference stress [1, 24].

It can be observed that at the reference stress the component creep behaviour is insensitive to the magnitude of the material exponent m, and so m could assume a wide range of values without significantly affecting the creep response. Specifically, if m ∞ we have the case of a perfectly plastic material [25]. Thus Sim [27] proposed:

$$\sigma_o = \frac{P}{P_{coll}}\,\sigma_y \qquad \ldots \quad (4.3)$$

where P is the load on the component, and P_{coll} is the collapse load of the component assuming perfect plasticity at the yield stress σ_y. This approximation is an upper bound on the reference stress, and is thus a conservative design approach [1].

MacKenzie [26] has provided a very useful collection of reference stresses for various cases of beams, cylinders, and axisymmetric plates. In the following sections, [26] is used extensively, and attempts will be made to elaborate on the list of cases by establishing the reference stress for a circular cross section beam in bending. Further, in an attempt to find a reference stress for turbine blade applications, a centrifugally loaded tapered beam will be considered, as well as a tapered cantilever under non-uniform windage loads.

4.1 Reference stresses for circular cross section beams in bending

For a circular beam cross section of radius r the equilibrium and strain relations are:

$$M = 2\int_{-r}^{+r} \sigma y [r^2-y^2]^{\frac{1}{2}}\ dy \qquad \text{and} \qquad \dot{\epsilon} = \dot{\kappa} y$$

and in conjunction with the Norton creep relation eq. (4.1) yields:

$$M = 4\sigma_o \left[\frac{\dot{\kappa}}{\dot{\epsilon}_o}\right]^{1/m} \int_0^r y^{(m+1)/m} [r^2-y^2]^{\frac{1}{2}}\ dy$$

By transforming $y=r/2(t+1)$ a geometry independent integral I is obtained:

$$M = \sigma_o \left[\frac{\dot{\kappa} r}{2\dot{\epsilon}_o}\right]^{1/m} r^3\ I \quad \text{with} \quad I = \int_{-1}^{+1} (t+1)^{(m+1)/m} [1+\tfrac{1}{4}(t+1)^2]^{\frac{1}{2}}\ dt$$

If the reference stress is :

$$\sigma_o = \alpha \frac{M}{r^3}$$

the dimensionless curvature-rate becomes a function of m and α only:

$$\frac{\dot{\kappa} r}{\dot{\epsilon}_o} = 2\left[\frac{1}{I\ \alpha}\right]^m$$

A high order Gauss Quadrature procedure was used to evaluate the integral I, and thus the non-dimensional curvature rate above, for various α and m, as summarised in table 4.1.

Table 4.1: Non-dimensional curvature rates for selected α and m

α \ m	1	3	5	7	9	11
0.75	1.6920	1.8050	1.8292	1.8368	1.8386	1.8376
0.752	1.6882	1.7908	1.8050	1.8030	1.7950	1.7846
0.80	1.5870	1.4874	1.3246	1.1692	1.0286	0.9036
0.85	1.4936	1.2400	0.9782	0.7648	0.5960	0.4638

Using an initially arbitrary estimate for the reference stress of $\alpha=0.85$, the non-dimensional curvature rate is evaluated at $m_1=3$ and $m_2=7$ (see table 4.1). Sim's method of equation (4.2) can be used to obtain a good estimate for the reference stress:

$$\alpha = 0.85\left[\frac{1.2400}{0.7648}\right]^{1/(3-7)} = 0.753$$

The remaining values in table 4.1 are included for completeness and comparison, and are reproduced in fig. (4.1) to show that for $\alpha=0.752$ the curvature rate is not affected by changes in material exponent m.

Thus for a circular cross section beam in bending, if:

$$\sigma_o = 0.752\,\frac{M}{r^3} \quad \text{then} \quad \kappa = 1.79\,\frac{\epsilon_o}{r}$$

where ϵ_o is the creep of a uniaxial tension test at σ_o.

By comparison, the limit load approach of equation (4.3) can be used to obtain a further approximation to the reference stress:

$$M_{coll} = 2\sigma_o\frac{\pi}{2}r^2\,\frac{4r}{3\pi} \quad \text{so} \quad \sigma_o = 0.75\,\frac{M}{r^3}$$

From fig. (4.1) it is clear that the reference stress ($\alpha=0.75$) predicted by the limit load approach is a very good approximation to the "exact" reference stress ($\alpha=0.752$). However, the limit load method has the drawback that it provides no indication of the proportionality constant β between component and tension specimen deformations.

fig.(4.1): A ROUND CROSS-SECTION BEAM IN BENDING

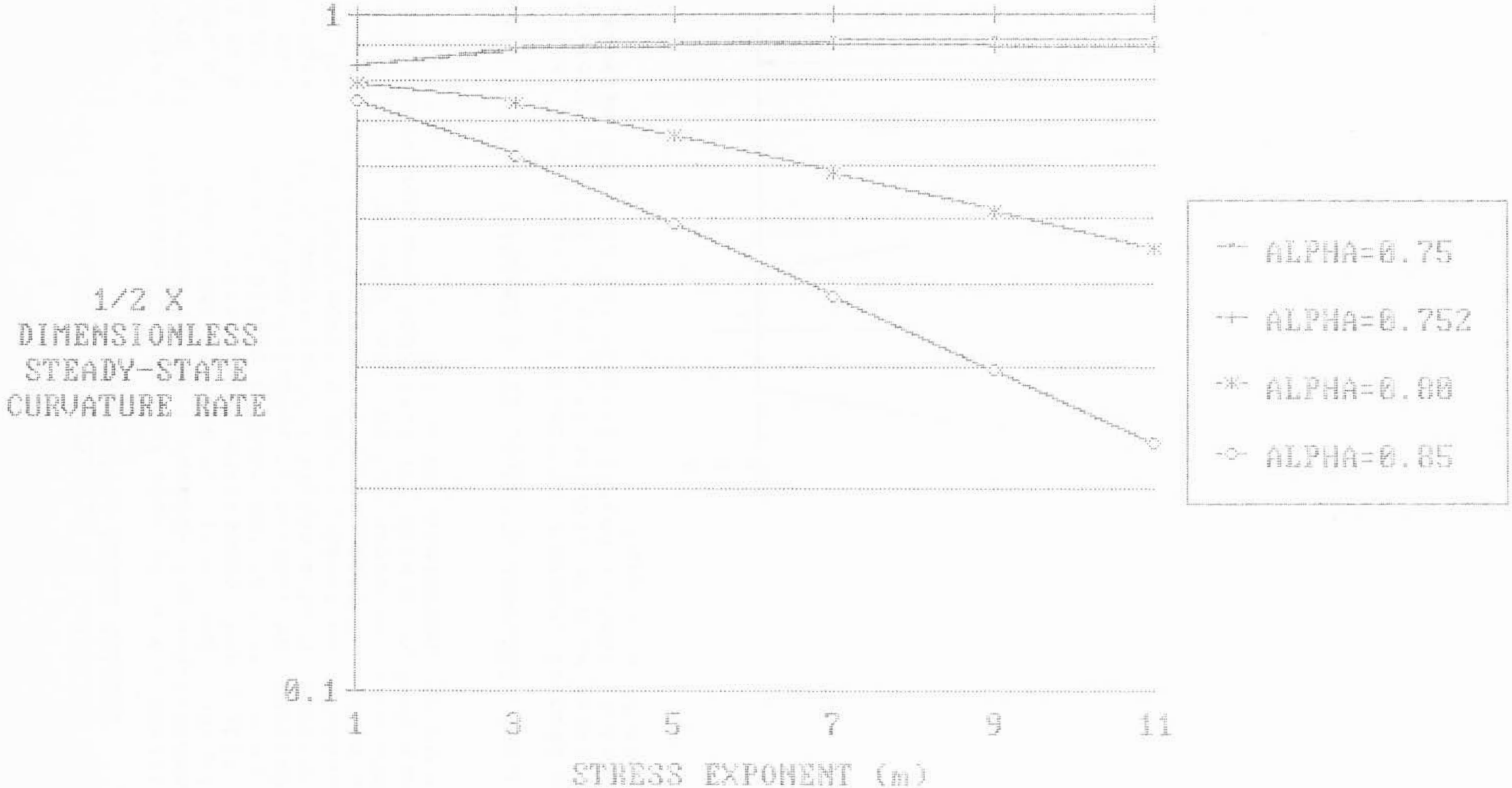

4.2 Estimates of reference stresses for turbine blade applications.

Attempts will be made to model alternately the effects of centrifugal and windage loads on turbine blades, by analysing a tapered cantilever. In view of the complexity in geometry, loading and temperature distribution, it should be stated at the outset that the results should be treated with caution. Besides the simplistic geometry and load modelling, the assumption of a constant blade temperature is especially suspect, as creep is highly temperature dependent, and substantial temperature variations between blade root and tip are known to occur in practice. However, the following analyses are presented with the view that poor approximations are better than no approximations at all.

4.2.1 Reference stresses for a spinning tapered beam.

A beam of length L is mounted on a rigid disk radius r_D, and rotates with an angular velocity $\dot{\theta}$. The root cross sectional area A tapers linearly towards the tip. The material of density ρ is used.

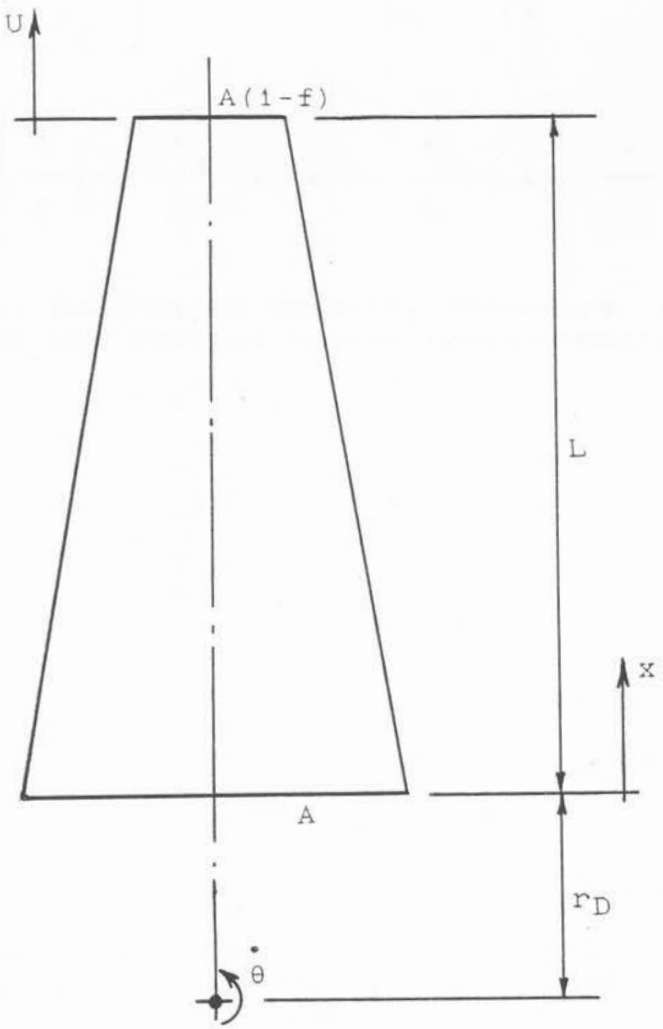

fig. (4.2) A spinning tapered beam

The cross sectional area at any distance x from the root is:

$$A(x) = A(1-\xi f) \qquad \text{with} \quad \xi = x/L$$

Equilibrium requires:

$$\sigma_x(x) = \int_x^L \rho\dot{\theta}^2 (x+r_D)\, A(1-\xi f)\, dx$$

Evaluating the integral yields:

$$\sigma_x(\xi) = \rho\dot{\theta}^2 AL^2 \left[\frac{1}{2}\left[1 - \frac{fr_D}{L}\right](1-\xi^2) + \frac{r_D}{L}(1-\xi) - \frac{f}{3}(1-\xi^3) \right]$$

Norton creep and compatibility require:

$$\dot{\epsilon}(x) = \dot{\epsilon}_o \left[\frac{\sigma_x(x)}{\sigma_o}\right]^m \qquad \text{and} \qquad \frac{\partial \dot{u}}{\partial x} = \dot{\epsilon}_x$$

so that:

$$\dot{u} = \dot{\epsilon}_o L \left[\frac{\rho\dot{\theta}^2 AL^2}{\sigma_o}\right]^m \int_0^1 \left[\frac{1}{2}\left[1 - \frac{fr_D}{L}\right](1-\xi^2) + \frac{r_D}{L}(1-\xi) - \frac{f}{3}(1-\xi^3) \right]^m d\xi$$

To facilitate a Gauss Quadrature solution procedure, the limits of integration are changed by the transformation:

$$\xi = 1/2(t+1)$$

to obtain:

$$\frac{2\dot{u}}{\dot{\epsilon}_o L} = \left[\frac{\rho\dot{\theta}^2 AL^2}{\sigma_o}\right]^m I$$

with:

$$I = \int_{-1}^{+1} \left[\frac{1}{2}\left[1 - \frac{fr_D}{L}\right](1-\tfrac{1}{4}(t+1)^2) + \frac{r_D}{L}(1-\tfrac{1}{2}(t+1)) - \frac{f}{3}(1-1/8(t+1)^3) \right]^m dt$$

This integral I is not independent of geometry, so specific values of f and r_D/L should be chosen, thereafter I is only a function of the material exponent m. As an example, set f=1/2 and r_D/L=1/3. If the reference stress is taken to be:

$$\sigma_o = \alpha\, \rho\dot{\theta}^2 AL^2$$

then the non-dimensional blade tip displacement rate is:

$$\frac{\dot{U}}{\dot{\epsilon}_o L} = \frac{1}{2}\left[\frac{I(m)}{\alpha^m}\right]$$

The non-dimensional blade tip displacement rate is evaluated numerically by Gaussian Quadrature for two arbitrary values of m. So the reference stress (ie. α) is obtained by Sim's method of equation (4.2), so that $\alpha=0.513$. In table 4.2 the non-dimensional blade tip displacement rate evaluated at the reference stress ($\alpha=0.513$) is confirmed to be independent of the material exponent m. It should be noted that the figures quoted apply only for geometries defined by $f=1/2$ and $r_D/L=1/3$.

Table 4.2: Non-dimensional blade tip displacement rates for selected m.

α \ m	1	3	5	7	9
0.513	0.6226	0.4484	0.4117	0.4117	0.4444

Thus for a spinning tapered beam with $f=1/2$ and $r_D/L=1/3$, if

$$\sigma_o = 0.513\ \rho\dot{\theta}^2 A L^2 \quad \text{then} \quad U = 0.43\ \dot{\epsilon}_o L$$

4.2.2 Reference stresses for a tapered cantilever.

Creep bending of a turbine blade will be modelled by a tapered cantilever rigidly fixed at the root. In the case of bending, the shape of the cross sectional area greatly affects the creep behaviour, as the difference in reference stress for rectangular and circular cross sections indicate. So approximating an airfoil section with a rectangular shape is suspect. However, the beam dimensions can be chosen so that the outer fibre stresses in the beam are comparable with the maximum stresses expected in the blade. Also, as the airfoil chord angle varies between the blade root and tip, the principal bending planes vary in orientation. In this analysis, however, the complex out-of-plane bending is approximated to be planar.

The windage loads are approximated by a parabolically varying distributed load such that pressures are zero at the root and tip, and the maximum pressure occurs at a distance 1/3 from the tip. So:

$$w(x) = \frac{27W}{4}\,\xi^2(1-\xi) \quad \text{with} \quad \xi = \frac{x}{L}$$

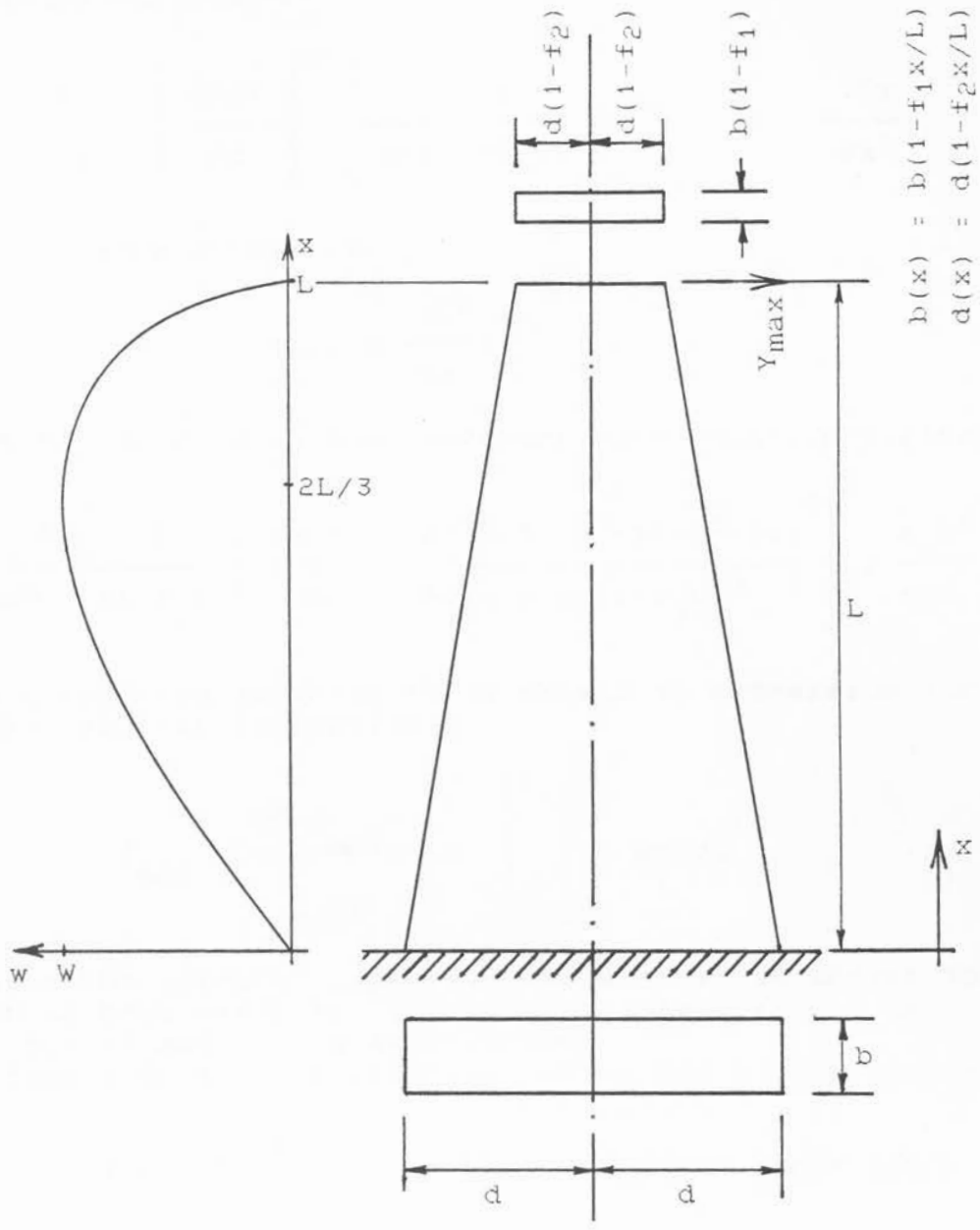

fig. (4.3) A tapered cantilever under non-uniform load

The shear force and bending moment are obtained by integration and applying the appropriate boundary conditions. So the bending moment is:

$$M(x) = \frac{27WL^2}{80}\left[\frac{5}{3}\xi(\xi^3-1) - \xi^5 + 1\right] \quad \text{and} \quad \xi = \frac{x}{L}$$

The curvature rate is:

$$\dot{\kappa} = \frac{\dot{\epsilon}_o}{d(x)} \left[\frac{2m+1}{2m}\right]^m \left[\frac{M(x)}{b(x)\, d^2(x)\, \sigma_o}\right]^m = \frac{\partial^2 \dot{y}}{\partial x^2}$$

and the reference stress is:

$$\sigma_o = \alpha \frac{WL^2}{bd^2}$$

Substituting M, b, d in the curvature rate equation yields:

$$\frac{\partial^2 \dot{y}}{\partial \xi^2} = \frac{\dot{\epsilon}_o L^2}{d\alpha^m} \left[\frac{1}{(1-f_2\xi)}\left[\frac{(2m+1)}{m} \frac{27[5/3\xi(\xi^3-1)-\xi^5+1]}{160(1-f_1\xi)(1-f_2\xi)^2}\right]^m\right] = \frac{\dot{\epsilon}_o L^2}{d\alpha^m} I$$

which is integrated numerically to obtain an expression for the non-dimensional tip deflection:

$$\dot{Y}_{max} = \frac{\alpha^m \dot{y}_{max} d}{\dot{\epsilon}_o L^2} = \int_0^1 \int_0^1 I \, d\xi \, d\xi$$

To evaluate the integral, specific values must be chosen for the taper in beam width f_1, and in beam height f_2. As an example, $f_1=1/2$ and $f_2=1/2$ were chosen.
Using a finite difference technique where for a step size $\Delta\xi=h$ we have:

$$I(\xi_i) = \frac{1}{h^2}\left[\dot{Y}_{i-1} - 2\dot{Y}_i + \dot{Y}_{i+1}\right] \quad \text{with error } O(h^2)$$

The boundary conditions for the fixed end require:

$$Y_0=0 \quad \text{and} \quad \frac{Y_1-Y_0}{h} \approx 0 \text{ i.e. } Y_1=0$$

With these starting values the iterative scheme

$$\dot{Y}_{i+1} = 2\dot{Y}_i - \dot{Y}_{i-1} + h^2 I(\xi_i) \qquad i=0, 1 \ldots n$$

can be applied successively for each increment $\Delta\xi$ along the beam to obtain the maximum deflection $Y_{max}=Y_n$. Taking $\Delta\xi=0.02$ estimates for Y_{max} can be made for various values of m, the creep exponent, shown in table 4.3 . Sim's technique in equation (4.2) is then used to obtain an estimate for α, and thus for the reference stress:

$$\alpha = \left[\frac{5.831E-5}{6.370E-3}\right]^{1/(7-3)} = 0.309$$

Further trials around this value of α have shown that for α=0.312 the non-dimensional tip deflection is even less dependent on the creep exponent, as the comparison in table 4.3 shows.

Table 4.3: Non-dimensional blade tip displacement rates for selected α and m.

α \ m	3	5	7	9	11	
	6.37E-3	5.98E-4	5.83E-5	5.86E-6	6.01E-7	$\dot{Y}_{max}$
0.309	0.3160	0.2115	0.2168	0.2284	0.2453	$\frac{\dot{Y}_{max}}{\alpha^m}$
0.312	0.2097	0.2016	0.2026	0.2094	0.2205	

Thus for a tapered cantilever with f_1=1/2 and f_2=1/2 under windage loads W, if:

$$\sigma_o = 0.312\,\frac{WL^2}{bd^2} \quad \text{then} \quad Y_{max} = 0.204\,\epsilon_o\frac{L^2}{d}$$

4.2.3 Thin walled cylinders

Lastly, results for thin walled cylinders [26] of radius r and wall thickness t under pressure p can be easily derived, so only the results from [26] are presented here.

For a closed end cylinder if:

$$\sigma_o = \frac{\sqrt{3}}{2}\frac{pr}{t} \quad \text{then} \quad -\epsilon_r = \epsilon_\theta = \frac{\sqrt{3}}{2}\epsilon_o \quad \text{and} \quad \epsilon_z = 0$$

For an open ended cylinder if:

$$\sigma_o = 1\frac{pr}{t} \quad \text{then} \quad \epsilon_r = \epsilon_z = -\tfrac{1}{2}\epsilon_o \quad \text{and} \quad \epsilon_\theta = \epsilon_o$$

5.0 Creep and damage predictions using FEM.

The Finite Element Method has been developed into a potent and versatile tool for stress analysis. Tremendous advances have also been made in the use of non-linear material constitutive models. Several material models have been refined to a point that they are now part of a standard library of user subroutines available in many finite element packages [31].

Also for creep analysis, the ABAQUS [31] finite element package provides a versatile library subroutine. The creep laws that are available are time hardening or strain hardening Norton and Bailey power laws:

$$\frac{\partial \epsilon_{cre}}{\partial t} = a\sigma_e^{m}\, t^{n}$$

involving the v. Mises stress and creep strain rate. An option also exists to use a hyperbolic sine law [3] for stress rather than a power law. With these program features, primary and secondary creep of complex geometries can be predicted with ease. Also the stress redistribution behaviour during primary creep is correctly modelled. The major disadvantage of this library subroutine however is that tertiary creep and damage accumulation are not included. Life assessments can thus not be made with this approach.

A final option within the creep analysis module of the ABAQUS package provides the possibility for the user to define his own creep constitutive law via a USER-CREEP subroutine. This option has been extensively investigated as a possible way to define a creep-damage material model. Creep and damage are defined as internal state variables. The evolution laws for damage and creep could be correctly defined, and their numerical integration proceeded stably and with acceptable accuracy. Primary creep stress redistribution behaviour was found to concur with known results [1]. However, during tertiary creep, the stress redistribution due to damage accumulation was absent. Thus erroneous rupture times were predicted. Damage accumulation causes a progressive reduction of the stiffness of the component, so that the elastic stress and strains change. As the USER-CREEP interface provides no means to modify the stiffness, tertiary stress redistribution cannot be correctly modelled from within the USER-CREEP program module. For this reason, this approach was aborted.

The ABAQUS package does however provide the possibility for a user to define his own material model in a very general way through the UMAT subroutine [31]. This requires a comprehensive definition from first principles of the material constitutive model. The basic equations of the displacement Finite Element Method will be presented [32], and specific attention is devoted to incorporating the concept of damage. The form of the material model evolves from these basic FEM equations.
The displacements and strains within an element are expressed as functions of the nodal displacements q:

$\underset{\sim}{u}(x,y,z) = \underset{\sim}{H}\underset{\sim}{q}$; $\underset{\sim}{\epsilon}(x,y,z) = \underset{\sim}{\epsilon}_{el}(x,y,z) + \underset{\sim}{\epsilon}_{cr}(x,y,z) = \underset{\sim}{B}\underset{\sim}{q}$

H is the displacement interpolation matrix of shapefunctions, and **B** is the strain-displacement matrix obtained by appropriately differentiating **H**. The elastic strain is related to stress:

$$\underset{\sim}{\sigma}(x,y,z) = \underset{\sim}{E}\underset{\sim}{\epsilon}_{el}(x,y,z) \quad \text{with} \quad \underset{\sim}{\sigma}(x,y,z) = \frac{\sigma_N(x,y,z)}{(1-\omega)}$$

Virtual Work considerations require, summing over all elements in the structure and integrating over the element:

$$\sum \int_V \delta S = \sum \int_V \delta W \qquad \ldots \quad (5.1)$$

Considering the RHS of equation (5.1), the virtual work done by active node forces, body forces and area forces is:

$$\sum \int_V \delta W = \sum \delta \underset{\sim}{q}^T \underset{\sim}{R}_F + \sum \int_{V_N} \delta \underset{\sim}{q}^T \underset{\sim}{H}^T \underset{\sim}{b} \, \partial V_N + \sum \int_{A_N} \delta \underset{\sim}{q}^T \underset{\sim}{H}^T \underset{\sim}{p} \, \partial A_N$$

$$= \delta \underset{\sim}{q}^T \sum \left(\underset{\sim}{R}_F + \underset{\sim}{R}_b + \underset{\sim}{R}_a \right) \qquad \ldots \quad (5.2)$$

The LHS of equation (5.1) is the strain energy:

$$\sum \int_V \delta S = \sum \int_V \delta \underset{\sim}{\epsilon}^T \underset{\sim}{\sigma} \, \partial V$$

The volume of material ∂V that is strained is not equal to the volume ∂V_N defined by the component geometry, due to the presence of voids. For n normal to A, $\partial V = \partial A \, \partial n$, but since $\partial A = \partial A_N (1-\omega)$ the volume of stressed material is $\partial V = \partial V_N (1-\omega)$. So:

$$\sum \int_V \delta S = \sum \int_{V_N} \delta \underset{\sim}{\epsilon}^T \underset{\sim}{\sigma} (1-\omega) \, \partial V_N \qquad \ldots \quad (5.3)$$

Incidentally, the substitution $\sigma_N = \sigma(1-\omega)$ into equation (5.3) cannot be used, as the actual -and not the nominal- stress are related to strain by $\sigma = E\epsilon_{el}$. Substituting for stresses and strains yields:

$$\sum \int_V \delta S = \delta \underset{\sim}{q}^T \sum \int_{V_N} \mathbf{B}^T \mathbf{E} \mathbf{B} (1-\omega) \, \partial V_N \cdot \underset{\sim}{q} + \delta \underset{\sim}{q}^T \sum \int_{V_N} \mathbf{B}^T \mathbf{E} \underset{\sim}{\epsilon}_{cr} (1-\omega) \, \partial V_N \qquad \ldots \quad (5.3a)$$

As damage is a scalar, we can set:

$$\mathbf{D}(\omega) = \mathbf{E} \, (1-\omega) \qquad \ldots \quad (5.4)$$

so that the element stiffness is:

$$\mathbf{K}(\omega) = \int_{V_N} \mathbf{B}^T \mathbf{D} \mathbf{B} \, \partial V_N$$

The pseudo creep load vector is:

$$\underset{\sim}{R}_{cr} = \int_{V_N} \mathbf{B}^T \mathbf{D} \underset{\sim}{\epsilon}_{cr} \, \partial V_N$$

so that finally equation (5.1) becomes:

$$\sum \mathbf{K}(\omega) \underset{\sim}{q} = \sum \left(\underset{\sim}{R}_F + \underset{\sim}{R}_b + \underset{\sim}{R}_a + \underset{\sim}{R}_{cr} \right) \quad . \; . \; . \quad (5.5)$$

This is a standard static creep Finite Element problem with a non-linear material. Equation (5.4) gives the form of the damaging material model. The statement $\mathbf{D}=\mathbf{E}(1-\omega)$ should however not be read to imply that the material properties of the load bearing material decrease. Clearly, the Youngs Modulus and Poisson Ratio are constant for a given temperature, and do not change as a result of damage. What is stated however, is that due to damage progressively less material is available to bear load, so that the component stiffness must decrease.

The equilibrium equation (5.5) is solved with an incremental strategy using the Newton tangent stiffness method. The state variables and stiffnesses are updated after each iteration. Loads are applied incrementally, and the creep evolution equation determines how the pseudo creep load vector is applied with respect to time t. As the iterations converge to the equilibrium solution, a set tolerance on out-of-balance forces determines when equilibrium is achieved. This tolerance also controlles the size of the time increments, as the stresses should vary as little as possible within a time step. From the equilibrium solution the total strain and nominal stresses are obtained at the end of every time step:

$$\underset{\sim}{\epsilon} = \mathbf{B}\underset{\sim}{q} \qquad \text{and} \qquad \underset{\sim}{\sigma}_N = \mathbf{D}(\mathbf{B}\underset{\sim}{q} - \underset{\sim}{\epsilon}_{cr})$$

For the UMAT subroutine to function correcty, certain required operations must be performed [31]:

1) The appropriate material Jacobian matrix (=D) must be updated to reflect conditions at the end of the time increment.

2) The nominal stresses must be updated to be the stress tensor at the end of the time increment.

3) All solution dependent state variables, in this case t, ω $\epsilon_{crij}, \sigma_{Nij}, \sigma_{ij}$, must be updated to the end of the increment. So the evolution equations for damage and creep strain must be stably integrated within the subroutine.

4) Any energy measures that might be appropriate, should be updated.

The main program passes the state of the material (i.e. $\tau, \Delta\tau, t, \omega, \sigma_{ij}, \epsilon_{ij}, \Delta\epsilon_{ij}, \epsilon_{crij}, D$) at the beginning of the time step to the subroutine. The updated state at the end of the time step must be returned to the main program.

A UMAT subroutine has been successfuly coded in Fortran, and includes the following features:

1) The first load-step provides the static elastic solution to the problem. UMAT supplies the appropriate isotropic stress-strain relationship at t=0, i.e. D=E. The material is presumed to be in a virgin state i.e. $\omega=0$, and no initial stresses or creep strains are present. The elastic loading is instantaneous.

2) The second load-step provides the creep solution subsequent to elastic loading, up to complete separation of the component. Complete rupture creates singularities in the stiffness matrix, causing the analysis to stop.

3) Fully 3-dimensional, plane stress, plane strain, axisymmetric, or uniaxial situations can be dealt with depending on the choice of elements. The material stiffness is initially homogeneous and isotropic (ie. Hooke's Law), but is progressively reduced by the scalar damage (equation (5.4)).

4) The state variables are evaluated at the Gauss Integration Points of each element, at the end of each time step.

5) Scalar damage accumulation proceeds as in equations (2.17) and (2.18). Tests to ensure positive τ_R, and thus positive damage increment $\Delta\omega$, are included. Should the maximum principal stress be in compression, damage accumulation ceases, and no damage is deemed to exist for the duration of compression. So equations (2.17a) and (2.18a) apply. The total accumulated damage is however retained, and is reactivated whenever a tensile state returns.

6) Rupture is deemed to have occurred whenever $\omega>0.95$, in which case damage and creep accummulation stop and stresses are set to zero. Also, failed material has zero stiffness. A test to ensure that damage never equals or exeeds 1.0 is included, as $\omega\geq1$ has unpredictable effects and the computations break down. At very high values of damage the equations become ill-conditioned, caused by either extremely small or extremely large numbers. At this stage the numerical integration can become unstable. From experience the damage integration should be terminated for $\omega\geq0.95$ to prevent such instability. The other alternative is to reduce the time increments even further, and so delay the onset of numerical instability to higher values of damage (say 0.98). Exeedingly small time steps and a lot of extra computer time are neccessary to proceed stably from $\omega=0.95$ to $\omega=0.98$, yet very little additional infomation is gained.

7) Creep strain accumulates subject to the time-hardening assumptions. Equation (2.19) is used, noting that $\epsilon_{cr}=\lambda_{cr}\epsilon_o$. After rupture, creep strain remains constant in tension. For

compressive maximum principal stress, the form of the creep rate equation changes and equation (2.19a) becomes appropriate.

8) In the main ABAQUS program, the transformed time τ is tallied. It is thus neccessary to transform τ back to the real time domain t at every time step. Real time is the 1st state variable defined, damage is the 2nd, followed by all creep strains and then all actual stresses. $\sigma=\sigma_N/(1-\omega)$ in tension, and $\sigma=\sigma_N$ in compression.

9) Explicit numerical integration has been used with respect to the changing stresses. A fully implicit algorithim has not been achieved. Further improvements in accuracy and/or reductions in computer run time could be expected from an implicit formulation.

In order to validate the UMAT subroutine coding, several test cases have been run. The material that was chosen to be modelled is a conventionally cast Nickel superalloy MAR-M 246. The operating temperature is 900 C. Experimental data [19] was used to obtain best estimates for the material constants by a curve fitting process. The method and the difficulties experienced with this process are elaborated on in section (3.2). The material constants that were used are listed in table (5.1):

Table 5.1: MAR-M 246 at 900 C

a	m	n	b	K=p	α	E	σ_o
1.5E-76	8.4	1.076	1.72E-76	8.5	1.0	155E9	290E6

In the various test runs the loads were chosen so that a reference stress of 290 [MPa] is appropriate. In general however, the relationship between applied load, geometry, and reference stress is not known with certainty. So here, the loads that result in a reference stress of 290 [MPa] are only approximated, and are obtained by estimation and iteration.

5.1 Uniaxial test cases

Predictions for a uniaxial tension specimen can be compared directly with available experimental data points (denoted +) in fig.(5.1a) for a load of 290 [MPa], and in fig.(5.1b) for a load of 340 [MPa]. Rupture lives of 450 hours and 130 hours respectively are predicted. The correlation of the predictions with experimental values essentially only indicates that the curve fitting procedure to obtain the material constants in table 5.1 has been successful. Yet again, the extreme sensitivity of the predictions to data scatter, and the high errors that can result, are highlighted.

In fig.(5.1c) a compressive load of 290 [MPa] is applied to a uniaxial specimen. As damage is suppressed in compression, no tertiary creep is predicted, and the steady state creep rate is as expected, constant. This model predicts the steady state

creep could continue ad infinitum, as no rupture criterion in compression has been incorporated. However the creep strain rate in fig (5.1c) compares well with the minimum creep strain rate from data [19].

A simple configuration to test primary and tertiary stress redistribution is the statically indeterminate two bar model shown in fig. (5.2a). Members 1 and 2 have lengths of 100 and 50 [mm] respectively, and have a cross sectional area of 200 [mm^2]. A constant load of 110 [KN] is applied, and it is estimated that this results in a reference stress of approximately 290 [MPa]. After elastic loading, primary stress redistribution occurs between the two members, shown in fig. (5.2d and e), and the steady-state is attained after about 50 hours. Although damage accumulates from the outset in fig. (5.2c), it only significantly affects behaviour during the 100 hours prior to rupture. As damage accumulates, tertiary stress redistribution in fig. (5.2d and e) occurs so as to transfer loads away from the most highly damaged member. The less damaged member is called upon to bear the extra load. So the nominal stresses reduce in member 2 and increase in member 1. Although the load in member 2 decreases, the damage there accumulates at such a high rate that the actual stress continues to rise.
Member 2 fails first followed a few minutes later by member 1. Upon rupture after a life of 620 hours, both the nominal and the actual stresses reduce to zero.

Also, the response of a uniaxial specimen to variable loads is discussed. In the first load case, a load of 290 [MPa] is applied to a specimen, and after 400 hours this load is steadily reduced until the specimen is completely unloaded 100 hours later (curve 1 in fig. (5.3a)). Damage in fig. (5.3c) accumulates rapidly up to t=400 hours, but as the load is reduced, the rate at which damage accumulates drops rapidly as the damage rate is proportional to stress to the k-th power. The actual stress (curve 2 in fig. (5.3a)) rises progressively further above the nominal stress (curve 1) due to ever increasing damage. In fig. (5.3b) the total strain rate also increases due to the accumulation of damage. However as the unloading begins, transitory primary creep is observed between t=400 and t=420 hours. Thereafter the strain rate is constant, i.e. a new steady state is attained. When the specimen is completely unloaded, the elastic strain has been entirely recovered, and only the accumulated creep strains cause a permanent set.

As a second load case the response to a cyclic load of 290 [MPa], alternating between tension and compression every 100 hours, is presented. The load variation (i.e. the nominal stress) is shown as curve 1 in fig. (5.4a). The damage, shown in fig. (5.4c), accumulates only during the tensile phase, and is not present during the compressive phase. Thus the actual stress (curve 2) and the nominal stress (curve 1) in fig. (5.4a) are equal only during the compressive phase, whereas in tension the actual stress rises increasingly further above the nominal stress due to increasing damage. The stress overshoot to below -290 [MPa] at t=700 for instance, illustrates the numerical stability problems discussed earlier. After rupture and separation after 835 hours, both nominal and actual stress

correctly reduce to zero. The strain history is shown in fig. (5.4b). The creep strain rate remains constant during all the compressive phases as it should, whereas damage accumulation causes a progressive increase in creep strain rate during the tensile phases. The elastic strain "jumps" at t=100, 200, . . . , 800 should also progressively increase because damage causes a reduction in specimen stiffness. This is however less apparent due to the graph scaling. The lifetime is predicted to be 835 hours, of which 435 hours were cumulatively spent under tension. This compares favourably with the 450 hours rupture life predicted for the same load constantly applied (fig. (5.1a)). To thus say that the component lifetime under cyclic load involving a compressive phase, is two times higher than the component lifetime under constant tension, is a fairly good initial estimate.

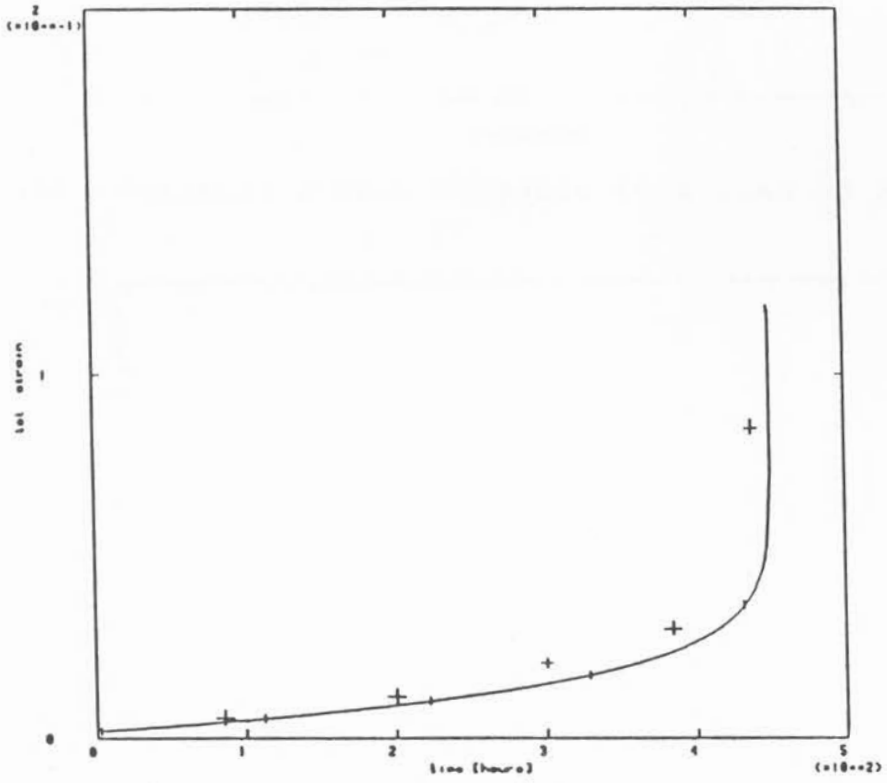

fig. (5.1a) **Uniaxial Strain Response to a Load of 290 MPa**

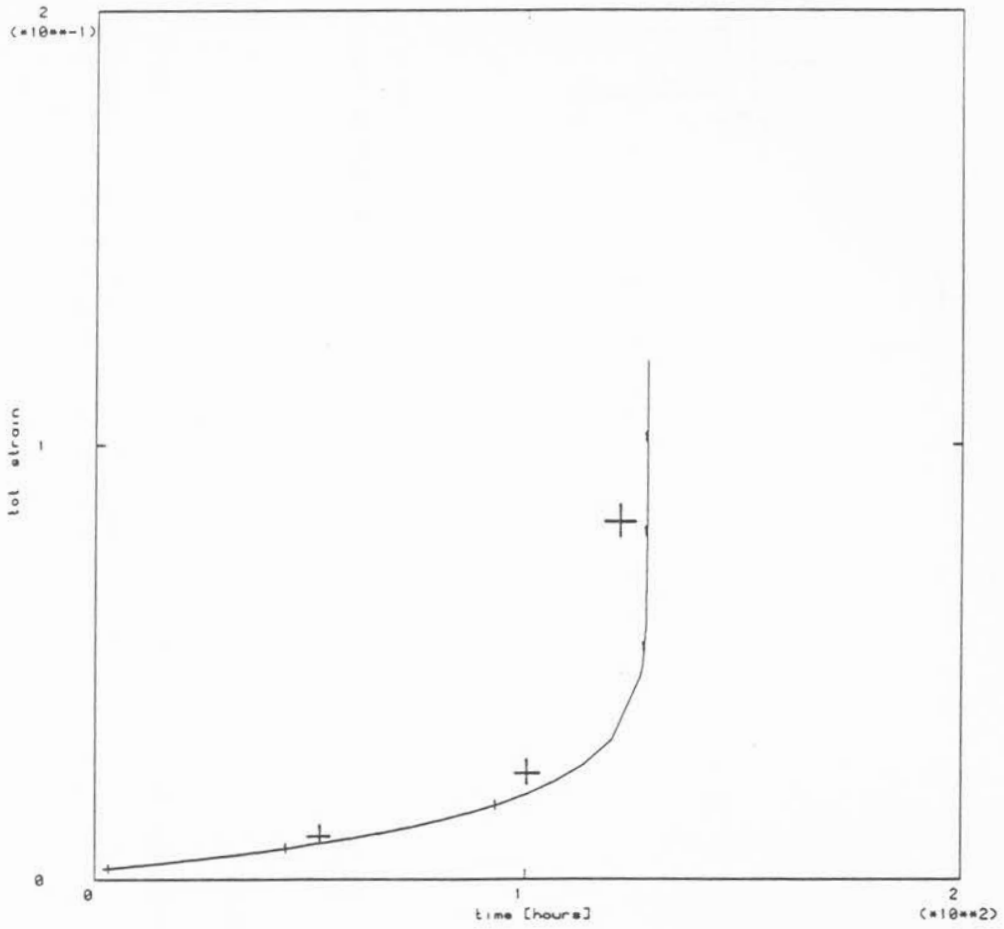

fig. (5.1b) Uniaxial strain response to a load of 340 MPa

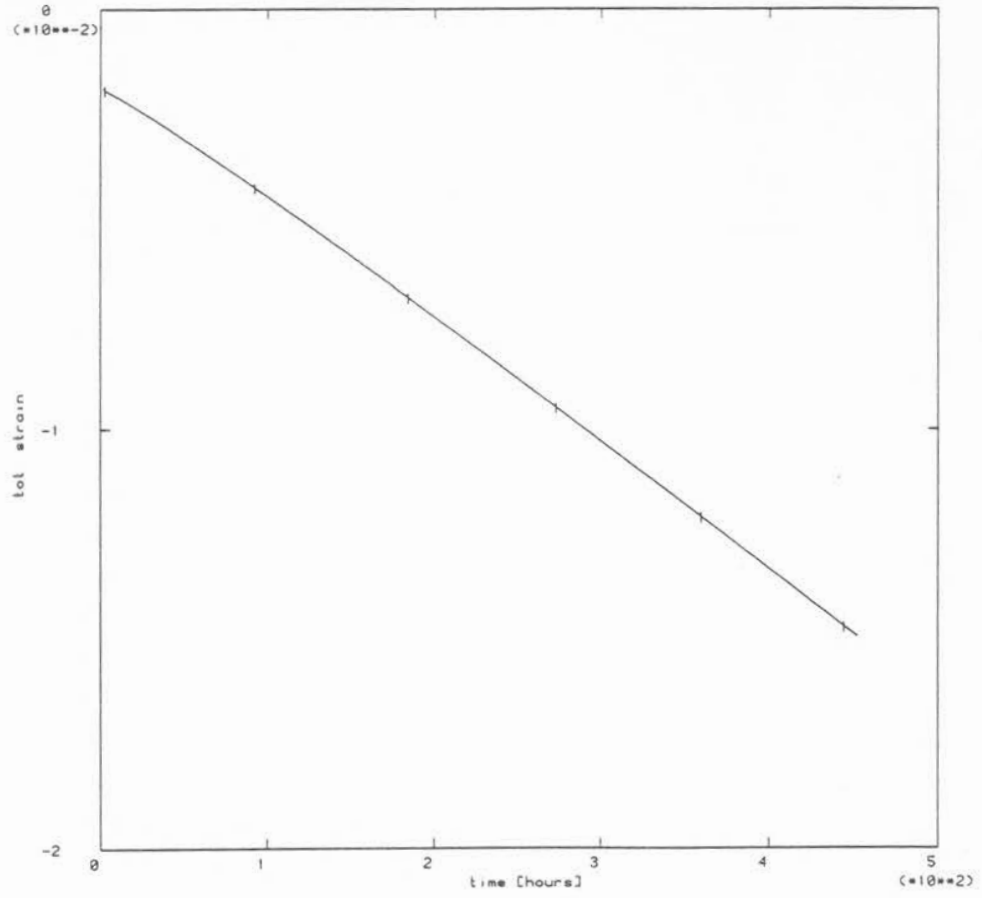

fig. (5.1c) Uniaxial strain response to a compressive load of 290 MPa

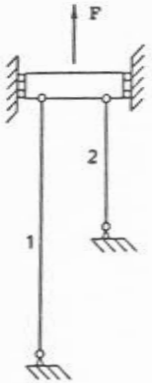

fig. (5.2a)

Two Bars in Tension

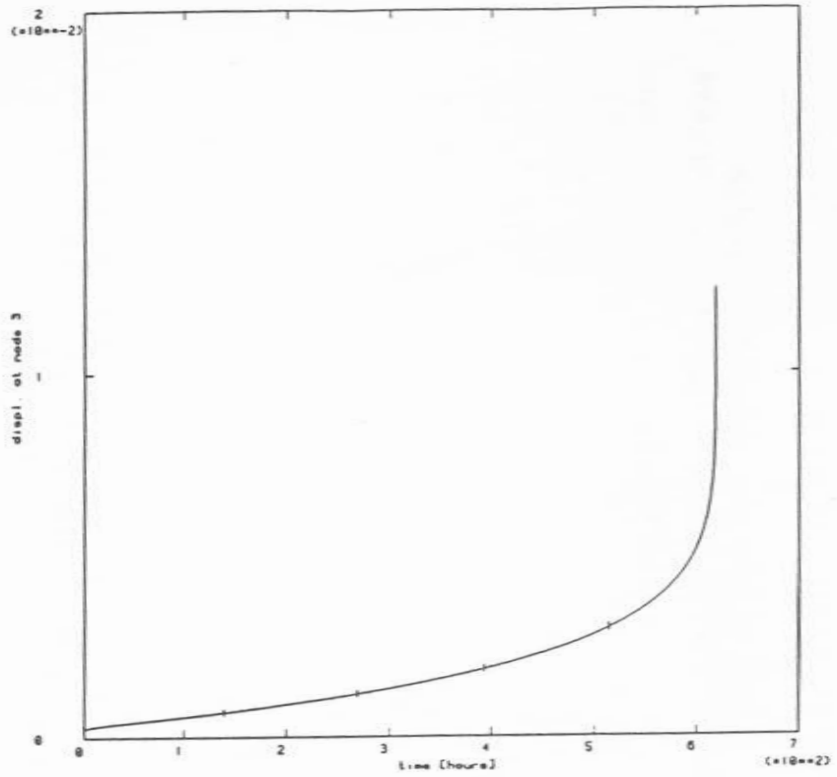

fig. (5.2b) **Crosshead Displacement in m**

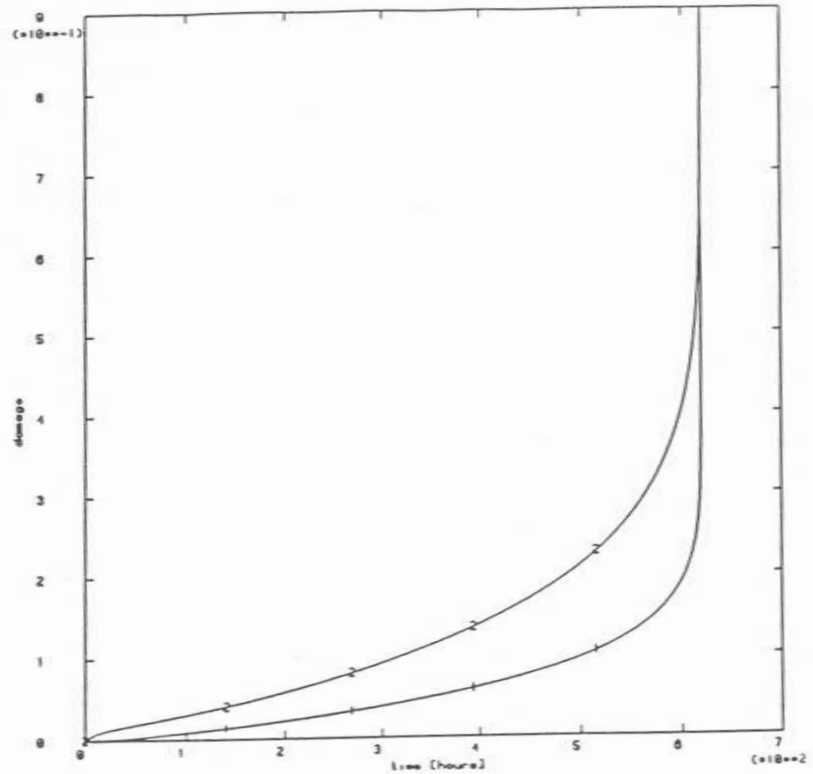

fig. (5.2c) **Damage History in Members 1 and 2**

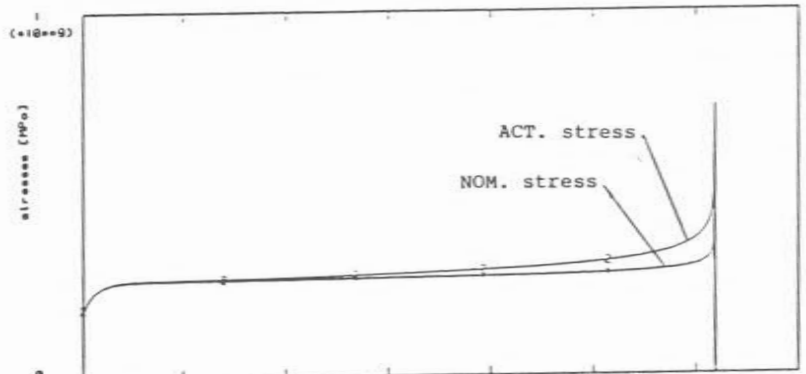

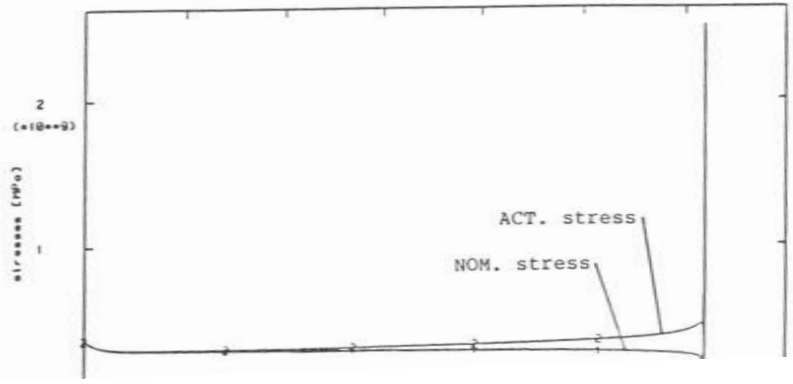

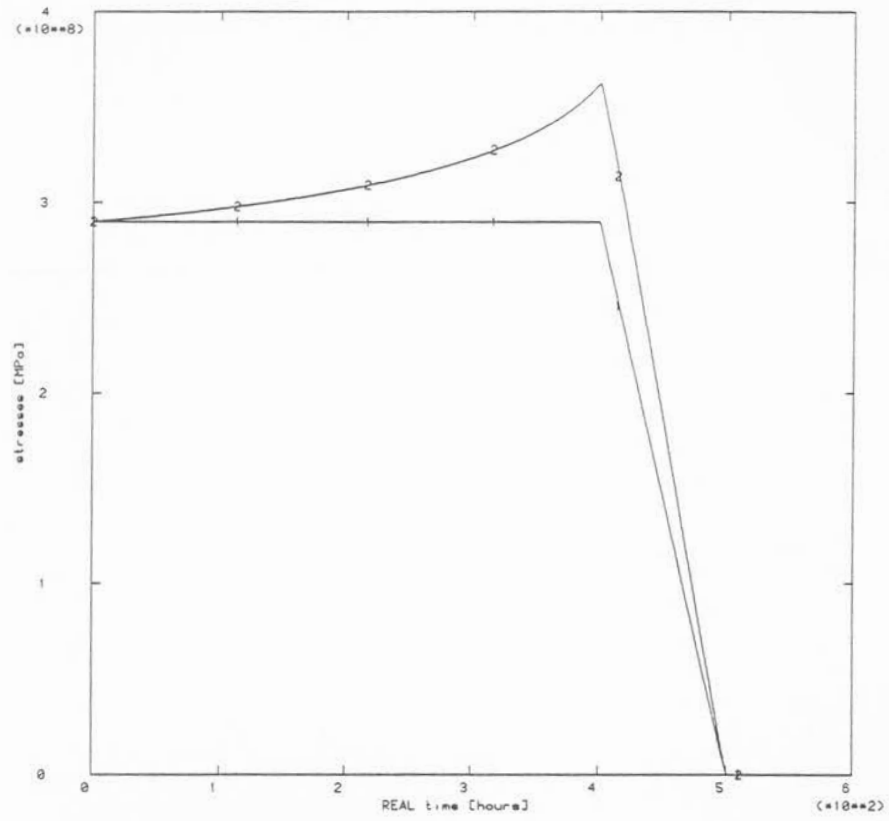

fig. (5.3a) Nominal (1) and actual (2) stress histories - ramp unloading

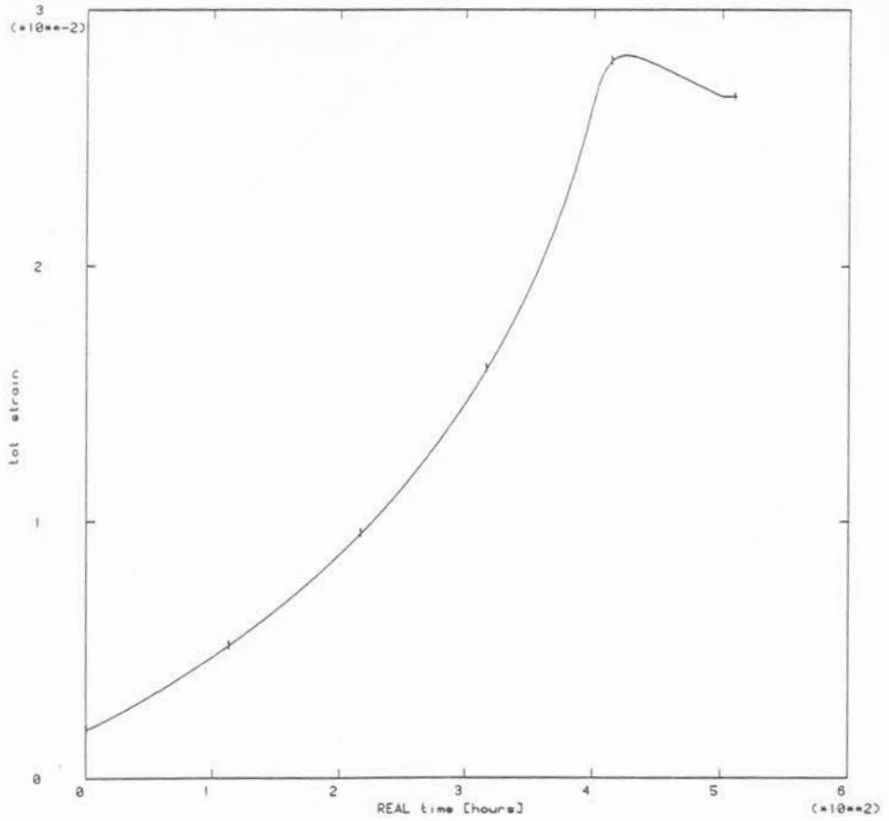

fig. (5.3b) Strain history - ramp unloading

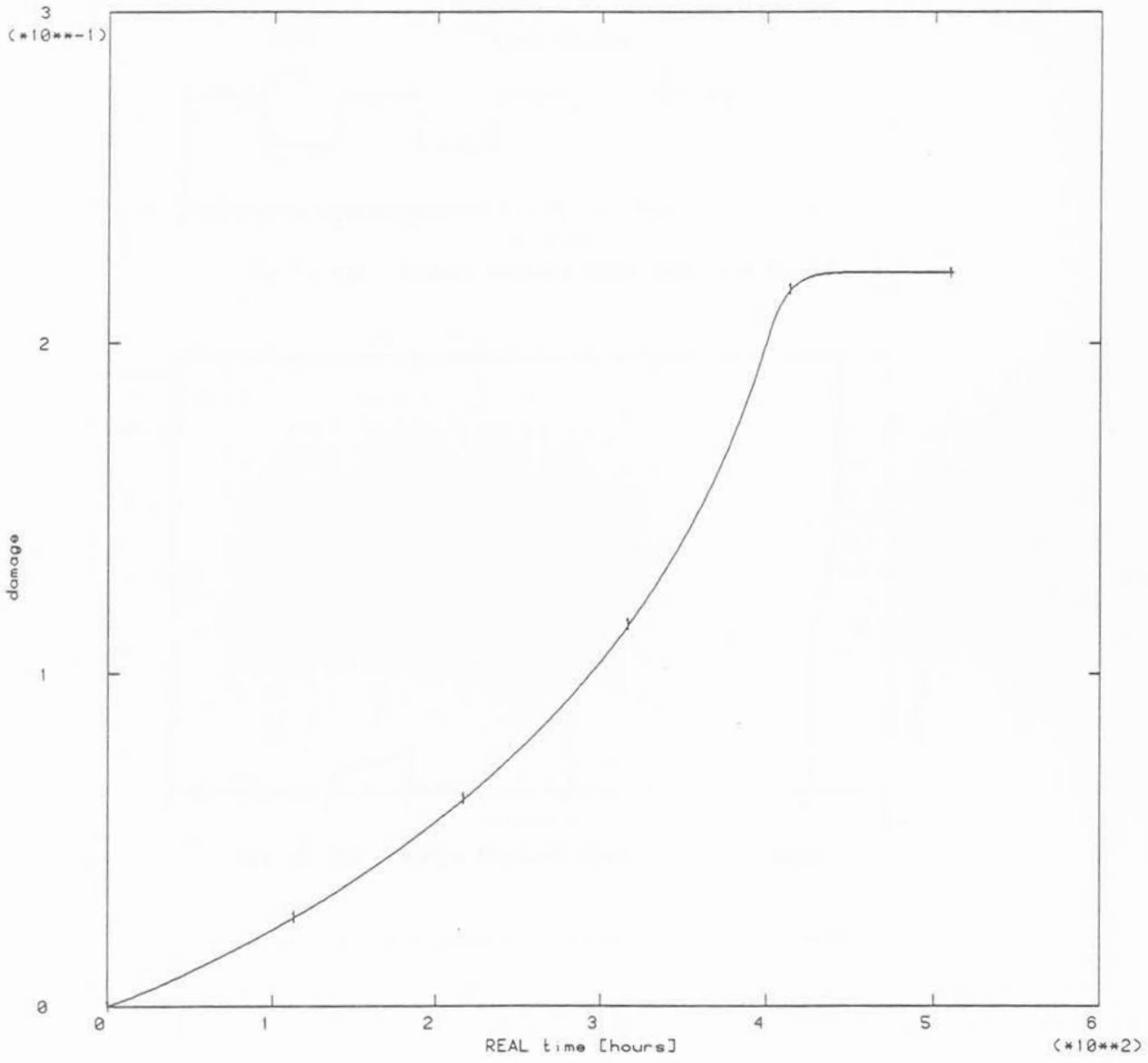

fig. (5.3c) Damage history - ramp unloading

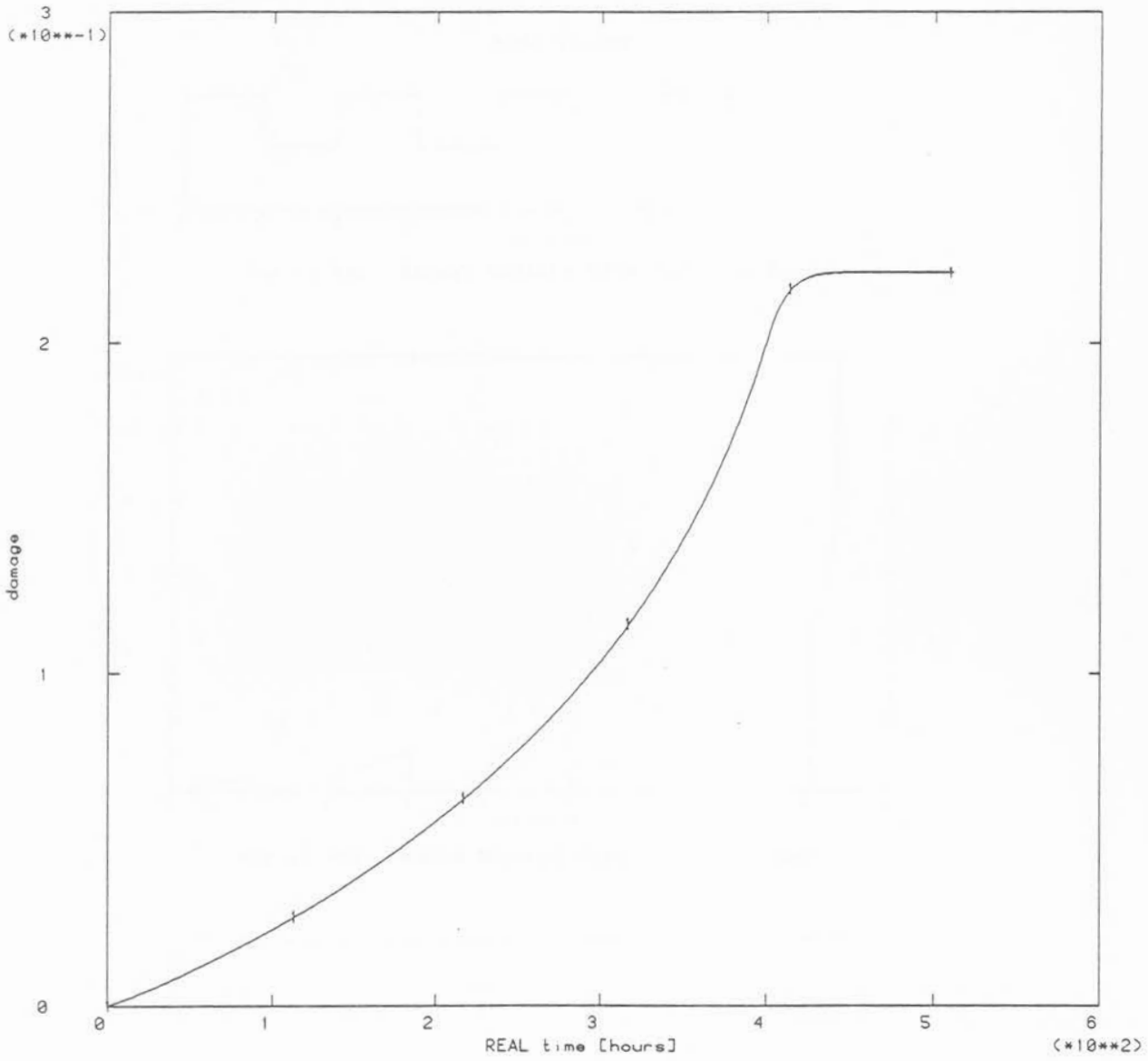

fig. (5.3c) Damage history - ramp unloading

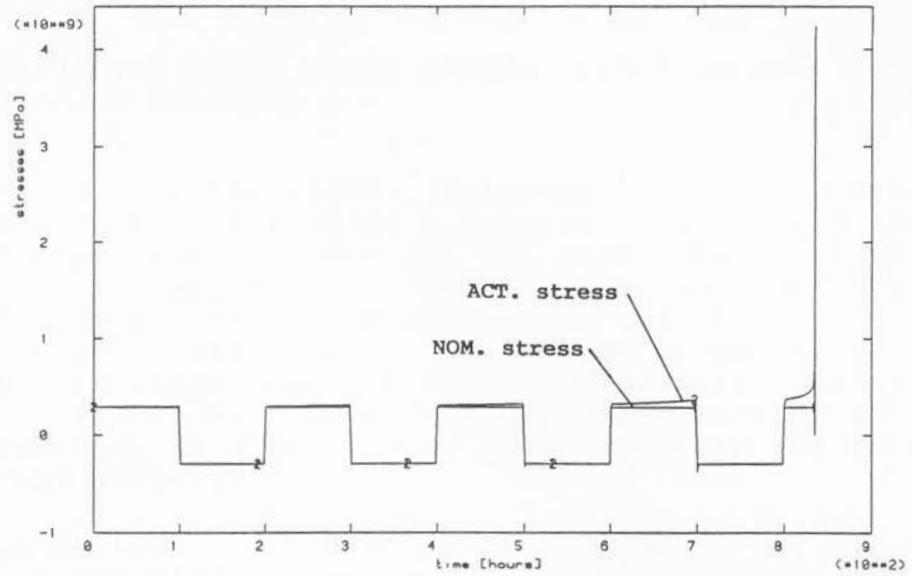

fig. (5.4a) Stress History With Variable Loads

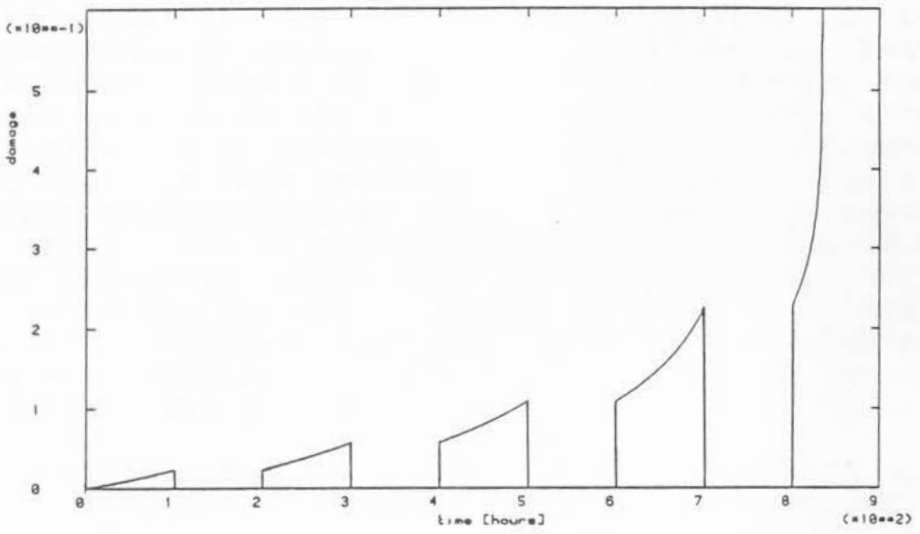

fig. (5.4b) Damage History With Variable Loads

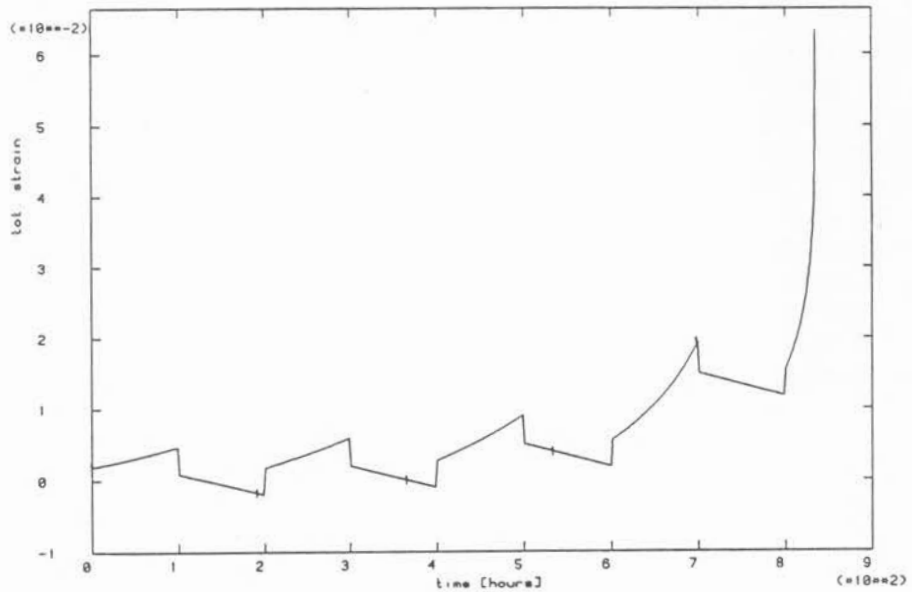

fig. (5.4c) Total Strain History With Variable Loads

5.2 Validation under plane stress, plane strain, axisymmetric, and 3D conditions

Plane strain, plane stress, axisymmetric, and 3D brick elements were all in turn subjected a uniaxial distributed load of 290 [MPa] in the y direction. The resulting total strain behaviour for all the four cases concurred exactly with the predictions for the uniaxial case in fig. (5.1a), for all the integration points sampled. The damage accumulation and the nominal and actual σ_{yy} history at integration points is shown in fig. (5.5a) and fig. (5.5b) respectively. As expected no difference in ω and σ_{yy} behaviour between the four element types was noticeable.

The σ_{xx} history ($=\sigma_{rr}$ for axisymm. element) for all element types is depicted in fig. (5.5c). Although σ_{xx} is correctly zero for the largest part of the lifetime, significant errors occur just prior to rupture. The high errors just before rupture can be ascribed to the fact that at very high damage values the structure stiffness is very low, and therefore the numerical algorithim has increasing difficulty converging. Reducing the time step will result in smaller errors; however, the instability persists because as the stiffness tends to zero, a zero time increment would be neccessary for stability. The analyst should ensure that the time increment is sufficiently small to confine the error accumulation as close as possible to rupture. The predictions close to rupture should thus be treated with extreme suspicion. Apart from the numerical difficulties, the fact that final failure is caused by plastic collapse and not creep should further underline the suspicion. However, as errors are confined to times just prior to failure, the creep analysis for the preceding history is still valid.

The σ_{zz} history for the 3D brick element, and the $\sigma_{\theta\theta}$ history for the axisymmetric element have a similar appearance as σ_{xx} in fig. (5.5c), and similar error behaviour occurs at rupture. For the plane strain case the σ_{zz} evolution is shown in fig. (5.5d), where the effect of progressively reducing stiffness becomes apparent.

When the plane stress, plane strain, axisymmetric or 3D brick elements are subjected to a compressive distributed load of 290 [MPa], the same total strain history as in fig. (5.1c) is obtained. The constant strain rate clearly indicates that no damage is accumulated in compression. Therefore this behavioural aspect of the constitutive model is correctly reproduced in the subroutine coding. Also, the magnitude of the constant strain rate in fig. (5.1c) in compression is in close agreement with the magnitude of the minimum strain rate in fig. (5.1a) in tension. As the load magnitudes in tension and compression are equal, a similarity in the minimum strain rates should not be suprising.

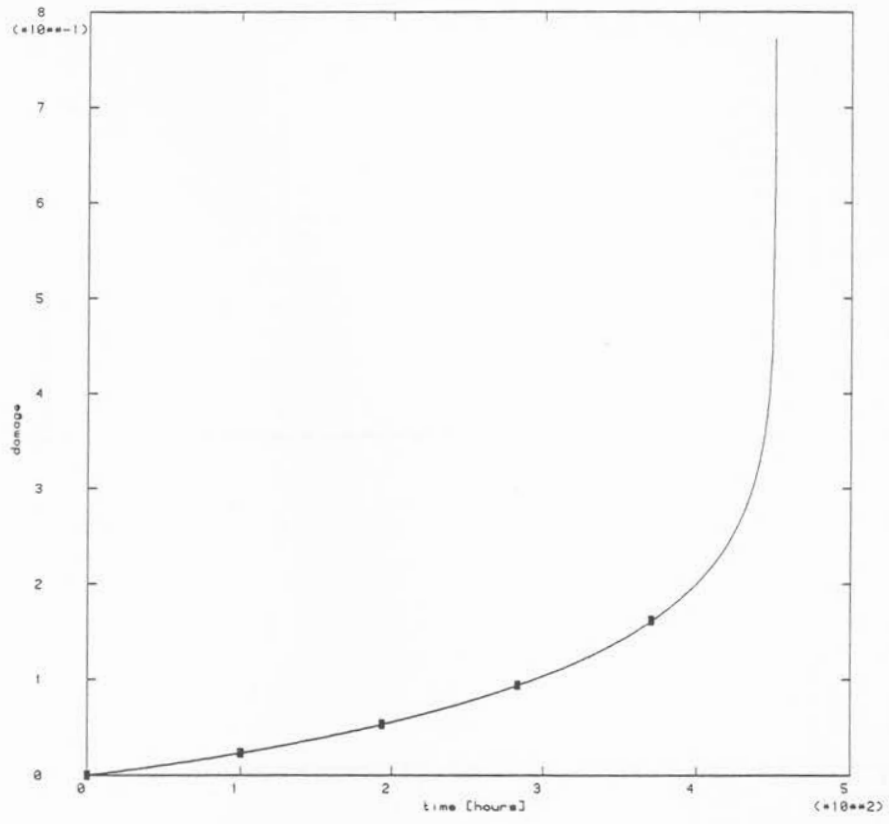

fig. (5.5a) Damage history

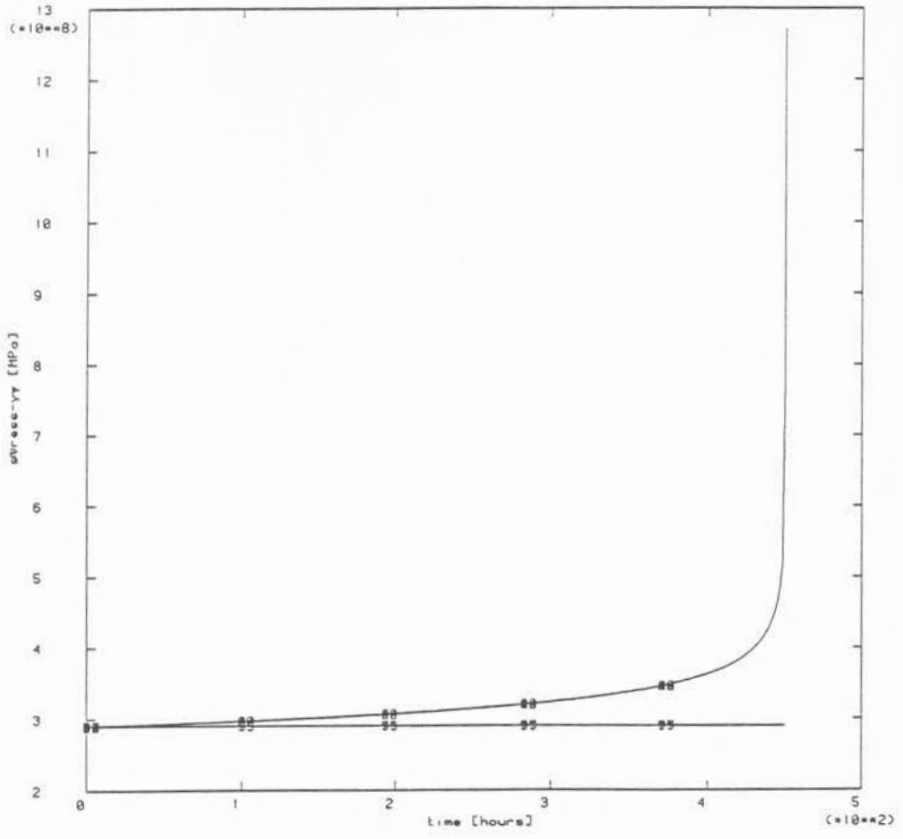

fig. (5.5b) Stress σ_{yy} history

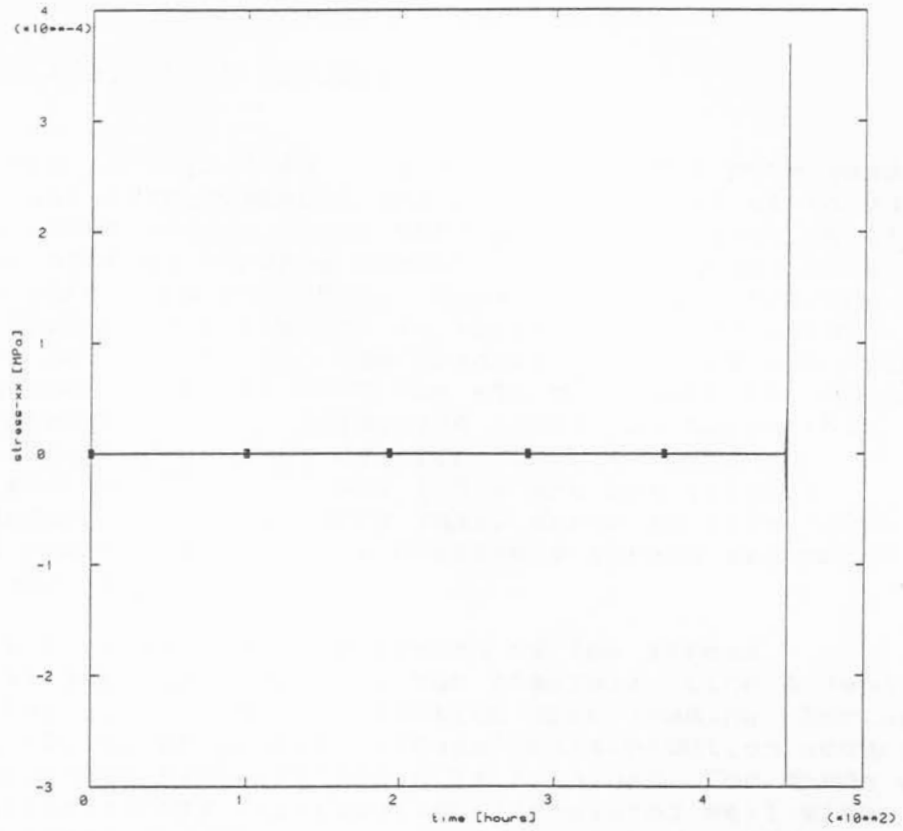

fig. (5.5c) Stress σ_{xx} history, and σ_{zz} history for a brick element

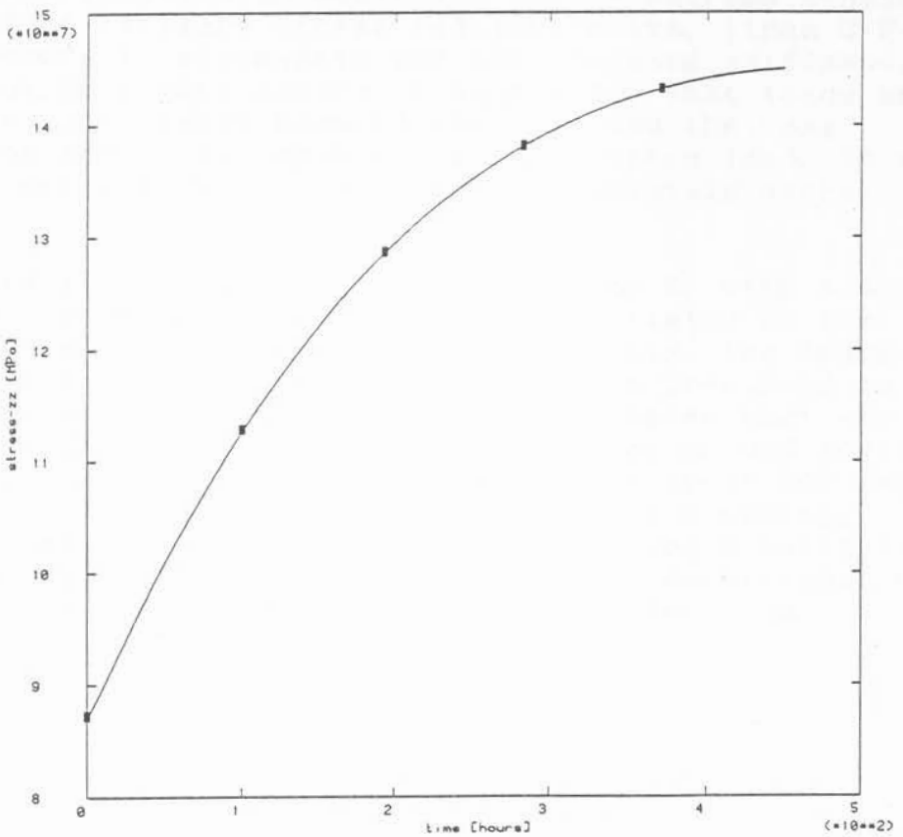

fig. (5.5d) Stress σ_{zz} history in plane strain

5.3 Model verification in bending

A beam, depicted in fig. (5.6a), is subjected to a pure bending moment. The nodal displacements are constrained so as to ensure that plane sections remain plane throughout the lifetime of the component. The applied bending moment has been chosen such that the reference stress is 290 [MPa]. Thus the beam curvature history will appear very similar in shape to the uniaxial strain history in fig. (5.1a). The predicted life of 494 hours in bending should correlate with the 450 hour life for uniaxial tension. The discrepancy in predicted lives indicates that estimates of the reference stress for the bending case (reviewed in section 4.0, [1] and [26]) are not totally accurate. However, the relatively small error in life (10%) that resulted indicates that the reference stress estimates are still useful and valuable.

Fig. (5.6b) illustrates the progression of the stress distribution at various stages in the analysis. Line A depicts the initial elastic stress distribution upon loading. During the following 150 hours primary stress redistribution occurs until a steady state distribution B is attained. The shape of this steady state stress distribution correlates well with findings from other sources [1]. In fig. (5.6c) the damage evolution at various times is shown. As expected, no damage accumulates under compressive loads. Damage accumulates fastest where the stress is highest. The damage accumulation C-F causes weakening and a reduction in stiffness in the extreme tension fibres. Therefore tertiary stress redistribution, lines C-F in fig. (5.6b), occurs to accomodate for the changing stiffness. The redistribution always occurs in such a way that loads are reduced in the most highly damaged regions, and the less damaged regions are called upon to bear the extra load. So the neutral axis, originally at z=0, shifts to maintain overall equilibrium.

Damage accumulates in fig. (5.6c) until at time E, with a mere 0.5% lifetime remaining, a crack is fully initiated at the extreme tension surface, where $\omega=1$. Subsequently, the crack rapidly grows inward (F) and total collapse is predicted to occur after a life of 494 hours. The high stresses that are predicted to occur immediately prior to failure should however be viewed with caution. At stress levels above about 600 [MPa], the behaviour is dominated by extensive plastic yielding, rather than creep-damage growth. As instantaneous plasticity effects are not included in this analysis, the conditions just prior to complete plastic collapse are poorly modelled.

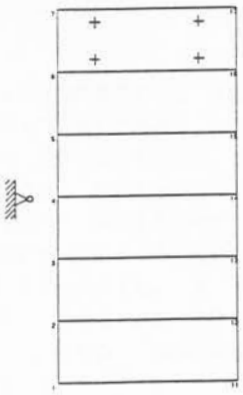

	t	t/t_f %
A	0	0
B	150	30,4
C	373	75,5
D	478	96,7
E	492	99,5
F	494	100

fig. (5.6a) Element Arrangement in Bending

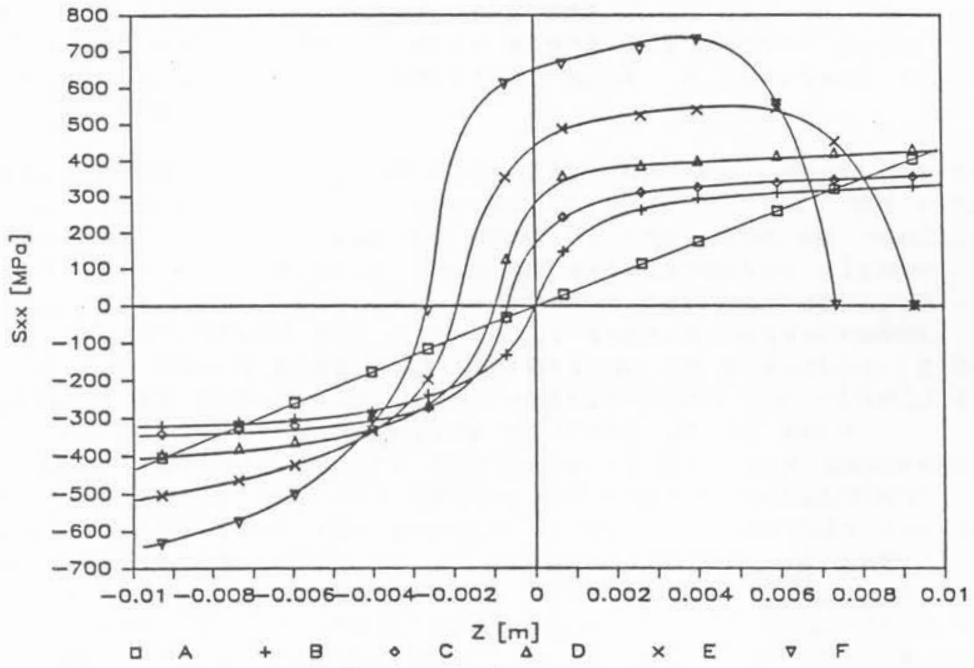

fig. (5.6b) Actual Stress Distributions Across beam Section

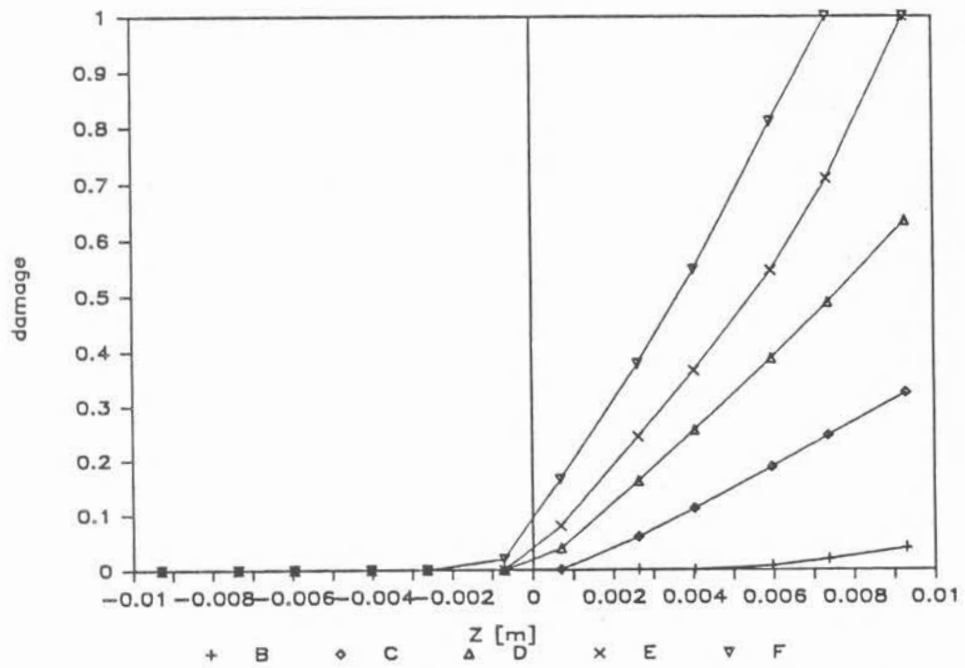

fig. (5.6c) Damage Distributions Across Beam Section

5.4 Predictions for a notched axisymmetric tension specimen

With a notched axisymmetric tension specimen we demonstrate the effects of geometric stress concentrations on creep and damage evolution, and the resulting stress redistributions. In the previous two sections only very simple situations were examined in order to ascertain whether the subroutine model behaves as it should, and where pitfalls and errors can be expected. In this more complex example, a further step is taken towards analysing realistic design problems. The total interaction of stress gradients, creep, damage and stress redistribution is a feature of this case.

A specimen of 20mm diameter with an annular notch of 3mm is modelled with a mesh consisting of 8 noded quadratic axisymmetric elements, shown as frame C in fig. (5.7a). An axis of revolution exists vertically along the centre line, and there is symmetry about the horizontal r-axis. A constant tensile load of 120 MPa is applied.

The displacement history of node 222, on the upper extremity along the centre line, is plotted in fig. (5.7b). The intention with this history plot was to predict the type of readings that one would expect to obtain from an extensometer clipped across the notch. The typical creep behaviour becomes apparent: Without sophisticated and continual strain measurement, the behaviour A-C could give the impression of a stable, elastic situation. Even non-destructive examination for cracks etc. does not reveal that a damaging process is at work. Catastrophic failure occurs suddenly (C-F), and apparently without warning or special cause. Of course subsequent micrographs show that the growth of microvoids has caused failure, but while creep is in progress there is very little that could reveal timeously when failure is likely. With the latest non-destructive testing technology, cracks of 0.1 mm can be detected. Therefore the earliest stage when cracks could be detected in this case would be at time C with a mere 8 hours (3% of the total lifetime) remaining. As in practice the rupture time is not known accurately, a sophisticated NDT would have to be conducted at a *maximum* interval of about every 7 hours in order to detect and prevent catastrophic failure. The logistics and practicability of such a test programme become a problem.

Fig. (5.7c) shows the stress distributions σ_{zz} across the throat section of the specimen, at various times throughout the history. The elastic stress distribution is shown as line A. The effect of primary stress redistribution is to reduce the elastic stress concentration at the notch root, until the steady state B is attained. For the largest part of the specimen life (B-C) the stress distribution remains fairly static. Intuitively, one might expect the highest stresses at the notch root. In fact, the highest steady state stresses occur in the adjoining subsurface. Damage thus accumulates fastest just below the surface. The damage accumulates until at a time C in fig. (5.7a) a crack is fully initiated with only 3% of the total lifetime remaining. Regions shaded black indicate failed regions, where $\omega=1$. The subsequent rapid propagation of this crack is traced by the damage plots C-F in fig. (5.7a).

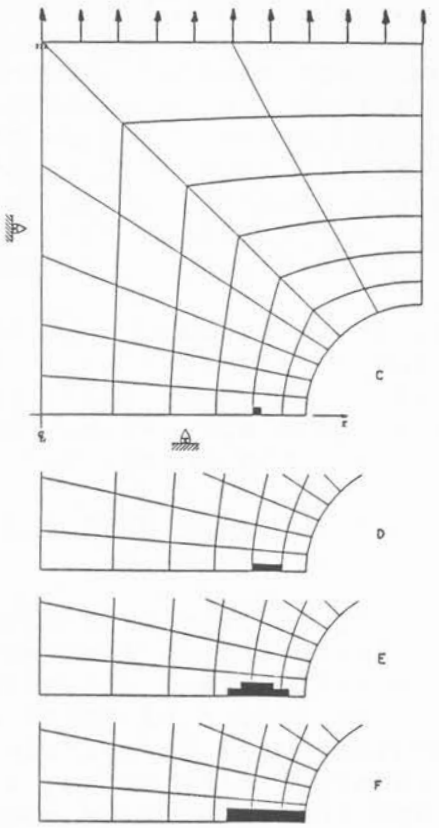

fig. (5.7a) Damage Evolution in an Axisymmetric Tension Specimen

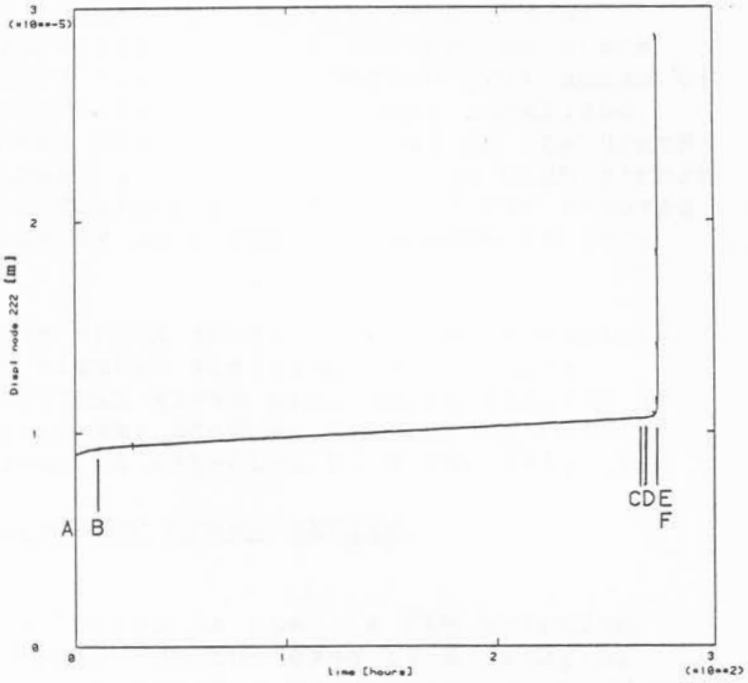

fig. (5.7b) Displacement History, node 222

	remaining life,h	t/t_f %
A	274	0
B	261,6	4,5
C	8,8	96,8
D	3,0	98,9
E	2,7	99,0
F	minutes	100,0

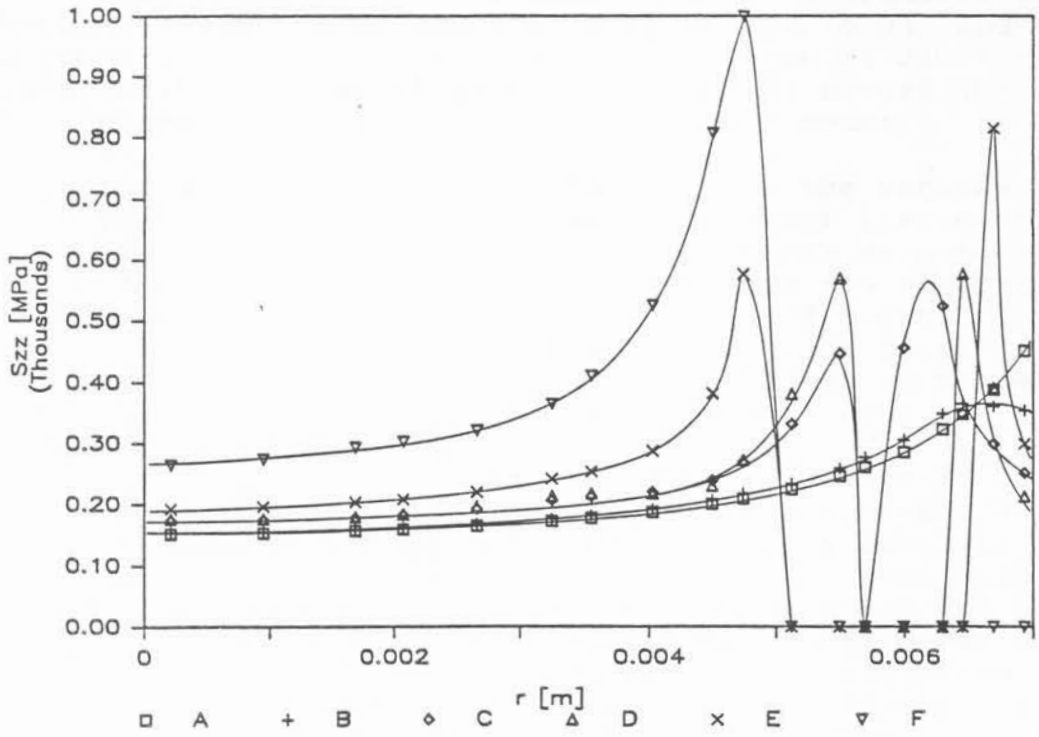

fig. (5.7c) Actual Stress Distributions Across the Throat Section

The stress behaviour during crack propagation is shown by curves C-F in fig. (5.7c). Stresses are zero across the crack surface, however they are very high in the region just ahead of the crack front. Damage accumulation is thus very localised, and limited to the high stress regions just ahead of the crack front. The crack will propagate into this region of high stress. Even at an advanced stage of failure F, the damage far removed from the crack is low; typically at r=3mm the damage is less than 1%.

The very high stresses in the crack front just before rupture (F) indicate that extensive plastic yielding has occurred. Realising that the creep analysis gives misleading results in such cases, the creep analysis was stopped at time F, and instantaneous plastic collapse is expected to occur after 274 h.

5.4.1 Mesh sensitivity studies for creep damage

Whenever a softening material model is used, a FEM solution is dependent on the mesh refinement. In the case of a damaging material, $D=E(1-\omega)$ as microvoids cause a reduction in stiffness. In order to establish to what extent the creep solution is sensitive to mesh refinement, the axisymmetric notch problem was re-run with different mesh sizes. Boundary conditions and loads were identical for all runs. The number of elements across the throat were taken as a measure of mesh refinement.

For 4 elements across the throat, the damage evolution and stress distributions are shown in fig. (5.8a) and fig. (5.8b) respectively. A rupture time of 276.3 hours was predicted. The original mesh, 6 elements across the throat, is discussed at length in section 5.4, and fig. (5.7a-c). Here a rupture time of 274 hours was predicted. Refining the mesh to 8 elements across the throat yielded the damage evolution in fig. (5.9a) and the stress behaviour in fig. (5.9b), with a lifetime of 260.9 hours. The finest mesh size investigated, 16 elements across the throat, yielded a predicted lifetime of 260.1 hours.

Comparing the damage and stress behaviour for the various levels of mesh refinement, it becomes clear that the location where the crack initiates (frames C) varies from mesh to mesh. Results from finer meshes further substantiate the observation that damage accumulation is very localised, and limited to a very small plastic region just ahead of the crack front. Although the location and extent of damage appear to be mesh sensitive, the stress and strain magnitudes are not.

The sensitivity of predicted rupture times to mesh size is shown in fig. (5.10). Rupture times converge to a steady value of 260 hours with increasing mesh refinement. In absolute terms however, the rupture life is not so sensitive to mesh size: The difference in predicted rupture life for the crudest and finest mesh is only 6% . Crude meshes are however less conservative. As mentioned in previous sections, the difference between *actual* and predicted rupture times can be high (30%+), due to problems associated with data scatter, and refining the mesh will not alleviate these problems. Thus there is little merit in using fine meshes.

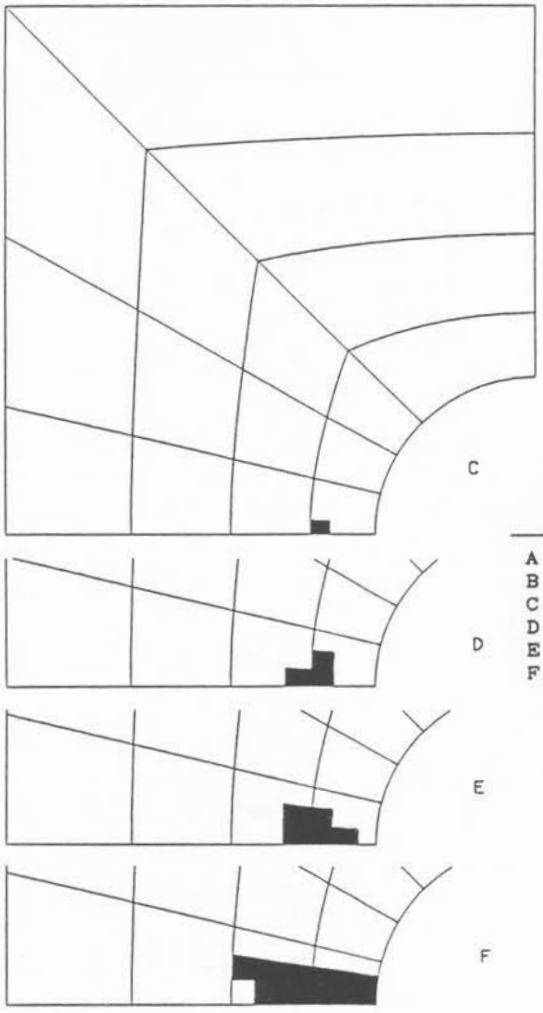

	remaining life [h]	t/tF %
A	276.3	0.0
B	206.0	25.5
C	25.3	90.9
D	2.4	99.1
E	0.5	99.8
F	0.0	100.0

fig. (5.8a) Damage evolution in an axisymmetric tension specimen

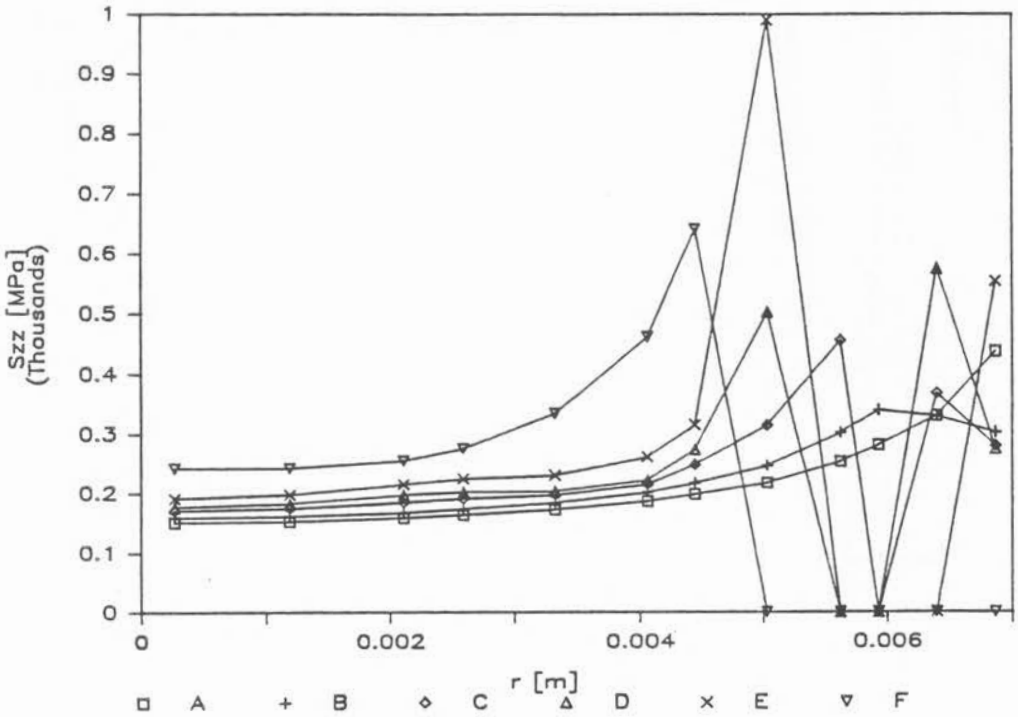

fig. (5.8b) Actual stress distribution across the throat section

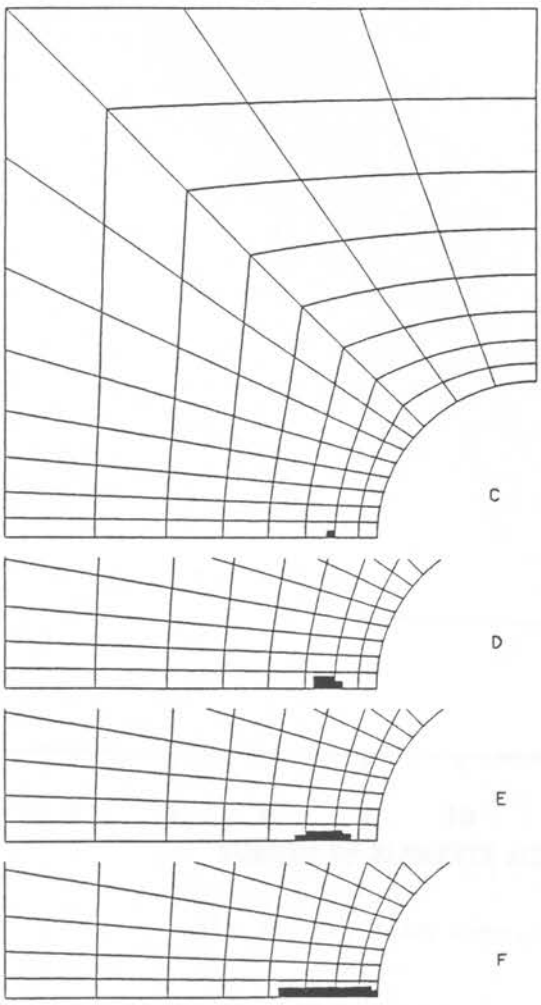

	remaining life [h]	t/tF %
A	260.9	0.0
B	190.6	26.9
C	5.4	97.9
D	0.3	99.8
E	0.1	99.9
F	0.0	100.0

fig. (5.9a) Damage evolution in an axisymmetric tension specimen

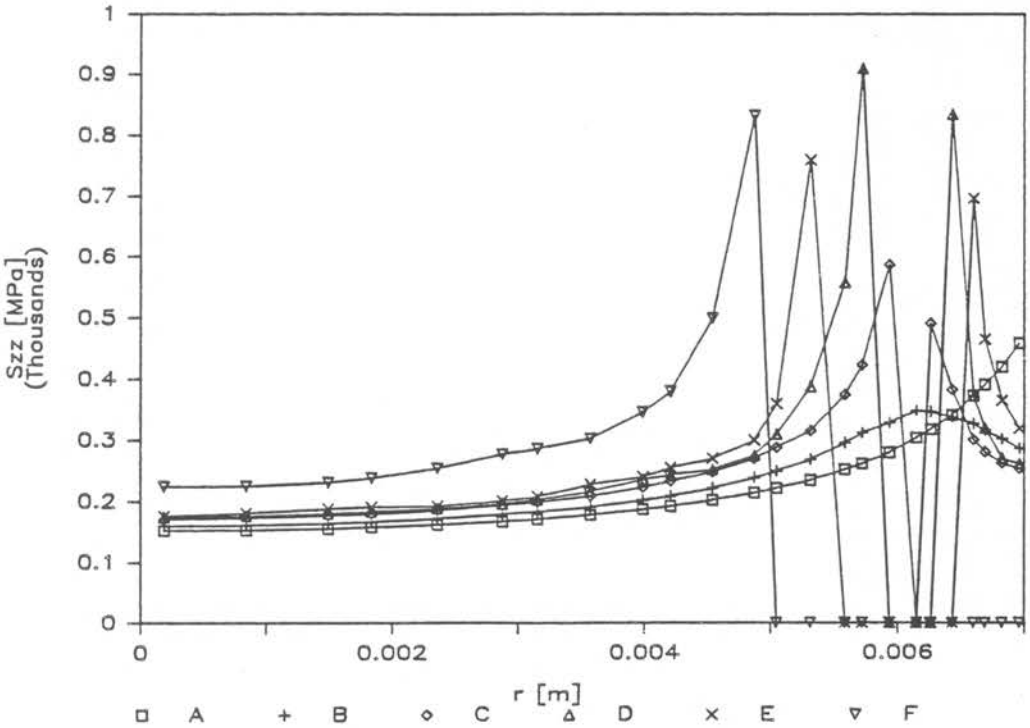

fig. (5.9b) Actual stress distribution across the throat section

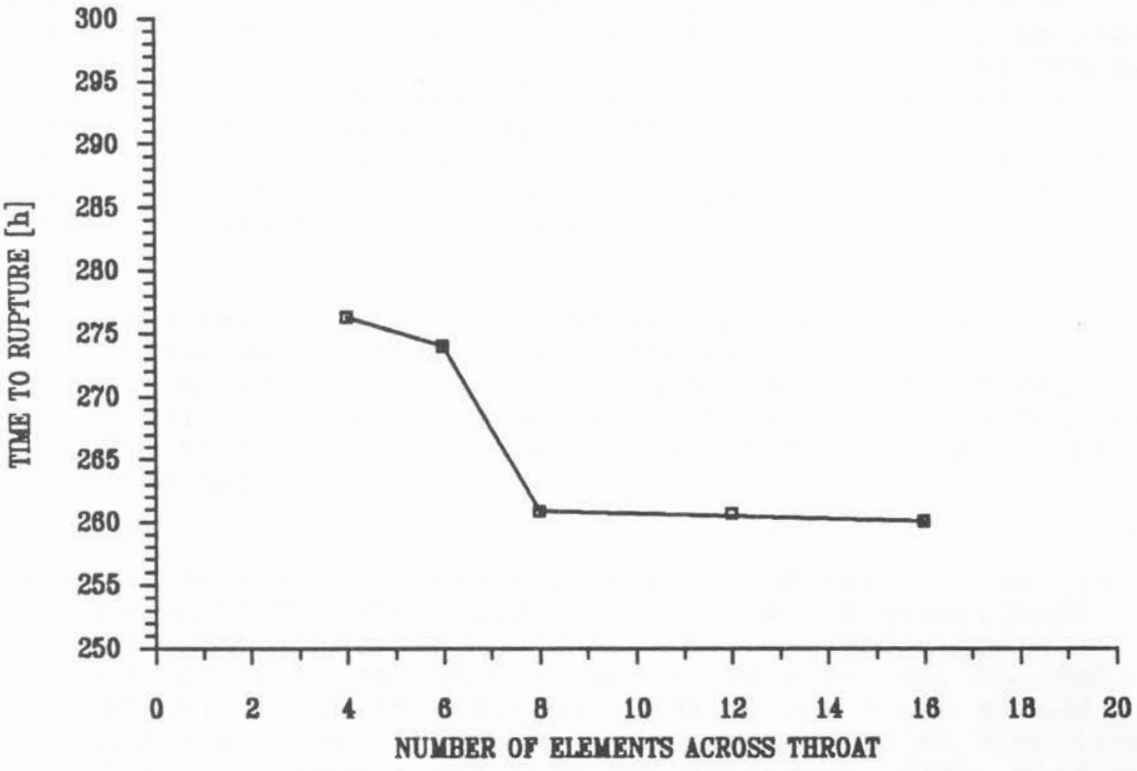

fig. (5.10) Mesh sensitivity

6.0 Conclusions

1) By employing a creep-damage theory, it is possible to estimate when a simple component subject to creep is likely to fail. Kachanov's scalar damage theory, and a Norton power law for creep have been utilised with some success to predict creep failure under simple loading conditions. However, non conservative errors of 30% are estimated to apply to these life predictions. The causes of these inaccuracies should be sought in three problem areas:

   i) Experimental data is often incomplete, and the data points can scatter widely. The material constants extracted from such experimental data, and the resulting predictions are very sensitive to scatter in source data. The need for comprehensive and accurate material tests is once again stressed.

   ii) The solution procedure itself is subject to simplifying assumptions. Here, explicit integration algorithims were employed, and so small time increments are necessary to maintain accuracy. In practice, the FEM solution requires extremely small time steps during primary creep, or whenever damage is high at some Gauss Point. So many iterations are necessary. Also, within each iteration the current stiffness matrix must be evaluated and inverted, and load vectors at each DOF evaluated. So even for relatively small problems (DOF<500) long computer times are needed. As an example, 30 h CPU time on a Vax8550 were necessary for the finest mesh in fig. (5.10). As real design problems would be much larger than the test cases presented here, their computing times and costs would be very high indeed.

      It is however expected that algorithim refinements involving implicit integration schemes will provide improved accuracy and computer performance.

   iii) The constitutive model does not correctly model all the aspects of observed behaviour. Some simplifying assumptions that were made will have to be re-evaluated, so as to refine and improve the creep damage model. Here, the temperatures were assumed to be constant throughout. However even slight temperature variations have a significant effect on the resulting creep behaviour. Not only are creep and damage rates (i.e. the material constants) very sensitive to temperature changes, but different micro-mechanical processes dominate at different temperatures. The transition from brittle to ductile type behaviour can occur quite easily. This, as well as the possibility for large (plastic) strain behaviour needs to be accounted for more thoroughly.

The scalar damage theory is by now dated, and has been found to be inadequate. Most importantly, scalar damage cannot correctly model the directional behaviour of voids, and the anisotropic responses that result from non proportional loading. Some recent developments of the Kachanov damage theory involve tensorial representations of damage [30]. These tensor-damage developments appear promising.

Despite these shortcomings, the use of Kachanov's notion of scalar damage has made significant inroads into the problem of creep and creep rupture.

2) The approximate reference stress techniques are useful further tools for creep analysis. They were formulated largely in response to the problem areas mentioned above, and ameliorate many of the difficulties. Reference stress computations are relatively simple to perform, but judgement and a lot of experience is necessary to correctly interpret and apply the results. Reference stress techniques are still often the only *practical* approach to real design situations.

3) With such analysis techniques, the designer should be able to enhance the safety and reliability of compoments in the creep range. Armed with an estimate of when a component is likely to fail, appropriate maintainence and replacement policies can be specified.

6.1 References

[1] PENNY; R. K. "Design for Creep" McGraw-Hill, London, 1971

[2] DORN; J. E. "Some Fundamental Experiments on High Temperature Creep" J. Mech. Phys. Solids 3, 85-116, 1955

[3] McVETTY; P. G. "Creep of Metals at Elevated Temperatures- the Hyperbolic sine Relation between Stress and Creep-rate" Trans. ASME 65, 761-769, 1943

[4] KACHANOV; L. M. "Time to Rupture under Conditions of Creep" (in Russian) Izv. Ak. Nauk. SSSR, Otd. Tekh. Nauk. 8, 1958

[5] COLLINS; J. A. "Failure of Materials in Mechanical Design" J. Wiley, N. Y., 1981

[6] KENNEDY; A. J. "Processes of Creep and Fatigue in Metals" Oliver and Boyd, 1962

[7] WARD; I. M. "Mechanical Properties of Solid Polymers" Wiley Interscience, 1971

[8] LEE; E. H. "The Influence of Viscoelastic Material Properties on Design Problems" Conf.: Thermal loading and creep in structures and components. Inst. Mech. Eng., 1964

[9] GITTUS; J. "Creep, Viscoelasticity and Creep Fracture in Solids" Appl. Science Publ., London, 1975

[10] MENDELSOHN; A. "Plasticity: Theory and Applications" McMillan, N. Y., 1968

[11] FREDERICK; C. O. and LEWIS; D. J. "Primary Deformation in Beams" Conf.: Thermal loading and creep in structures and components. Inst. Mech. Eng., 1964

[12] MARRIOTT; D. L. and LECKIE; F. A. "Some Observations on the Deflections of Structures during Creep" Conf.: Thermal loading and creep in structures and components. Inst. Mech. Eng., 1964

[13] KENYON; J. L. and WEBSTER; G. A. et. al. "An Investigation of the Application of Fracture Mechanics to Creep Cracking" Conf.: Creep and fatigue in elevated temperature applications. Mech. Eng. Publ., London, 1974

[14] RABOTNOV; Y. N. "Creep Problems in Structural Members" North-Holland Publ., London, 1969

[15] PENNY; R. K. "The Usefulness of Engineering Damage Parameters during Creep" Metals and Materials 8, 278-283, 1974

[16] HOFF; N. J. "The Necking and Rupture of Rods subject to Constant Tensile Loads" J. Appl. Mech. 20, 105-108, 1953

[17] WOODCROFT; D. A. "A Critical Assessment of the Life Fraction Rule under Non-steady Stress and Temperature" Conf. : Creep and fatigue in elevated temperature applications. Mech. Eng. Publ., London, 1974

[18] HULT; J. "Structural Creep Behaviour under Alternating Load" Conf. : Creep and fatigue in elevated temperature applications. Mech. Eng. Publ., London, 1974

[19] HARRISON; G. F. and TILLY; G. P. "The Static and Cyclic Creep Properties of Three Forms of a Cast Nickel Alloy" Conf. : Creep and fatigue in elevated temperature applications. Mech. Eng. Publ., London, 1974

[20] HAYHURST; D. R. "Stress Redistribution and Rupture due to Creep in a Uniformly Stretched Thin Plate Containing a Circular Hole" J. Appl. Mech. 40, 244-250, 1973

[21] KRAJCINOVIC; D. "Distributed Damage Theory of Beams in Pure Bending" J. Appl. Mech. 46, 592-596, 1979

[22] WILSHIRE; B. and OWEN; D. R. J. (Ed.) "Engineering Approaches to High Temperature Design" Pinridge Press, 1983

[23] PENNY; R. K. and LECKIE; F. A. "The Mechanics of Tensile Testing" Int. J. Mech. Sci. 10, 265-273, 1968

[24] MARRIOTT; D. L. "A Review of Reference Stress Methods for Estimating Creep Deformation" IUTAM Symposium on creep in structures 1970, Ed. : Hult; J., Springer Verlag, 1972

[25] KRAUS; H. "Creep Analysis" J. Wiley & Son, N. Y., 1980

[26] MacKENZIE; A. C. "On the Use of a Single Uniaxial Test to Estimate Deformation Rates in Some Structures Undergoing Creep" Int. J. Mech. Sci. 10, 441-453, 1968

[27] SIM; R. G. "Reference Stress Concepts in the Analysis of Structures during Creep" Int. J. Mech. Sci. 12, 561ff, 1970

[28] LECKIE; F. "Constitutive Equations of Creep Deformation and Rupture and their Application" in: BERNASCONI; G. and PIATTI; G. (Eds.) "Creep of engineering materials and structures" Appl. Sc. Publ., London, 1978

[29] HAYHURST; D. R., DIMMER; P. R. and MORRISON; C. J. "Development of Continuum Damage in Creep Rupture of Notched Bars" Phil. Trans. R. Soc. A311, London, 1984

[30] MURAKAMI; S. and OHNO; N. "A Continuum Theory of Creep and Creep Damage" in: PONTER; A. R. S. and HAYHURST; D. R. (Eds.), "Creep in Structures" Springer Verlag, Berlin, 1981

[31] HIBBITT, KARLSON and SORENSEN Inc. "Abaqus User Manual" Version 4. 7, Providence, Rhode Island, 1988

[32] BATHE; K. J., "Finite Element Proceedures in Engineering Analysis" Prentice-Hall, 1982

Appendix A: Integrals for rectangular and circular cross sections.

For a rectangular section width=b and height=2d.

$$dS_N = \eta d^2 \, d\xi \qquad \text{with} \qquad \eta = \frac{b}{d}$$

$\sigma > 0$	$\sigma \leq 0$
$I_1 = \eta d^2 \int_{-1}^{+1} (1-\omega) \, d\xi$	$I_1 = \eta d^2 \int_{-1}^{+1} d\xi$
$I_2 = \eta d^3 \int_{-1}^{+1} (1-\omega)\xi \, d\xi$	$I_2 = \eta d^3 \int_{-1}^{+1} \xi \, d\xi$
$I_3 = \eta d^4 \int_{-1}^{+1} (1-\omega)\xi^2 \, d\xi$	$I_3 = \eta d^4 \int_{-1}^{+1} \xi^2 \, d\xi$
$I_4 = \eta d^2 \int_{-1}^{\lambda_{cr}} (1-\omega) \, d\xi$	$I_4 = \eta d^2 \int_{-1}^{\lambda_{cr}} d\xi$
$I_5 = \eta d^3 \int_{-1}^{\lambda_{cr}} (1-\omega)\xi \, d\xi$	$I_5 = \eta d^3 \int_{-1}^{\lambda_{cr}} \xi \, d\xi$
$I_6 = \eta d^2 \int_{-1}^{X} m(1-\omega) \, d\xi$	$I_6 = \eta d^2 \int_{-1}^{X_N} m \, d\xi$
$I_7 = \eta d^3 \int_{-1}^{X} m(1-\omega)\xi \, d\xi$	$I_7 = \eta d^3 \int_{-1}^{X_N} m\xi \, d\xi$
$I_8 = B\eta d^2 \int_{-1}^{X} k+1 \, d\xi$	$I_8 = 0$
$I_9 = B\eta d^3 \int_{-1}^{X} k+1 \xi \, d\xi$	$I_9 = 0$

For a circular section, diameter=2d

$$dS_N = 2d^2 \sqrt{(1-\xi^2)}\, d\xi$$

$\sigma > 0$	$\sigma \leq 0$
$I_1 = 2d^2 \int_{-1}^{+1} (1-\omega) \sqrt{(1-\xi^2)}\, d\xi$	$I_1 = 2d^2 \int_{-1}^{+1} \sqrt{(1-\xi^2)}\, d\xi$
$I_2 = 2d^3 \int_{-1}^{+1} (1-\omega)\xi \sqrt{(1-\xi^2)}\, d\xi$	$I_2 = 2d^3 \int_{-1}^{+1} \xi \sqrt{(1-\xi^2)}\, d\xi$
$I_3 = 2d^4 \int_{-1}^{+1} (1-\omega)\xi^2 \sqrt{(1-\xi^2)}\, d\xi$	$I_3 = 2d^4 \int_{-1}^{+1} \xi^2 \sqrt{(1-\xi^2)}\, d\xi$
$I_4 = 2d^2 \int_{-1}^{\lambda_{cr}} (1-\omega) \sqrt{(1-\xi^2)}\, d\xi$	$I_4 = 2d^2 \int_{-1}^{\lambda_{cr}} \sqrt{(1-\xi^2)}\, d\xi$
$I_5 = 2d^3 \int_{-1}^{\lambda_{cr}} (1-\omega)\xi \sqrt{(1-\xi^2)}\, d\xi$	$I_5 = 2d^3 \int_{-1}^{\lambda_{cr}} \xi \sqrt{(1-\xi^2)}\, d\xi$
$I_6 = 2d^2 \int_{-1}^{\sum_1^m} (1-\omega) \sqrt{(1-\xi^2)}\, d\xi$	$I_6 = 2d^2 \int_{-1}^{\sum_1^N m} \sqrt{(1-\xi^2)}\, d\xi$
$I_7 = 2d^3 \int_{-1}^{\sum_1^m} (1-\omega)\xi \sqrt{(1-\xi^2)}\, d\xi$	$I_7 = 2d^3 \int_{-1}^{\sum_1^N m} \xi \sqrt{(1-\xi^2)}\, d\xi$
$I_8 = B2d^2 \int_{-1}^{\sum_1^{k+1}} \sqrt{(1-\xi^2)}\, d\xi$	$I_8 = 0$
$I_9 = B2d^3 \int_{-1}^{\sum_1^{k+1}} \xi \sqrt{(1-\xi^2)}\, d\xi$	$I_9 = 0$

Appendix B: Program listing

```
10 REM                  CREEP IN A BEAM-ELEMENT
30 REM                 ==========================
50 CLEAR
55 KILL "CR401DAT.PRN":KILL "CR402DAT.PRN":KILL "CR403DAT.PRN"
60 DEFDBL A-Z:DEFSNG I,J
70 DIM S(40),SACT(40),SACTDOT(40),DAM(40),TRUPT(40),LCR(40),SUM(9)
75 REM  use: A=a*E*SO^M-1)
77 REM  and: B=b/a/E*SO^K+1-M)as a and b are too small!
80 READ D,E,A,B,M,K,N,SO
90 DATA 0.01,155D9,9.730D-3,1.510D-2,8.4,8.5,1.076,290D6
110 REM
120 INPUT "MOMENT=",MOM:INPUT "P AXIAL=",P
130 INPUT "TIME(HOURS) OF NEXT LOAD-CHANGE=",TIMNEXT
140 TNEXT=A*TIMNEXT^N
240 REM
250 REM             evaluate integrals   -1st set
260 REM
270 SUM(1)=0:SUM(2)=0:SUM(3)=0:SUM(4)=0:SUM(5)=0
280 FACTOR=4
290 FOR I=1 TO 39 STEP 2
300     IF S(I)<=0 THEN GOSUB 2000 ELSE GOSUB 3000
310 NEXT I
320 FACTOR=2
330 FOR I=2 TO 38 STEP 2
340     IF S(I)<=0 THEN GOSUB 2000 ELSE GOSUB 3000
350 NEXT I
360 FACTOR=1
370 I=0:IF S(I)<=0 THEN GOSUB 2000 ELSE GOSUB 3000
380 I=40:IF S(I)<=0 THEN GOSUB 2000 ELSE GOSUB 3000
390 SUM(1)=2*D*D/60*SUM(1):SUM(2)=2*D*D*D/60*SUM(2)
400 SUM(3)=2*D*D*D*D/60*SUM(3):SUM(4)=2*D*D/60*SUM(4)
410 SUM(5)=2*D*D*D/60*SUM(5)
420 REM
430 REM             equilibrium equation & stresses
440 REM
450 DET=1/(SUM(1)*SUM(3)-SUM(2)*SUM(2))
460 LO=DET*(SUM(3)*(P/SO+SUM(4))-SUM(2)*(MOM/SO+SUM(5)))
470 CURV=DET*(SUM(1)*(MOM/SO+SUM(5))-SUM(2)*(P/SO+SUM(4)))
510 FOR I=0 TO 40
520     SACT(I)=LO+CURV*D*(I-20)/20-LCR(I):S(I)=SACT(I)*(1-DAM(I))
550 NEXT I
567 REM
570 REM             evaluate integrals   2nd set
580 REM
590 SUM(6)=0:SUM(7)=0:SUM(8)=0:SUM(9)=0
600 FACTOR=4
610 FOR I=1 TO 39 STEP 2
620     IF S(I)<=0 THEN GOSUB 2500 ELSE GOSUB 3500
630 NEXT I
640 FACTOR=2
650 FOR I=2 TO 38 STEP 2
660     IF S(I)<=0 THEN GOSUB 2500 ELSE GOSUB 3500
670 NEXT I
680 FACTOR=1
690 I=0:IF S(0)<=0 THEN GOSUB 2500 ELSE GOSUB 3500
700 I=40:IF S(20)<=0 THEN GOSUB 2500 ELSE GOSUB 3500
710 SUM(6)=2*D*D/60*SUM(6):SUM(7)=2*D*D*D/60*SUM(7)
```

```
720 SUM(8)=2*B*D*D/60*SUM(8):SUM(9)=2*B*D*D*D/60*SUM(9)
740 REM
750 REM              evaluate rate equations  & stress-rates
760 REM
790 LODOT=DET*(SUM(3)*(SUM(6)+SUM(8))-SUM(2)*(SUM(7)+SUM(9)))
800 CURVDOT=DET*(SUM(1)*(SUM(7)+SUM(9))-SUM(2)*(SUM(6)+SUM(8)))
810 FOR I=0 TO 40
820     IF S(I)<=0 THEN SACTDOT(I)=LODOT+CURVDOT*D*(I-20)/20-
        A*SGN(S(I))*(ABS(S(I)))^M
830     IF S(I)>0 THEN SACTDOT(I)=LODOT+CURVDOT*D*(I-20)/20-
        A*SGN(SACT(I))*(ABS(SACT(I)))^M
840 NEXT I
850 REM
860 REM              choose time-incriment
870 REM
880 DT=1/5/B/(K+1)/(ABS(SACT(40)))^K
890 FOR I=0 TO 40
900     IF (SACT(I)<>0) AND (SACTDOT(I)<>0) THEN
        ABA=.1*ABS(SACT(I)/SACTDOT(I))
910     IF ABA<DT THEN DT=ABA
920     IF S(I)<=0 THEN TRUPT(I)=9.99999E+09 ELSE
        TRUPT(I)=1/(K+1)/B/(ABS(S(I)))^K
960 NEXT I
970 IF TNEXT=0 THEN GOTO 980 ELSE IF (TNEXT-T)<DT THEN DT=TNEXT-T
973 REM
976 REM              print results & check for rupture or new loads
979 REM
980 GOSUB 5000
985 GOSUB 1800
987 IF TNEXT=0 GOTO 992
990 IF T=TNEXT GOTO 120
992 IF STFLAG=1 THEN PRINT "   RUPTURED!":END
995 REM
997 REM              go to next time-step
1000 REM
1010 FOR I=0 TO 40
1030     IF S(I)>0 THEN BBB=(1-DAM(I)^(K+1)-DT/TRUPT(I)
1040     IF S(I)>0 THEN LCR(I)=LCR(I)+1/B/(K+1-M)*
         (ABS(S(I))^(M-K)*((1-DAM(I)^(K+1-M)-BBB^(1-M/(K+1)))
1045     IF S(I)<=0 THEN LCR(I)=LCR(I)+DT*SGN(S(I))*(ABS(S(I)))^M
1050     IF S(I)>0 THEN DAM(I)=1-BBB^(1/(K+1))
1070     IF DAM(I)>.9 THEN STFLAG=1
1080 NEXT I
1090 PRINT T,DT
1096 T=T+DT
1100 GOTO 240
1800 REM
1801 REM              print subroutine
1802 REM
1810 OPEN "CR401DAT.PRN" FOR APPEND AS 1
1820 TIME=(T/A^(1/N)
1830 TFAIL=T+TRUPT(40)*(1-DAM(40)^(M+1)
1840 CURVATURE=CURV/E*SO:STRAINO=LO/E*SO:
     STRMX=STRAINO+CURVATURE*D
1845 ACA!=T:AAA!=TIME:BCB!=STRAINO:CCC!=CURVATURE:ERE!=STRMX
1850 PRINT #1,ACA!,AAA!,BCB!,CCC!,ERE!
1860 CLOSE 1
1870 IF (T=TNEXT) OR (T=0) THEN GOSUB 1970
1875 TPR=TPR+1
```

```
1880 IF (TPR/10<>INT(TPR/10)) AND (T<>TNEXT) THEN RETURN
1890 OPEN "CR402DAT.PRN" FOR APPEND AS 2
1892 CDC!=T:CNC!=TIME
1895 PRINT #2,CDC!,CNC!
1896 PRINT #2,
1900 FOR I=0 TO 40
1910     Z=D*(I-20)/20:STRESS=SO*SACT(I):STRESSN=SO*S(I)
1915     DCD!=Z:DDD!=STRESS:DAMAG!=DAM(I):TRU!=TRUPT(I):DED!=STRESSN
1920     PRINT #2,DCD!,DDD!,DAMAG!,TRU!,DED!
1930 NEXT I
1940 CLOSE 2
1960 RETURN
1970 OPEN "CR403DAT.PRN" FOR APPEND AS 3
1975 CSC!=T:CNC!=TIME:CFC!=P:CGC!=MOM
1980 PRINT #3,CSC!,CNC!,CFC!,CGC!
1990 CLOSE 3
1995 RETURN
1999 STOP
2000 REM
2010 REM   integ.summ. subroutine      1st set  -for neg. stress
2020 REM
2025 RT=SQR(1-(I-20)*(I-20)/400)
2030 SUM(1)=SUM(1)+FACTOR*RT
2040 SUM(2)=SUM(2)+FACTOR*RT*(I-20)/20
2050 SUM(3)=SUM(3)+FACTOR*RT*(I-20)*(I-20)/400
2060 SUM(4)=SUM(4)+FACTOR*RT*LCR(I)
2070 SUM(5)=SUM(5)+FACTOR*RT*(I-20)/20*LCR(I)
2080 RETURN
2499 STOP
2500 REM
2510 REM    integ.summ. subroutine      2nd set  -for neg. stress
2520 REM
2525 RT=SQR(1-(I-20)*(I-20)/400)
2530 SUM(6)=SUM(6)+FACTOR*RT*SGN(S(I))*(ABS(S(I)))^M
2540 SUM(7)=SUM(7)+FACTOR*RT*(I-20)/20*SGN(S(I))*(ABS(S(I)))^M
2550 RETURN
2999 STOP
3000 REM
3010 REM    integ.summ. subroutine   1st set   -for pos. stress
3020 REM
3025 RT=SQR(1-(I-20)*(I-20)/400)
3030 SUM(1)=SUM(1)+FACTOR*(1-DAM(I))*RT
3040 SUM(2)=SUM(2)+FACTOR*(1-DAM(I))*RT*(I-20)/20
3050 SUM(3)=SUM(3)+FACTOR*(1-DAM(I))*RT*(I-20)*(I-20)/400
3060 SUM(4)=SUM(4)+FACTOR*(1-DAM(I))*RT*LCR(I)
3070 SUM(5)=SUM(5)+FACTOR*(I-20)/20*(1-DAM(I))*RT*LCR(I)
3080 RETURN
3499 STOP
3500 REM
3510 REM    integ.summ. subroutine   2nd set   -for pos. stress
3520 REM
3525 RT=SQR(1-(I-20)*(I-20)/400)
3530 SUM(6)=SUM(6)+FACTOR*(1-DAM(I))*RT*SGN(SACT(I))*
     (ABS(SACT(I)))^M
3540 SUM(7)=SUM(7)+FACTOR*(1-DAM(I))*RT*(I-20)/20*SGN(SACT(I))*
     (ABS(SACT(I)))^M
3550 SUM(8)=SUM(8)+FACTOR*RT*SGN(SACT(I))*(ABS(SACT(I))^(K+1)
3560 SUM(9)=SUM(9)+FACTOR*RT*(I-20)/20*SGN(SACT(I))*
     (ABS(SACT(I))^(K+1)
3600 RETURN
```

Appendix C: ABAQUS USER MATERIAL subroutine listing

```
C=======================================================================
C       FILE : MATNOCOM.FOR                                  ABAQUS v 4.7
C
C          USER MATERIAL SUBROUTINE for Creep including Damage
C          ===========================
C
C       -  Full 3D, plane stress, axisymmetric, plane strain
C          and uniaxial cases possible
C       -  Material stiffness reduces: E(1-w)
C       -  Time hardening assumptions,   Isothermal conditions
C       -  Not a large strain formulation, no plasticity
C       -  Accurate creep and damage integration over interval
C       -  Explicit integration only
C       -  2 Steps needed: STEP1: Elastic loading, STEP2: Creep
C       -  Creep: Norton power law:Creep=a * STRESS**XM * t**XN
C                                          (1-w)**XM
C       -  Scalar damage: Rabotnov :Dam =b * STRESS**XK * t**XN
C                                          (1-w)**XP
C       -  To prevent unduly large or small numbers use
C          non-dimensional form. So define and input:
C          AA = a * E * SO**(XM-1)&BB = b /a /E * SO**(XK+1-XM)
C       -  Damage>=0.95 is considered FAILED, so damage & creep
C          accumulation ceases. Set STATEV(2)=1.0 so
C          DDSDDE(i,j)=0.0 & nom. and act. stresses=0.0
C       -  Elastic: stress = EE*(1-w)*elastic strain
C       -  Total strain: STRAN(i)=elastic strain + creep strain
C       -  If the max. principal stress is less than 0.0,
C          damage accumulation will be suppressed, and damage
C          set to 0     i.e. NO damage in COMPRESSION !
C       -  Input deck interface:
C                  *MATERIAL,NAME=xxxxxx
C                  *USER MATERIAL,CONSTANTS=10
C                  EE,POISS,AA,XM,SO,BB,XK,XP    =PROPS(1 to 8)
C                  XALPHA,XN                     =PROPS(9 to 10)
C                  *DEPVAR
C                  aa                            =2(NTENS+1)
C       -  Material stiffness matrix size (NTENS):
C                  3D   pl stress  pl strain  axisymm  uniaxial
C          NTENS    6       3          4         4         1
C          NDI      3       2          3         3         1
C          NSHR     3       1          1         1         0
C       -  Additional state variables defined:
C                   real time:   STATEV(1)
C                      damage:   STATEV(2)
C                creep strains:   STATEV(3 .. 2+NTENS)
C             actual stresses:    STATEV(3+NTENS .. 2*NTENS+2)
C       -  H. Sieburg  (AMRU/UCT)                    1. August 1988
C-----------------------------------------------------------------------
      SUBROUTINE UMAT(STRESS,STATEV,DDSDDE,SSE,SPD,SCD,
     &RPL,DDSDDT,DRPLDE,DRPLDT,
     &STRAN,DSTRAN,TIME,DTIME,TEMP,DTEMP,PREDEF,DPRED,CMNAME,
     &NDI,NSHR,NTENS,NSTATV,PROPS,NPROPS,COORDS,DROT)
      IMPLICIT REAL*8 (A-H,O-Z)
      DIMENSION STRESS(NTENS),STATEV(NSTATV),DDSDDE(NTENS,NTENS),
     &DDSDDT(NTENS),DRPLDE(NTENS),STRAN(NTENS),DSTRAN(NTENS),
     &PS(3),PREDEF(1),DPRED(1),PROPS(NPROPS),COORDS(3),
     &SDEVND(6),DELSTRAN(6)
C-----------------------------------------------------------------------
```

```
C           Pass material constants.
      EE = PROPS(1)
      POISS = PROPS(2)
C           AA = a*EE*SO**(XM-1)
      AA = PROPS(3)
      XM = PROPS(4)
      SO = PROPS(5)
C           BB = b/a/EE*SO**(XK+1.0-XM)
      BB = PROPS(6)
      XK = PROPS(7)
      XP = PROPS(8)
      XALPHA = PROPS(9)
      XN = PROPS(10)
C-----------------------------------------------------------------
C
C           1) Update D matrix
C
C           Initialise DDSDDE(i,j) = 0.0
      DO 20 I=1,NTENS
        DO 10 J=1,NTENS
          DDSDDE(I,J) = 0.0D0
 10     CONTINUE
 20   CONTINUE
C           Evaluate Eff. stress, Princ. stresses, Stress
C           deviator tensor & their non-dim. counterparts
      LSTR = 1
      CALL SPRINC(STRESS,PS,LSTR)
      IF ( ABS(PS(1)).GT.ABS(PS(3)) ) THEN
        SPRINMAX = PS(1)
      ELSE
        SPRINMAX = PS(3)
      ENDIF
      SPRMAXND = SPRINMAX/SO
C
      CALL SINV(STRESS,SINV1,SINV2)
      SINV2ND = SINV2/SO
C
      DO 90 I=1,NDI
        SDEVND(I) = (STRESS(I) - SINV1)/SO
 90   CONTINUE
      IF ( NSHR.GT.0.0 ) THEN
        DO 100 I=1,NSHR
          LSH = NDI+I
          SDEVND(LSH) = STRESS(LSH)/SO
 100    CONTINUE
      ENDIF
      SCOMND = XALPHA*SPRMAXND + (1.0D0-XALPHA)*SINV2ND
C
C
      IF ( SPRMAXND.LT.0.0 ) THEN
C           NO damage in compression - void closure
        DAMAGE = 0.0D0
      ELSE
C           Damage in tension
        DAMAGE = STATEV(2)
      ENDIF
C
```

```
      IF ( DAMAGE.LT.0.95 ) THEN
C
C          Material has NOT failed yet: Material stiffness
C          exists & DDSDDE(i,j) not equal to 0.0  Define
C          upper half of DDSDDE(i,j) for a case a) thru d)
C
C          Case a)  -----  full 3D
C
        IF ( NTENS.EQ.6.0 ) THEN
          CONST = EE*(1.0D0-DAMAGE)/(1.0D0+POISS)/
     &    (1.0D0-2.0D0*POISS)
          DO 30 I=1,NDI
            DDSDDE(I,I) = CONST*(1.0D0-POISS)
 30       CONTINUE
          DO 40 I=1+NDI,NTENS
            DDSDDE(I,I) = CONST*(1.0D0-2.0D0*POISS)/2.0D0
 40       CONTINUE
          DDSDDE(1,2) = CONST*POISS
          DDSDDE(1,3) = CONST*POISS
          DDSDDE(2,3) = CONST*POISS
        ENDIF
C
C          Case b)  -----  plane stress
C
        IF ( ( NDI.EQ.2.0 ).AND.( NSHR.EQ.1.0 ) ) THEN
          CONST = EE*(1.0D0-DAMAGE)/(1.0D0-POISS**2.0D0)
          DDSDDE(1,1) = CONST
          DDSDDE(2,2) = CONST
          DDSDDE(4,4) = CONST*(1.0D0-POISS)/2.0D0
          DDSDDE(1,2) = CONST*POISS
        ENDIF
C
C          Case c)  -----  axisymmetric & plane strain
C
C          For pl.strain, E(zz)=0.0 is ensured by main program.
        IF ( ( NDI.EQ.3.0 ).AND.( NSHR.EQ.1.0 ) ) THEN
          CONST = EE*(1.0D0-DAMAGE)/(1.0D0+POISS)/
     &    (1.0D0-2.0D0*POISS)
          DO 50 I=1,NDI
            DDSDDE(I,I) = CONST*(1.0D0-POISS)
 50       CONTINUE
          DDSDDE(4,4) = CONST*(1.0D0-2.0D0*POISS)/2.0D0
          DDSDDE(1,2) = CONST*POISS
          DDSDDE(1,3) = CONST*POISS
          DDSDDE(2,3) = CONST*POISS
        ENDIF
C
C          Case d)  ------  uniaxial
C
        IF ( ( NDI.EQ.1.0 ).AND.( NSHR.EQ.0.0 ) ) THEN
          DDSDDE(1,1) = EE*(1.0D0-DAMAGE)
        ENDIF
C
C          Define all symmetric terms in DDSDDE matrix
C          i.e. bottom half
        DO 70 I=1,NTENS
          DO 60 J=1,NTENS
            DDSDDE(J,I) = DDSDDE(I,J)
 60       CONTINUE
 70     CONTINUE
```

```
C
C           For the case DAMAGE.GT.0.95 the material is
C           considered failed.  So DDSDDE(i,j)=0.0D0 from
C           initialisation is OK.
        ENDIF
C-----------------------------------------------------------------
C
C           2) Evaluate real time, and update damage, creep
C              strains, elastic strain increments, and stresses
C              at END of time increment
C
        IF ( (TIME + DTIME).GT.1.0 ) THEN
C
C           Creep loading - STEP2
C           Update REAL time at END of time step
C           (1.0=static STEP1 "time")
          STATEV(1) = ((TIME+DTIME-1.0D0)/AA)**(1.0D0/XN)
          IF ( DAMAGE.GE.0.95 ) THEN
C           Material has failed:
C           set STATEV(2)=1.0, no damage accumulation
C           set STRESS(i)=0.0, & no creep accumulation
            STATEV(2) = 1.0D0
            DO 80 I=1,NTENS
              STRESS(I) = 0.0D0
              ISTR = 2+NTENS+I
              STATEV(ISTR) = 0.0D0
 80         CONTINUE
          ELSE
C            Material has NOT failed yet:
            IF ( SPRMAXND.LE.0.0 ) THEN
C            NO damage in compression - void closure
              DCRCON = 3.0D0/2.0D0*SO/EE*DTIME*
     &         SINV2ND**(XM-1.0D0)
              DAMEND = STATEV(2)
              DAMAGE = 0.0D0
            ELSE
C            Damage accumulates in tension - evaluate Trupt
              TRUPT = 1.0D0/BB/(XP+1.0D0)/(ABS(SCOMND)**XK)
              XINC = (1.0D0-STATEV(2))**(XP+1.0D0) - DTIME/TRUPT
              IF ( XINC.LE.0.0 ) THEN
C             Cause this iteration to ABORT
                DAMAGE = 1.1D0
              ELSE
C             Update creep strain & el.strain increments,
C             & damage at END of time step.
                YINC = ((1.0D0-STATEV(2))**(XP+1.0D0-XM))
     &           -XINC**(1.0D0-XM/(XP+1.0D0))
                DCRCON = 3.0D0/2.0D0/BB*SO/EE/(XP+1.0D0-XM)*YINC*
     &           (ABS(SINV2ND)**(XM-1.0D0))/(ABS(SCOMND)**XK)
                DAMEND = 1.0D0 - XINC**(1.0D0/(XP+1.0D0))
                DAMAGE = DAMEND
              ENDIF
            ENDIF
C
C           Test if failure has occurred during THIS time step.
            IF ( DAMAGE.GE.1.0 ) THEN
C           Failure HAS occurred during this time step.
C           Cause out-of-balance forces to REDUCE TIME STEP
C           and to ABORT THIS iteration.
```

```
              DO 105 I=1,NTENS
                STRESS(I) = 0.0D0
 105          CONTINUE
            ELSE
C            Failure has NOT occurred during this time step.
              STATEV(2) = DAMEND
              DO 110 I=1,NTENS
                DCRSTRAN = DCRCON*SDEVND(I)
                ICR = 2+I
                STATEV(ICR) = STATEV(ICR) + DCRSTRAN
                DELSTRAN(I) = DSTRAN(I) - DCRSTRAN
 110          CONTINUE
C            Update stress increments & thus stresses
              DO 130 I=1,NTENS
                DSTRESS = 0.0D0
                DO 120 J=1,NTENS
                  DSTRESS = DSTRESS + DDSDDE(I,J)*DELSTRAN(J)
 120            CONTINUE
                STRESS(I) = STRESS(I) + DSTRESS
C            Update ACTUAL stresses
                ISTR = 2+NTENS+I
                IF ( SPRMAXND.LE.0.0 ) THEN
                  STATEV(ISTR) = STRESS(I)
                ELSE
                  STATEV(ISTR) = STRESS(I)/(1.0D0-STATEV(2))
                ENDIF
 130          CONTINUE
            ENDIF
          ENDIF
        ELSE
C
C             Elastic loading --- STEP1
          DO 150 I=1,NTENS
            DSTRESS = 0.0D0
            DO 140 J=1,NTENS
              DSTRESS = DSTRESS + DDSDDE(I,J) * DSTRAN(J)
 140        CONTINUE
            STRESS(I) = STRESS(I) + DSTRESS
 150      CONTINUE
        ENDIF
C-----------------------------------------------------------------
C             Optional print control data at every pass:
C         WRITE(6,*) ' REAL TIME= ',STATEV(1),' DAMAGE= ',
C        &STATEV(2),' CRSTRAN(yy)= ',STATEV(3),' SPRMAXND= ',
C        &SPRMAXND,' SCOMND= ',SCOMND,' TRUPT= ',TRUPT,' XINC= ',
C        &XINC,' YINC= ',YINC,' PS(I)= ',PS(1),PS(2),PS(3),
C        &' SINV1&2= ',SINV1,SINV2,' DCRCON= ',DCRCON
C         DO 170 I=1,NTENS
C           DO 160 J=1,NTENS
C             WRITE(6,*) ' DDSDDE(I,J)= ',DDSDDE(I,J)
C 160       CONTINUE
C 170     CONTINUE
C         DO 180 I=1,NTENS
C           WRITE(6,*) ,' SDEVND(I)= ',SDEVND(I)
C 180     CONTINUE
C-----------------------------------------------------------------
        RETURN
        END
C=================================================================
```

Appendix D: Notation

a	material creep constant
A	$=aE\sigma_0^{m-1}$
A, A_N	cross sectional area, undamaged (nominal) area
α	proportionality constant; material constant; d^2/A
b	material damage constant; characteristic dimension
B	$=(b\sigma_0^{k+1-m})/(aE)$
$\mathbf{B}$	strain-displacement interpolation matrix
β	$=d^4/I$
d	characteristic dimension
D_{ij}, D_{ijN}	non. dim. stress deviator tensor σ_{ij}/σ_0, σ_{ijN}/σ_0
$\mathbf{D}$	material stiffness matrix $=E(1-\omega)$
Δ	increment in . . .
e	position of the neutral axis
$E, \mathbf{E}$	Youngs Modulus, material stiffness matrix
$E_{1,2}$	Rheological spring constants
$\epsilon_x, \epsilon_{cr}$	total strain, creep strain
$\epsilon_R, \epsilon_{crR}$	total strain at rupture, creep strain at rupture
$\epsilon_{ij}, \epsilon_{crij}$	strain tensor, creep strain tensor
ϵ_0	reference strain $=(1/E)\sigma_0$
f, g	a function of . . .
$\mathbf{H}$	displacement interpolation matrix
$\eta, \eta_{1,2}$	$=b/d$, Rheological dashpot constants
I	Moment of Inertia; Integral
k	damage exponent
$\mathbf{K}$	element stiffness matrix
κ	beam curvature
l	length
L	$=(k+1)/(k+1-m)$
λ_x, λ_{cr}	non dimensional strains ϵ_x/ϵ_0 , ϵ_{cr}/ϵ_0
$\lambda_{ij}, \lambda_{crij}$	non dimensional strain tensor ϵ_{ij}/ϵ_0, $\epsilon_{crij}/\epsilon_0$
λ_{x0}	non dimensional strain at $x=\xi=0$
m	creep exponent
M, M_{coll}	bending moment, plastic collapse moment
n	time exponent
ν	Poisson's Ratio
ω	damage
p	damage exponent, pressure
P, P_{coll}	axial load, plastic collapse load
q	damage exponent; nodal displacements
Q	Activation energy
r	damage exponent; radius
R	Boltzmann constant
$\mathbf{R}_{F,b,a,cr}$	equivalent nodal load - force, body, area, creep
ρ	density
S	load bearing cross section area; strain energy
S_N	undamaged (nominal) cross section area
s_{ij}, s_{Nij}	stress deviator tensor, nominal stress deviator
σ_x	stress over the load bearing area
σ_{xN}	(nominal) stress over the undamaged area
σ_{ij}, Σ_{ij}	stress tensor, non dim. stress tensor σ_{ij}/σ_0
$\sigma_{ijN}, \Sigma_{Nij}$	nominal stress tensor, non dim. nominal tensor
$\sigma_e, \sigma_{Ne}, \Sigma_e, \Sigma_{Ne}$	v. Mises stress, nom., non dim., non dim. nom.
$\sigma_{1,2,3}, \sigma_{N1,2,3}$	principal stresses, nominal princ. stress
$\Sigma_{1,2,3}, \Sigma_{N1,2,3}$	non dim. $\sigma_{1,2,3}$
σ_y	yield stress
σ_0	reference stress

Σ_x, Σ_{xN}	non dimensional stresses σ_x/σ_o , σ_{xN}/σ_o
t, t_R	time, time to rupture
τ, τ_R	time parameter, time parameter to rupture
T	temperature
U, u	displacement
V	volume
w	characteristic dimension; distributed load
W	work done; max. distributed load
z	position in beam cross section
ξ	non dimensional position =z/d

$$\dot{(\ )} \quad \frac{\partial (\ )}{\partial \tau}$$